NTNU – Trondheim
Norwegian University of
Science and Technology

Higher Order Loads from Steep Waves on Drilling Risers

Balder Een Sture

Marine Technology
Submission date: May 2013
Supervisor: Carl Martin Larsen, IMT

Norwegian University of Science and Technology
Department of Marine Technology

NTNU Trondheim
Norwegian University of Science and Technology
Faculty of Engineering Science and Technology
Department of MarineTechnology

M.Sc. thesis 2013

for

Stud.tech. Balder Sture

HIGHER ORDER LOADS FROM STEEP WAVES ON DRILLING RISERS

Drilling risers are exposed to large hydrodynamic forces in the splash zone. These forces have normally been calculated by use of the well known Morison equation and linear wave theory. The purpose of the present project is to study the response from slamming loads caused by steep waves on a drilling riser. Such loads may lead to unwanted structural vibrations at the upper part of the riser and also of the hydraulic cylinders for heave compensation.

The computer program RIFLEX is well suited to carry out dynamic analyses of marine risers. However, slamming loads cannot be generated in a time domain simulation. The only way of including this effect is to pre-calculate these loads and prepare a data file with loads that can be applied during simulation. Some simplifications have to be accepted in this type of calculations, and the loads must replace drag forces that is automatically calculated by RIFLEX at the same location and time.

The purpose of the present work is to study the importance of these forces by use of RIFLEX for a set of relevant wave cases.

The work may be carried out in steps as follows

1. Literature study that should concentrate on methods for calculation of wave loads and load effects on slender marine structures. Classical and numerical methods should be included. References may be given to the pre-project that was completed during fall 2012.

2. Make a simple Matlab code for calculation of slamming loads from steep, irregular waves on a typical drilling riser. Statistics of slamming loads should be studied.

3. Describe the procedure for calculating slamming forces to be used in a Riflex simulation so that the sum of slamming forces and the drag forces calculated by Riflex becomes correct.

4. Carry out time domain simulations with and without slamming forces on a deep water drilling riser. Vary wave spectrum and give recommendations on the relevance of including slamming forces in marine riser analysis. Response of the hydraulic cylinders in the heave compensation system should in particular be studied.

The work may show to be more extensive than anticipated. Some topics may therefore be left out after discussion with the supervisor without any negative influence on the grading.
The candidate should in her/his report give a personal contribution to the solution of the problem formulated in this text. All assumptions and conclusions must be supported by mathematical models and/or references to physical effects in a logical manner.

The candidate should apply all available sources to find relevant literature and information on the actual problem.

The report should be well organised and give a clear presentation of the work and all conclusions. It is important that the text is well written and that tables and figures are used to support the verbal presentation. The report should be complete, but still as short as possible.

The final report must contain this text, an acknowledgement, summary, main body, conclusions and suggestions for further work, symbol list, references and appendices. All figures, tables and equations must be identified by numbers. References should be given by author name and year in the text, and presented alphabetically by name in the reference list. The report must be submitted in two copies unless otherwise has been agreed with the supervisor.

The supervisor may require that the candidate should give a written plan that describes the progress of the work after having received this text. The plan may contain a table of content for the report and also assumed use of computer resources.

From the report it should be possible to identify the work carried out by the candidate and what has been found in the available literature. It is important to give references to the original source for theories and experimental results.

The report must be signed by the candidate, include this text, appear as a paperback, and - if needed - have a separate enclosure (binder, DVD/ CD) with additional material.

Supervisor at NTNU is Professor Carl M. Larsen

Trondheim, February 2013

Carl M. Larsen

Submitted: January 2013
Deadline: 10 June 2013

Preface

The master thesis work has been carried out at the Norwegian University of Science and Technology (NTNU) in Trondheim, at the Faculty of Engineering Science and Technology during the spring semester 2013 during the fifth year of the Master of Science degree at the Department of Marine Technology. The subject of study was proposed by Professor Carl Martin Larsen.

The work can be considered a continuation of the project thesis work completed during the previous semester. A simple Matlab model for calculating slamming loads was developed, and a literature study conducted in order to gain more knowledge on the subject, laying the foundation for the master thesis.

I would like to express my gratitude towards Professor Carl Martin Larsen for the supervision of the work and his assuring guidance during the process. His encouragement and interest was always a motivation. I would also like to thank Elizabeth Passano and Andreas Amundsen at Marintek for their assistance with use of the Riflex software. Their knowledge of the program contributed greatly to the final result. I am also grateful for the invaluable input from fellow students, whose knowledge should never be underestimated.

Finally, I would like to thank my family for their never-ending support.

Trondheim, June 2013

Balder Sture

Summary

Drilling operations are conducted in increasingly harsher environments as the easily accessible oil fields are growing more scarce. Marine drilling risers are exposed to large hydrodynamic forces in the splash zone. Higher order hydrodynamic forces known as slamming loads can occur during especially severe sea states, as steep waves impact with offshore structures. These loads are of concern to the industry, because these loads may lead to structural vibrations. The upper part of the riser and the heave compensation system are especially exposed to slamming loads. The hydraulic cylinders of the compensation system are pretensioned and have short natural periods, and are of special concern with regard to short duration forces such as slamming.

This thesis will investigate the relevance of including slamming loads in the general load model for marine riser analyses. Riflex is a purpose-made computer simulation program to perform such marine riser analysis. Hydrodynamic loads from waves, formulated by Morison's equation, and current forces are included in the load model of Riflex. In order to include slamming loads in the simulation, a separate load file must be created and added to the load procedure of the program.

A slamming load model is developed in Matlab. The model is intended to reproduce the irregular sea elevation extracted from Riflex and formulate the resulting load as a wave impacts against the riser. A load file is produced and implemented to the simulation procedure in Riflex. The marine riser analysis is performed both with and without slamming loads incorporated in the load model for comparison reasons. It is vital to synchronize the loading with the wave and vessel motion simulated in Riflex. Extensive information of the Riflex riser model is transferred to the Matlab code, as well as the updated position of the riser. Five severe sea states are simulated.

The focus of the analysis is primarily on the hydraulic cylinders of the heave compensation system. Time series of the displacements are examined for any dynamic effects from the slamming loads. The displacements are found to be close to similar with and without slamming forces. Occasionally, slightly higher amplitudes are observed as the slamming loads act on the riser, but the standard deviations of the displacements reveal small differences. The largest differences manifest themselves in the sea states with the steepest waves. The response spectra both with and without slamming show no evidence of response in different frequency ranges.

The bending moments on the hydraulic cylinder are found to have higher amplitude oscillations in the case of large slamming loads. The differences in the bending moments standard deviation are slightly higher than for the displacements. At most, the largest observed maximum bending moment increases 27.39 %. At the least, 1.85 %.

The influence slamming loads have on fatigue life is also investigated. The accumulated damage was calculated with Miner-Palmgren summation, utilizing the rainflow counting technique to count stress cycles. The number of small stress amplitude cycles increase for all sea states when slamming is included. In addition there is a small increase of high stress amplitude cycles. This leads to a relatively large effect on accumulated damage. At most, the damage is increased with 133.67 %.

The effects of slamming loads are in this thesis found to coincide poorly with previous work on the subject. The differences most likely lie in the differences in approximations, especially with regards to wave kinematics. Linear wave theory is not well suited to deal with slamming loads, and higher order theories are most likely needed to describe the kinematics in steep waves properly. On the basis of this thesis, it does not appear relevant to include slamming loads in the general load model in marine riser analysis.

Sammendrag (Norwegian Summary)

Tiden for de lett tilgjengelig oljefeltene nærmer seg slutten, og i søken etter ny oljeutvinning foregår boreoperasjoner i stadig mer ekstreme værforhold. Borestrenger blir utsatt for store hydrodynamiske krefter i skvalpesonen. Høyere ordens krefter kjent som slammingkrefter kan opptre i særlig ekstreme sjøtilstander, når krappe bølger slår imot offshore konstruksjoner. Disse kreftene må tas til etterretning fordi de kan indusere strukturelle vibrasjoner. Den øvre delen av riseren og hivkompenseringssystemet er spesielt utsatt for disse slammingkreftene. De hydrauliske stempelstagene i kompenseringssystemet er utsatt for stort strekk, noe som bidrar til den korte egenperioden. Det er derfor knyttet særlig bekymring til disse i sammenheng med slammingkrefter.

Denne oppgaven vil undersøke nærmere betydningen av å inkludere slamminglaster i den generelle lastmodellen i analyser på slanke marine konstruksjoner. Riflex er et simuleringsprogram skreddersydd for analyser på slanke marine konstruksjoner. Lastmodellen til Riflex består av bølgelaster formulert av Morisons ligning, samt strømkrefter. For å implementere slammingkrefter i simuleringer i Riflex er det nødvendig å lage og inkludere en separat lastfil i programmets lastprosedyre.

En slamminglastmodell er utviklet i Matlab. Modellen er ment å reprodusere den irregulære sjøtilstanden generert i Riflex, og formulere den resulterende lasten når bølgene slår i mot riseren. En lastfil blir laget og implementert i simuleringsprosedyren i Riflex. Analysen blir gjennomført både med og uten slamminglaster i den generelle lastmodellen for å sammenligne. Det er avgjørende å synkronisere lasten med bølge- og fartøybevegelsen som er simulert i Riflex. Detaljert informasjon om riser-modellen blir overført til Matlab-programmet, i tillegg til oppdatert posisjon av riseren. Fem ulike sjøtilstander blir simulert.

Hensikten med analysen er å undersøke oppførselen til de hydrauliske stempelstagene i hivkompenseringssystemet. Tidsserier av forskyvningene er skrevet ut og gransket for dynamiske effekter fra slamminglastene. Forskyvningen med og uten slamminglaster er svært like. I tilfeller der høye slamminglaster opptrer, er det mulig å observere høyere amplituder eller små hopp. Forskjellene i standardavvikene til forskyvningene er imidlertid liten for alle sjøtilstandene, men størst for sjøtilstandene med de krappeste bølgene. Responsspektrene med og uten slamming viser ingenting som tyder på respons i ulike frekvensområder, noe som avviser at det opptrer strukturelle vibrasjoner i stempelstaget.

Bøyemomentene i stempelstaget viser større amplituder i svingningene der store slamminglaster inntreffer. Forskjellene i standardavvikene til bøyemomentene er noe større enn for forskyvningene. Det største maksimale bøyemomentet øker med 27.39 %, det minste med 1.85 %.

Det blir også undersøkt om slammingkrefter påvirker utmattingslevetiden til stempelstaget. Miner-Palmgren summasjon ble brukt for å beregne akkumulert skade, ved å bruke rainflow-telling av spenningsviddene. Antallet lave spenningssykler øker for alle sjøtilstander når slamming er inkludert. I tillegg blir det observert en viss økning i store spenningssykler. Samlet sett medfører dette en relativt stor påvirkning på utmattingslevetiden. På det meste øker akkumulert skade med 133.67 %.

Denne oppgaven konkluderer med at betydningen av slamminglaster er liten sammenlignet med tidligere arbeid på området. Forskjellene i resultatene skyldes nok ulike anvendelse av bølgekinematikken. Lineær teori er ikke godt egnet til å beskrive slamminglaster. Høyere ordens bølgeteorier vil være mer hensiktsmessig til å beskrive bølgekinematikken i steile, nærbrytende bølger. Med utgangspunkt i arbeidet i denne oppgaven, fremstår det ikke som relevant å inkludere slamminglaster i den generelle lastmodellen i analyser på slanke marine konstruksjoner.

Notation

Abbreviations

BOP	Blow-out preventer
CFD	Computational fluid dynamics
DAF	Dynamic amplification factor
DNV	Det Norske Veritas
FE	Finite element
FEM	Finite element method
ID	Inner diameter
JONSWAP	Joint North Sea wave project
LMRP	Lower marine riser package
MODU	Mobile offshore drilling unit
OD	Outer diameter
PM	Pierson-Moskowitz
RAO	Response amplitude operator
RFC	Rainflow cycles
ROPS	Roll-over protection structure
Std	Standard deviation
WAFO	Wave analysis for fatigue and oceanography
WT	Wall Thickness

Greek symbols

α	Spectral parameter
β	Slope of S-N curve, WAFO terminology
$\beta_{1,2}$	Wave directions
γ	Angular orientation, pipe-in-pipe coordinate system

γ	Spectral peakedness parameter
ε	Phase angle
ζ	Wave elevation
ζ_a	Wave amplitude
η_i	Motion of support vessel, i=1-6
$\eta_{1,2}$	Incremental slippage of contact points
λ	Wave length
ξ	Dimensionless length, pipe-in-pipe coordinate system
ρ	Sea water density
σ	Stress
τ	Time instant of pulse
ϕ	Potential flow
ψ	Stream function
ω	Angular frequency
ω_n	Natural frequency
ω_p	Peak frequency

Roman symbols

A	Cross section area
A_{33}	Added mass in heave
$\bar{a}$	Intercept of log N-axis of S-N curve
c	Damping coefficient
C_D	Drag coefficient
C_M	Mass coefficient
c(t)	Body submergence
C_s	Slamming coefficient, Campbell & Weynberg
D	Cylinder diameter
d	Water depth
D(t)	Accumulated damage at time t
E	Wave energy
F_x	Horizontal slam force
F_3	Vertical water entry force
g	Gravity constant
H	Wave height
H_s	Significant wave height
I	Pulse magnitude

I_i	Global base vector, pipe-in-pipe coordinate system
i_i	Master base vector, pipe-in-pipe coordinate system
j_i	Slave base vector, pipe-in-pipe coordinate system
K	Material constant
k	System stiffness
k	Wave number
m	System mass
N	Number of cycles to failure
p(t)	Pulse
p	Pressure
R	Radius of cylinder
$\mathbf{r}_{CA}$	Contact point position with respect to body A
$\mathbf{r}_{CB}$	Contact point position with respect to body B
s	Submergence, Campbell & Weynberg
$S(\omega_n)$	Spectrum
S_k^{RFC}	Rainflow cycle stress range
t	Time
T_n	Natural period
T_p	Peak period
u	Horizontal water particle velocity
V	Vertical body velocity
$\mathbf{X}_i$	Global coordinate system, pipe-in-pipe coordinate system
z_s	Wheeler stretched vertical coordinate

Contents

List of Figures

List of Tables

Chapter 1

Introduction

1.1 Motivation

Marine drilling risers are exposed to large hydrodynamic forces, as they extend the distance between the drilling deck and the sea bottom. These forces arise from currents and waves, and it is found that especially steep or breaking waves in the splash zone are prone to inducing large forces with short duration on the upper end of the drilling riser, and in some cases exciting structural vibrations. The hydraulic cylinders of the heave compensation system are more susceptible to damage from such pulse excitation. Directional wear lines found on worn pack boxes and cylinder rods indicate that they have been subjected to higher lateral loads than initially accounted for in their design. Replacement of such hydraulic cylinders is extremely costly and time consuming, and so it is of great interest to improve the design in order to meet the requirements posed by the environment. To accomplish this, it is important to make an accurate estimation of the forces to which the riser system is exposed to.

1.2 Previous work

Marine risers are a well documented field, and there is an abundance of literature and information about the subject. Non-linear hydrodynamic loads such as water entry, slamming and the similar are also extensively studied, as well as their application on circular objects, such as spheres, discs and cylinders. It is in the intersection between these loads and the properties of steep non-linear waves that the range of available literature is slightly more narrowed down.
The project thesis work conducted during the previous fall semester was a prelude to the present work. A more elaborate literature study was made on the topic of slamming loads and methods of estimation. A Matlab program was written to calculate the slamming loads from a single, regular wave, using the method and wave kinematics proposed by Nestegård in his paper on resonant vibrations on riser guide tubes due to slamming forces [8].
Nestegård studies the topic in great detail, and has been an important reference during the thesis work. DNV's recommended practice C205 [13] also refers to Nestegård, and provides simple

guidelines for the calculation of the slamming forces on vertical cylinders. Nestegårds work is a detailed discussion on the slamming forces introduced by steep waves on riser guide tubes. The tubes are relatively short tubular fittings in the splash zone that provide guidance and protection to various risers and cables. His work includes a proposed wave kinematic model. Response calculations are done using RIFLEX. Calculations were done for several cases of regular and irregular waves. Results from experiments conducted at Marintek on a model semi-submersible fitted with riser guide tubes, subjected to steep waves are also included, and compared with the theoretical estimations. The results were found to coincide well with each other.
Sten [29] also uses the slamming load formulations presented by Nestegård and the pre-process code WAVESLAM. A great amount of attention is given to the responses of the hydraulic cylinders and tensioner ring, and a detailed model of a hydraulic-pneumatic system is developed to describe the cylinder tension accurately. Sten provides two load models, the first composed of a normal wave load formulated by the Morison equation, the second including slamming forces in addition. The computed results of his analysis show a great variation between the two load models.
Various other contributions to the subject have been made, and will be discussed in more detail in Section 3.1.

1.3 Contributions

The contribution of this thesis is a method for calculating the slamming forces on a marine drilling riser or similar circular marine structure from a steep incident linear wave. The method includes generating an irregular linear wave elevation from Fourier components provided by Riflex, and deals with the details of the wave kinematics from the peak to the mean water line by implementing a stretching method. The slamming forces from the irregular wave are calculated based on fluid momentum theory and analytically fitted experimental data. The method is capable of including the updated position of the riser in question. A Matlab code is created to perform the calculations.

1.4 Outline of thesis

The master thesis is organized in the following way:

Chapter 2 provides an overview of the support vessel, marine drilling riser and heave compensation system, as well as the FE model.

Chapter 3 presents a literature study of related work that has been done regarding the subject and the various methods of estimating and calculating wave forces. It also includes a discussion with regards to wave theory and provides the necessary theory on the computation of slamming loads

Chapter 4 this chapter explains the theory of pulse excitation

Chapter 5 a short introduction to fatigue theory is given in this chapter

Chapter 6 explains the numerical implementation of the formulations and modeling in Matlab

Chapter 7 provides an overview and presents choices made concerning the simulation model

Chapter 8 displays and provides a discussion of the results obtained by the calculations

Chapter 6 concludes the findings and gives a recommendation on the significance of the inclusion of slamming loads. Proposes possible further work

Chapter 2

Marine risers and heave compensation system

2.1 Marine drilling risers

Marine risers include a wide variety of long, slender structures, defined according to their use. The main uses of risers are:

- Drilling
- Completion and workover
- Production
- Export

This thesis will focus on the typical drilling riser. As the name indicates, the drilling riser is used for drilling wells in the sea bed, and is typically used by semi-submersible drilling rigs or other types of mobile offshore drilling units (MODUs), which are often dynamically positioned to maintain their position under operations. The riser is therefore suspended between the floater and the sea floor, with an applied top tension to give the riser an additional stiffness contribution, see Figure 2.1.
The most commonly used type of drilling riser is the low-pressure riser, whose only internal pressure is that from the weight of the drilling-mud weight. In other words, the top of the riser is exposed to atmospheric pressure. The length of the riser is comprised of a number of riser joints, seen in Figure 2.2, called a string. A riser joint has an individual length of 15-23 meters. They are fastened together on installation to complete the entire distance from the floater to the sea bed. The main body of the riser is comprised of a central tube of 21 inches in diameter. Also fitted on the periphery of the central tube are a number of lines used for control of the blow-out preventer, BOP, and fluid flow, such as the kill and choke lines. As shown in Figure 2.1, the riser is connected to the seabed through the BOP and a lower marine riser package, LMRP. The BOP allows the riser to be disconnected from the well in the case of an emergency, closing

Figure 2.1: Drilling risers deployed from various MODUs

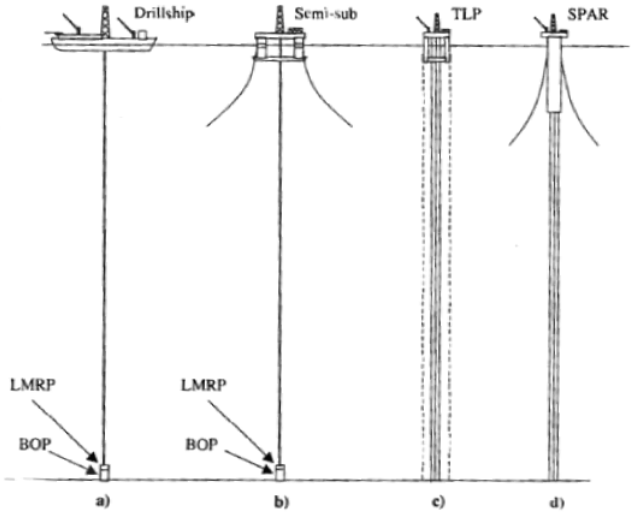

Figure 2.2: Drilling riser joint with buoyancy modules

the well. The LMRP is a flexible joint, allowing a certain degree of rotation, thus reducing bending moments at the end of the riser string. The upper end of the riser is a telescopic joint, or slick joint, that is comprised of two separate pipes that telescope into each other. This is in order to protect the riser from damage, and also to house the umbilici as they pass through the rotary table. The top end of the riser also includes a flex-joint and slip-joint, which takes axial displacement and rotation respectively [4].
Drilling risers are also commonly fitted with buoyancy modules on certain sections of the riser length. Due to hydrodynamic forces, the buoyancy modules are usually omitted near the surface to reduce the area, and with that the loads. They are also omitted towards the sea bottom, as the density of the modules must increase with the depth, thus increasing also the cost [27].
Top tension is applied to give an addition to the bending stiffness and carry the weight of the riser. The floater unit will naturally be subject to motions due to wave loads, so that a heave compensation system is necessary to provide constant tension, as is described in further detail in Section 2.2. The high frequency slamming loads are suspected to be an issue concerning the heave compensation system. It is necessary to estimate the loads which the system is subject to, to be able to improve the design. Slamming will subject the riser to large lateral loads, introducing bending moments. The result is metal-to-metal contact within the cylinders, producing wear lines [29].

2.2 Heave compensation system

It is necessary for all floating drilling units to include a heave compensation system in its drilling equipment to provide near constant tension on the drilling riser during heave motion of the vessel. It is usual for such a system to have a stroke capacity of around 15 m. The system consists mainly of the hydraulic cylinders, accumulators and air pressure vessels, see Figure 2.3. The cylinders, usually six in number, are attached to the riser through a tensioner ring using a shackle-and-eye connection, allowing rotation. This means that bending moments at the end of the cylinders are avoided. However, lateral forces on the riser may give rise to bending moments on the barrel and rod, such as those induced by slamming loads.
The working principle is that when the vessel heaves upwards, the cylinders extend to compensate for the additional length gained. Each cylinder is connected to a accumulator bank. During extension, oil will flow from the cylinder to the bank. In order to uphold a near constant tension, the accumulators are pressurized at a certain level with nitrogen. During the extension of a cylinder for example, the pressure will increase. For the opposite vessel movement, the cylinder will retract, reducing the pressure in the accumulator bank.

Figure 2.3: Heave compensation system

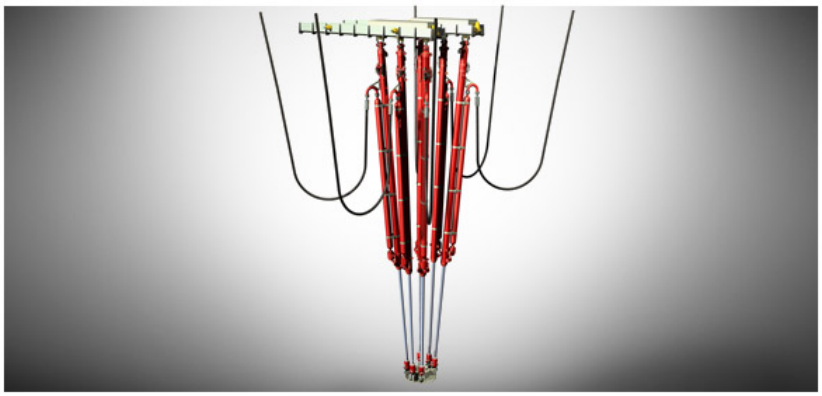

2.3 Riflex model

2.3.1 Drilling riser model

R. Sten has kindly provided the necessary files for the riser model. The model is built on the basis of information provided by Aker Solutions and the riser manufacturer Rexroth Bosch Group. The drilling riser is modeled in Riflex, and is complete with BOP, heave compensation system, upper flex joint located beneath the drill floor and buoyancy modules fitted to the riser at mid-depth. The model is visualized in Sima Riflex, as can be seen in Figure 2.4. The water

Figure 2.4: Marine riser layout

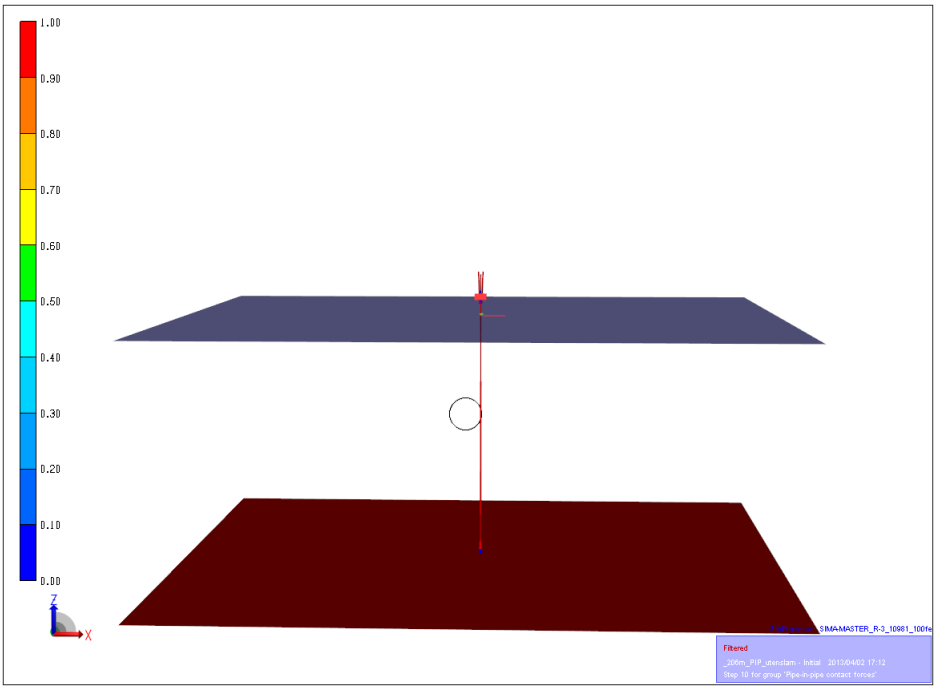

depth is 206 m, and with riser joints with lengths of 22.86 m, this requires 9 joints to run the entire length. On the sea bottom the riser is connected to the well with a BOP, seen at the lower end of the riser. At the top end, the riser is attached to the heave compensation system

on the vessel through the tensioner ring, which in turn is fastened to the six cylinders. The clearing between mean water level and the upper flex joint and tensioner ring is 9.9 m. The vessel motion is given by the RAO for the given semisubmersible. Some riser main data are provided in Tables 2.1 and 2.2

Table 2.1: Riser layout geometry, 206 m water depth

Type	**Description**	**Values**
Mariner riser	WT	22.225 mm
21" OD	OD	533.4 mm
	ID	488.95 mm
	Material	X-80 (552 MPa)
BOP	OD	5.5 m
	ID	476 mm
LMRP	OD	4.5 m
	ID	476 mm
Riser with	Max OD	1371.6 mm
buoyancy modules	Length	22.86 m
Tensioner joint/	Length	32.0 m
Telescopic joint	Maximum stroke	18.3
	OD (outer barrel)	660.4 mm
	WT (outer barrel)	25.4 mm
	OD (inner barrel)	527.3 mm
	WT (inner barrel)	19.1 mm
ROPS	OD	533.3 mm
	WT	22.225 mm
	Joint length	22.86 m

Some modifications on the model received from Sten were needed to accommodate for the slamming loads that are provided on a separate load file. Most importantly, the concentration of nodes from the mean water level up to the flexible joint were increased, as it is necessary to have a high resolution in this area due to the slamming loads. Line 8, located in the splash zone area, was split into two segments, where the segment on the surface side was provided with 250 nodes from elevation 0 m to 9.9 m, giving an element length of less than 0.04 m. This can be seen in Figure 2.5

Table 2.2: Riser stack-up, 206 m water depth

Description	Elevation [m]	Build-up length [m]
Drill floor/deck	40	
Tensioner hang-off	37.15	
Upper flex joint	35.5	1.3
Spacer joint	34.2	12.04
Slip-joint (60' telescopic joint)	22.2	11.79
Slip-joint (75' telescopic joint)	10.4	22.86
Tensioner ring	9.9	
Mean water level	0	
ROPS	-12.5	22.86
Riser joints/pup	35.3	20.22
Riser joints (buoyant)	-55.5	114.3
Riser joints	-169.8	22.86
Lower flex joint	-192.7	1.3
LMRP	-194	4.5
BOP	198.5	5.5
BOP lower end	-204	
Seabed	-206	

Figure 2.5: Riser nodes around mean water level

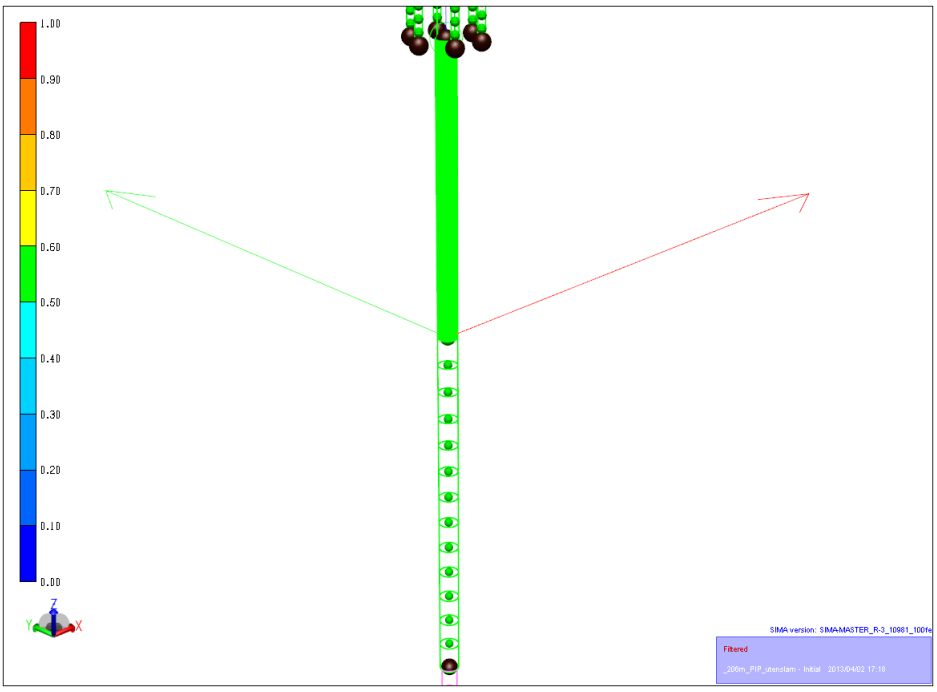

2.3.2 Vessel motion and transfer function

The top end of the drilling riser is connected to a floating structure, which in this case is a semi-submersible drilling rig of the type Aker H6e, currently the largest drilling semi type in the world. It operates with a draft of 23 meters, and is equipped with a dual drilling derrick, capable of undertaking two operations at once. The deck has the capacity of carrying three kilometers of marine risers, reducing its dependence on additional supply vessels [9].

Figure 2.6: Aker Barents

The transfer function relates the linear response of the vessel due to loading from a harmonic wave, and contains information of both amplitude and phase angle between load and response.

$$\eta_i(t) = \eta_{a,i} \sin(\omega t + \phi) \tag{2.1}$$

where X_a is the response amplitude and ϕ is the phase angle. Translation displacements along the x-,y- and z-axes are η_1, η_2 and η_3 respectively. Rotational displacements about the same axes are respectively η_4, η_5 and η_6. The velocity and acceleration are the first and second derivatives of the response respectively, and are simply given by:

$$\dot{\eta}_i = i\omega\eta_{a,i} \sin(\omega t + \phi) \tag{2.2}$$

$$\ddot{\eta}_i = -\omega^2\eta_{a,i} \sin(\omega t + \phi) \tag{2.3}$$

The motion of the support vessel in Riflex is described by the transfer function file, which gives the frequency dependent motion characteristic of the vessel in 6 degrees of freedom. The transfer function is plotted in Figure 2.7.

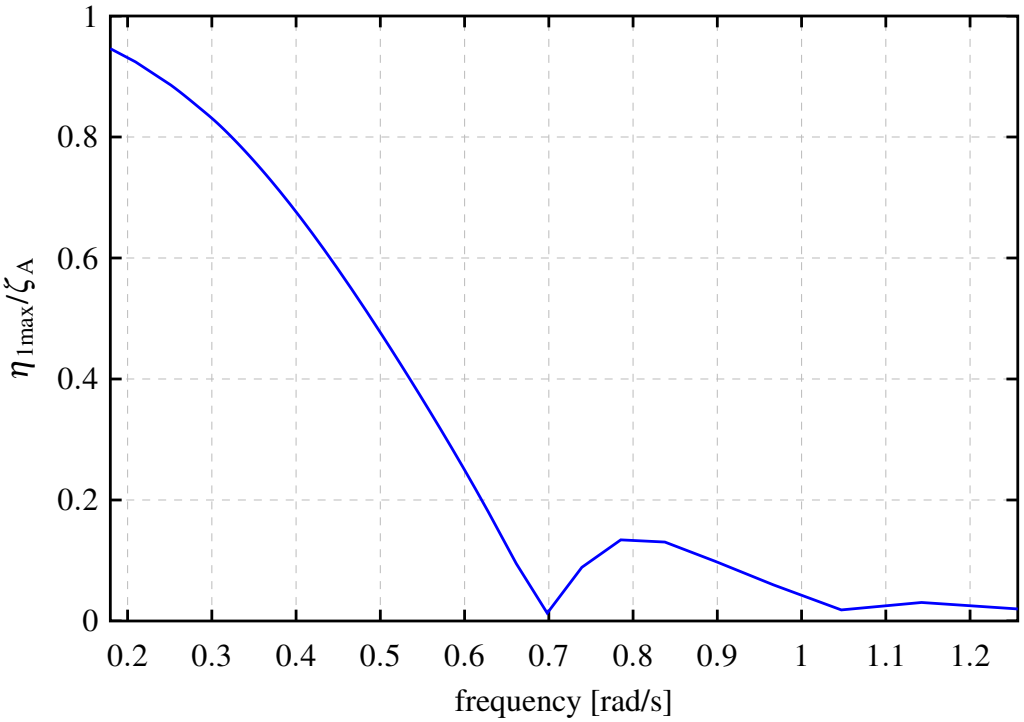

Figure 2.7: Support vessel transfer function

2.3.3 Pipe-in-pipe model in Riflex

The hydraulic cylinders of the tensioner system are modeled using a *pipe-in-pipe* approach in Riflex. The pipe-in-pipe model consists of a *master* and *slave pipe*, both with either beam or bar elements. The contact between the pipes is arranged by equipping all the FE nodes of the master pipe with contact components, while the slave pipe will experience contact with the master pipe through discrete element loads. The system consists of four different coordinate systems. Considering two cylinders, A being the master pipe and B the slave pipe:

- The global system with axes $\mathbf{X}_i$ and base vectors $\mathbf{I}_i$.
- The master element system located to the center of body A with axes y_i and base vectors $\mathbf{i}_i$.
- The slave element system located at body B with origin at node B1 with axes x_i and base vectors $\mathbf{j}_i$.
- The contact point system is located at point C on the circumference of body A. Local coordinate axes are s_i and base vectors $\mathbf{n}_i$, where the normal vector $\mathbf{n}_3$ is directed outward from the master body center.

This is illustrated in Figure 2.8. The position of the contact point C on the surface of cylinder body A with radius R_A and angular orientation γ is expressed as:

$$\mathbf{r}_{CA} = \mathbf{r}_A + R_A \sin\gamma\mathbf{i}_2 - R_A \cos\gamma\mathbf{i}_3 \tag{2.4}$$

Figure 2.8: Contact element coordinate systems

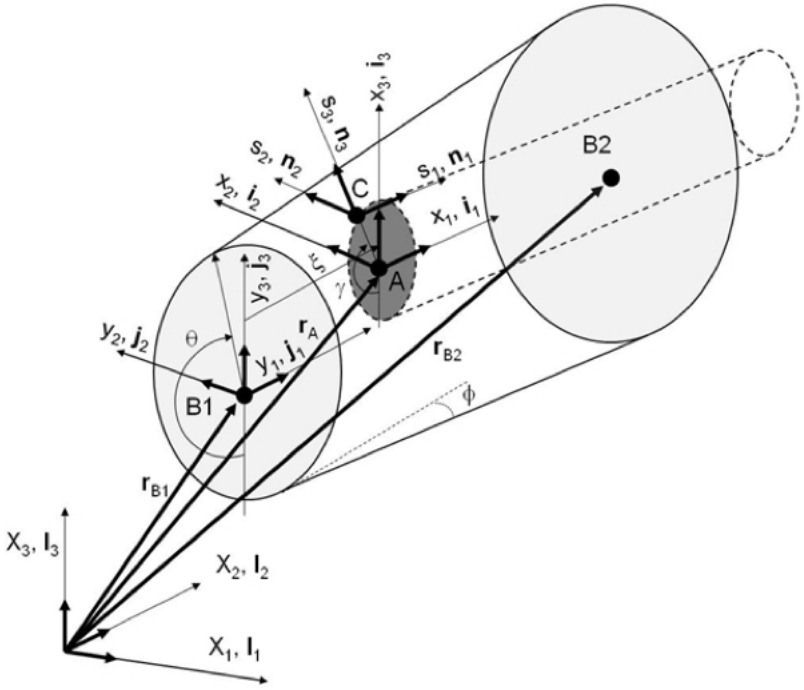

Likewise, point C may be expressed in terms of the slave body coordinate system:

$$\mathbf{r}_{CB} = \mathbf{r}_{B1} + [R_{B1}(1-\xi) + R_{B2}(\xi)][\sin\theta\mathbf{j}_2 - \cos\theta\mathbf{j}_3] \tag{2.5}$$

Where ξ is the dimensionless length coordinate along the slave element, $\mathbf{r}_{B1}$ and $\mathbf{r}_{B2}$ the radii at end 1 and 2 respectively at body B and θ is the angular rotation in the slave coordinate system. Contact occurs when:

$$g = (r_{CB} - r_{CA})\mathbf{n}_3 < 0 \tag{2.6}$$

Where g is the gap between the points in the different coordinate systems. If contact is obtained, there is also an incremental slippage between the points of the two bodies:

$$\Delta\eta_1 = (\Delta\mathbf{r}_{CB} - \Delta\mathbf{r}_{CA})\mathbf{n}_1 \tag{2.7}$$

$$\Delta\eta_2 = (\Delta\mathbf{r}_{CB} - \Delta\mathbf{r}_{CA})\mathbf{n}_2 \tag{2.8}$$

Further, the reaction force when contact is obtained is modeled with the application of a stiffness in the $\mathbf{n}_3$ direction with the parameter k, either taken as a constant or variable, dependent on whether elastic or hyper-elastic material law is used [28] [26].

The model in Sima is shown in Figures 2.9 and 2.10. Each hydraulic cylinder is composed of two lines, the cylinder rod and cylinder housing, each in turn are divided into two segments. The first rod on the segment is the rod itself, the second is the rod head. The pack-box at the bottom of the cylinder housing is described by one segment, the cylinder housing by the other.

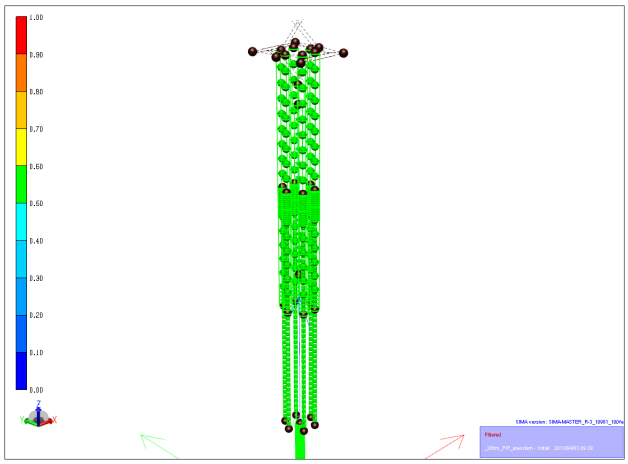

Figure 2.9: Total wave load on cylinder

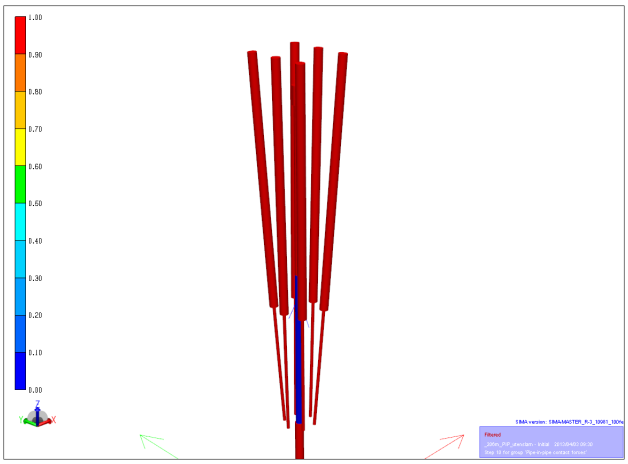

Figure 2.10: Wave load on each strip

Chapter 3

Higher order loads from steep waves

3.1 Overview

Slamming loads occur when a body impacts with water, and have high pressure peaks and short duration. A typical scenario in which slamming might be an issue is when the fore part of a ship bottom has exited the sea due to extreme weather conditions, resulting in an impact when it re-enters the water. Another concern is if extreme waves are permitted to impact against the underside of a platform. There are therefore requirements towards the minimum air gap between the platform deck and a 100 year design wave. Steep and/or breaking waves against platform columns have also proven to induce high pressure slamming loads, and is very closely related to the problem this thesis intends to discuss. For the large diameter of a platform column, the local pressure loads are of concern. For a typical drilling riser, with a diameter of only half a meter, it is the response of the entire structure that is the issue. Figure 3.1 shows a descriptive example of how a steep wave may impact against offshore structure members, and is also illustrative for the case of slamming loads on risers.

Figure 3.1: Wave run-up against platform columns

Slamming loads are of concern in the offshore industry due to the high pressure peaks and local forces induced, and in many cases it is important to completely avoid the occurrence

of slamming, for instance slamming against platform decks and undersides, green water on deck of ships and so on. In other cases, slamming cannot be avoided, for example against the columns of a platform or against caissons, riser and so on. Some cases and methods of estimating slamming loads are described in this section.

3.1.1 Methods for estimating slamming loads

Various methods have been implemented in the estimation of slamming loads on a whole range of marine structures. They can mainly be categorized into analytic, experimental and numerical methods, and are often used in conjunction with each other.

Analytical formulations for the slamming and water entry problem are presented by Wagner and von Karman [21], and are discussed in more detail in Sections 3.3.1 and 3.3.2. The theory they present has been implemented in an impact simulation tool developed by the *Institute for Fluid Dynamics and Ship Theory* at the *Hamburg University of Technology*. In addition, it contains some corrections for viscous effects, buoyancy, time-varying velocity, cavitation etc. [19]. They give the pressure as:

$$p(y) = k\rho \frac{Dv}{Dt}\sqrt{c^2 - y^2} + k\rho max(v,0)\frac{Dc^2}{Dt}\frac{1}{\sqrt{c^2 - y^2}} + \rho g\zeta \tag{3.1}$$

Lange and Rung [19] investigated the effects aeration of water has on impact loads and pressure upon forced water entry for a cylinder. Using model tests they were able estimate the coefficient k in Equation 3.1 with the results they obtained.

Nestegård [8] has also implemented the method presented by von Karman based on momentum theory in a numerical program named WAVESLAM. The program is capable of estimating the slamming load as an incident wave impacts against a circular pile, as well as including the loads from the Morison formulation. The results obtained from a regular incident wave with $T = 12s$ and $H = 12m$ are shown in Figures 3.2 and 3.3. The slamming load peaks occur simultaneously

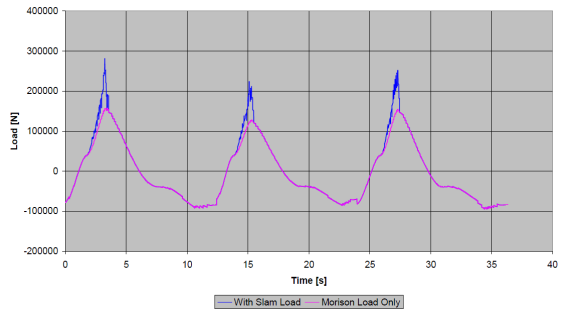

Figure 3.2: Total wave load on cylinder

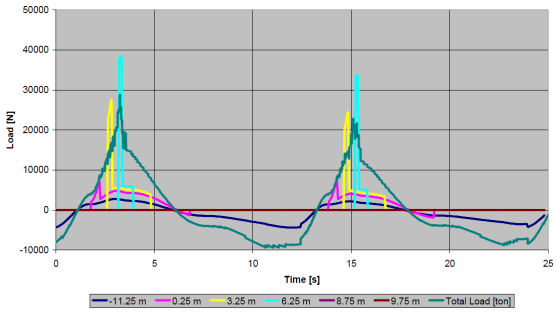

Figure 3.3: Wave load on each strip

with the maximum Morison load, leading to a high total load on the riser. The slamming load on the individual strips increase for strips at a higher location, meaning that the velocity with which the wave impacts also increases towards the wave crest.

Computational fluid dynamics, CFD, is a numerical method for solving partial differential

equations describing flow. The solution provides information about velocity and pressure distribution. The governing equations are Navier-Stokes, or Euler equations. The principle of CFD is the solution of these equations over a discretized mesh, and the solution is highly dependent on the quality of the mesh [24] There is a wide range of available CFD software, both commercial, open-source and in-house in the various research institutions involved in CFD problems. Commonly used programs for hydrodynamic use are for example STAR-CCM+ and OpenFOAM®.

Marintek uses a combination of model tests and computational fluid dynamics (CFD) in its research, and state that the two methods complement each other nicely. CFD provides a good way of describing in detail flow and pressure fields, while model tests are useful for the validation of the results obtained from CFD methods.

The *Wave Impact Load Joint Industry Project (JIP)* at Marintek is looking at various problems relevant for the offshore industry. One of the problems subjected to study was wave impact on the deck of an offshore platform. The problem was formulated with both simplified potential theory and with a CFD code (STAR-CCM+) and compared against model tests. The vertical and horizontal loading on the deck was estimated. However, it was found during model tests that subsequent impacting waves were effected by the diffraction of the previous wave, and so underestimating the load and showing the importance of validating results with experimental data [23].

Another problem undertaken by the JIP is the breaking wave impact on a platform column. Model tests where performed and CFD used to reproduce the tests. One of the challenges was to correctly model the motion history and velocity of the breaking wave. The model tests and results from the CFD analysis were found to coincide well [14].

A similar problem to which this thesis wishes to discuss, is the slamming loads on a offshore wind turbine by breaking waves. Jacobsen and Bredmose [16] approach the problem from a computational point of view, utilizing OpenFOAM® for the CFD analysis. Using second-order waves for the problem, the impacting wave was modelled by focusing the components of a discretized spectrum on the position of the pile of the wind turbine, creating a steep transient wave. As the impacting wave breaks on the cylinder, the impact will result in vertical velocity of the fluid, slamming against the underside of the platform. Both vertical forces on the platform and in-line forces on the cylinder itself are calculated for varying vertical locations of the platform, see Figure 3.4. The in-line forces seem to coincide well with the shape of the traditional Morison formulation, with an additional peak forming as the breaking wave impacts against the column.

Experiments and model tests are in addition to being a good way of studying slamming loads in itself, also a invaluable tool in validating results from CFD analysis. The CFD analysis done by Pakozdi, Kendon and Stansberg [14] were supplemented with model tests that could validate their results. Pressure sensors are mounted to the platform column and on the underside of the deck. The wavemaker was calibrated so that the wave generated in the model test was similar to

Figure 3.4: Impacting wave on offshore wind turbine. Resulting forces and moment at platform level of 6.04m

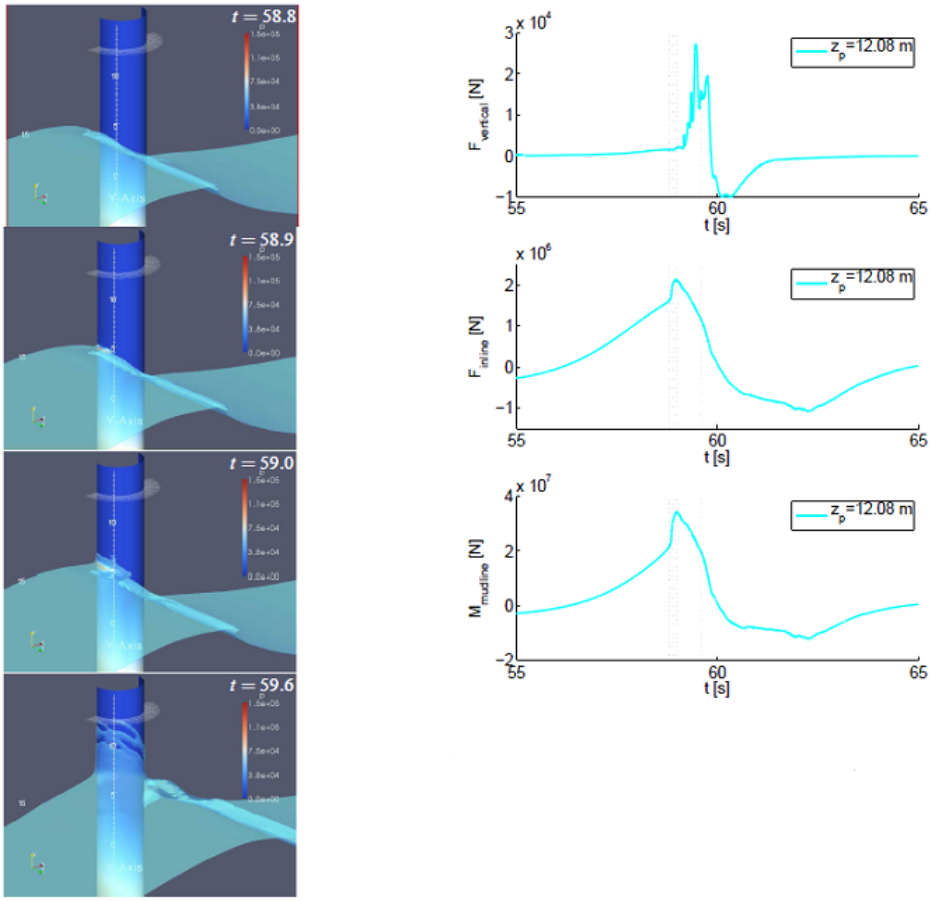

that modeled with numerical tools. The force of a breaking wave impacting against the model was measured, the results found in Figure 3.5

Figure 3.5: Slamming force measured by pressure sensors

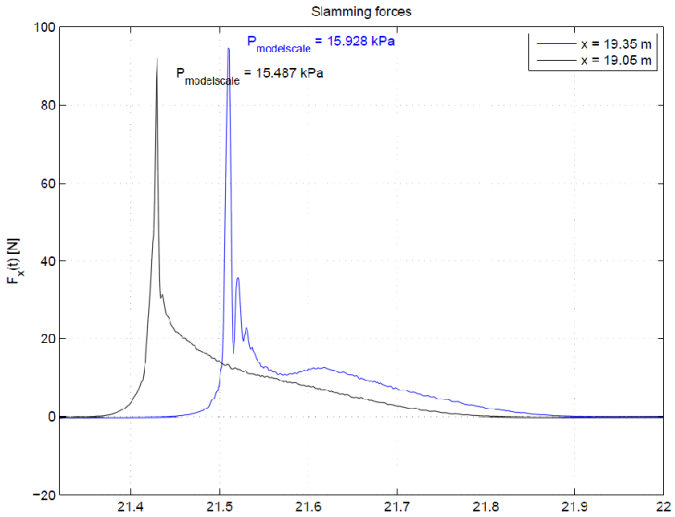

3.2 Modeling of sea waves

3.2.1 Linear wave theory

Ignoring the effects of diffraction from surrounding platform columns for simplicity, an incident regular wave on a marine riser can be described by linear potential theory. The wave elevation is given by:

$$\zeta(t) = \zeta_a sin(\omega t - kx) \tag{3.2}$$

$\zeta(t)$	wave elevation
ζ_a	wave amplitude
k	wave number
ω	wave angular frequency

As Section 3.3 describes, slamming loads are induced by a rapid rate of change of fluid momentum, and thus are more important with the presence of steep waves with high velocity. Linear wave theory has its limitations with regard to wave steepness, as the theory is based upon the condition that the horizontal velocity component u is small, i.e. that $k\zeta_a$ is small [25]. Because $k\zeta_a$ expresses the slope of the wave, this implies that the steepness of the wave is small. Figure 3.6 shows the range of application of increasingly higher order wave theories. Generally, in comparison with Stokes third-order waves, it can be said that the use of first-order regular waves is valid for a ratio up to $\frac{H}{\lambda} = \frac{1}{20}$ [10]. This means that for a wave with a period of $10s$ propagating in deep water, this corresponds to height of $7.8m$. With Stokes third-order waves it is possible to describe steepness ratios of up to $\frac{H}{\lambda} \approx \frac{1}{7}$, known as the *breaking limit* or *breaking criterion* as can be seen in Figure 3.6.

Riflex uses linear wave theory in the generation of irregular sea [1], so that this thesis will also

Figure 3.6: Ranges of validity for various wave theories

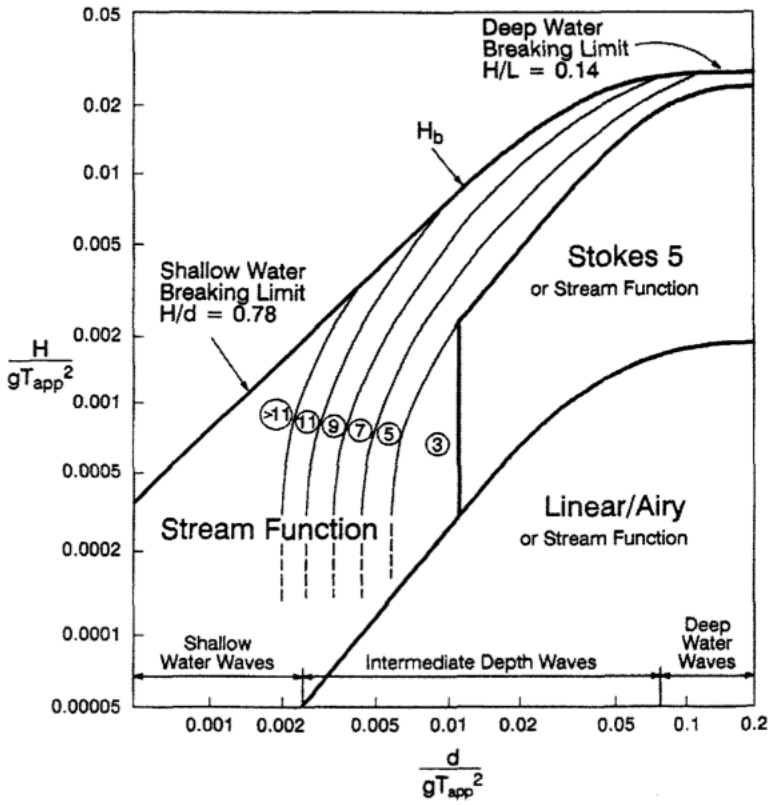

limit itself to the use of first-order waves. For practical use, its range of applicability is deemed sufficient enough for the present case.

A sea surface is notably not a single propagating sinusoidal wave, but can more realistically be described by a sum of waves with various frequencies, amplitudes and periods. Considering long-crested 2-D waves, this may written:

$$\zeta(x,t) = \sum_{j=1}^{N} \zeta_{aj} sin(\omega_j t - k_j x + \varepsilon_j) \tag{3.3}$$

- ζ_{aj} amplitude of wave component
- ω_j frequency component
- k_j component wave number
- ε_j phase difference

ε_j is a stochastic variable that is statistically independent and uniformly distributed between 0 and 2π. By relating the energy of a wave component with the amplitude, it is possible to introduce the spectrum for a irregular sea state. The total energy of an irregular sea state can be described by:

$$\frac{E}{\rho g} = \sum_{n=1}^{N} \frac{1}{2} \zeta_{An}^2 \tag{3.4}$$

E	energy per unit area
N	number of wave components
ζ_{an}	amplitude of component n

Now introducing the spectrum:

$$\frac{1}{2}\zeta_{An}^2 = S(\omega_n)\Delta\omega \tag{3.5}$$

$S(\omega)$	spectrum
$\Delta\omega$	frequency interval

Using Equations 3.4 and 3.5 and inserting into Equation 3.3, a wave elevation of an irregular sea state at a given position may be expressed by [7]:

$$\zeta(t) = \sum_{n=1}^{N} \sqrt{2S(\omega_n)\Delta\omega}\cos(\omega_n t + \varepsilon_n) \tag{3.6}$$

The principle is illustrated in Figure 3.7. A certain energy spectrum will represent the energy

Figure 3.7: Illustration of simulation of irregular waves from a wave spectrum

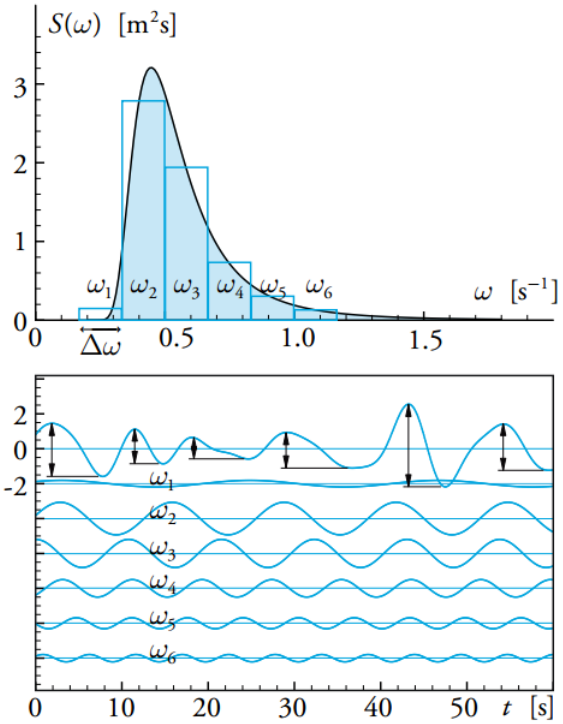

distribution of the wave elevation during a certain time interval at a specific location. This means that a spectrum at a certain site offshore may not be identical if they are measured during say three hour intervals 24 hours apart. For design purposes, it is common to make use

of standardized spectra, given by a set of parameters such as significant wave height and peak period.

3.2.2 Wave kinematics

As will be shown later in Section 3.3, the horizontal particle velocity of the wave is an important parameter in calculating the slamming load. It is therefore necessary to give detailed information about the velocity profile belonging to the entire wave front. The general expression for the horizontal fluid particle velocity for a regular first-order wave in deep water is given by [21]:

$$u = \omega \zeta_a e^{kz} \cos(\omega t - kx) \tag{3.7}$$

u horizontal water particle velocity

The horizontal water particle velocity is, as can be seen by Equation 3.7 in phase with the wave elevation, meaning that the maximum positiv velocity occurs at the wave crest, zero velocity at the mean water line and maximum negative velocity at the trough.
For the simulation of a irregular wave elevation, the horizontal water particle velocities are found in the same fashion of superpositioning the velocities of the wave components [21]:

$$u = \sum_{j=1}^{N} \omega_j \zeta_j e^{k_j z} \cos(\omega_j t - k_j x + \varepsilon_j) \tag{3.8}$$

The random phase angle ε is identical for ζ and u. It should be noted that linear wave theory assumes a constant fluid velocity from the mean water level to the free-surface elevation [21] as illustrated in Figure 3.8. For describing the kinematics more accuratly in the wave profile, it is possible to modify the depth-decay function by attaching it to the free-surface elevation, rather than the mean water level. This is done with a stretching method, which will be discussed in further detail in section 6.3.

A brief presentation of the kinematic model suggested by Nestegård [8] will be made here. The previous work by both Nestegård and Sten are based on this model, and so it seems appropriate for comparative reasons to discuss it in some detail. The model is intended to function as an approximation to the kinematics of waves that are close to breaking. The vertical variation is exponentially distributed, using the Wheeler stretching method from the crest and down. Horizontally, there is a sinusoidal variation so that the maximum velocity occurs beneath the crest and zero at the mean water level. The magnitude is approximated by using the phase velocity of the wave, and multiplying it with a factor, so that: $U_m = \alpha c$. α is dependent on wave steepness, varying from 1 for a breaking wave, to $k\zeta_A$ for a linear wave, resulting in Equation 3.7. [8] opts to use $\alpha = 0.3$ for all cases. Wave height and period are H=12 m and T=12 s for the

Figure 3.8: Horizontal velocity distribution under a wave crest and trough according to linear theory

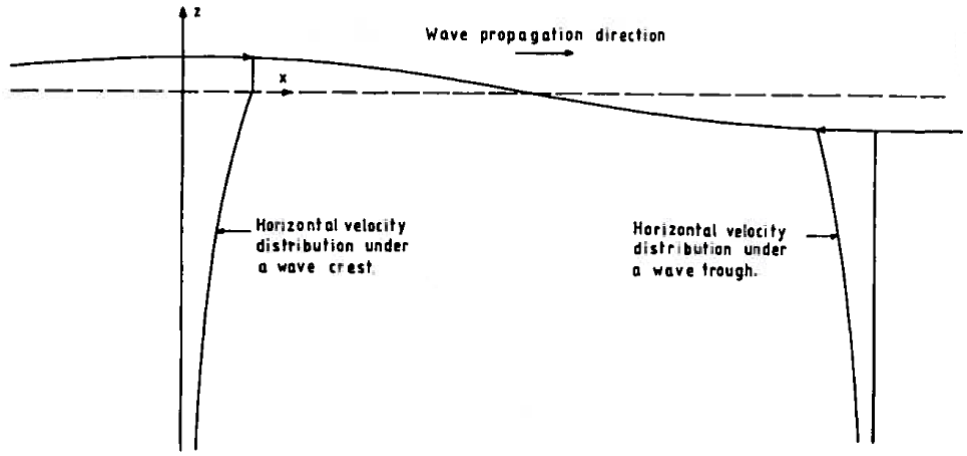

regular wave simulation and Hs=14.7 m and Tp=15.5 s for the irregular wave simulation, both of which are outside the area of application for linear theory. For T=12 s, this gives a phase velocity of 18.73 m/s. Using the approximation yields a particle velocity of 5.62 m/s, while linear theory estimates 3.14 m/s. In the simulation, the phase velocity was determined by measuring the wave elevation and time between two consecutive wave troughs.

3.2.3 Higher order wave theories

As explained in Section 3.2.1, linear wave theory has its limitations in the description of steep waves. Several higher order wave theories are more appropriate in describing steep waves as they have a higher *breaking limit* as shown in Figure 3.6. These wave theories include:

- Second-order Stokes Wave Theory
- Fifth-order Stokes Wave Theory
- Stream Function Theory

Stoke's second-order wave theory is a non-linear theory that introduces a second component of twice the wave frequency, but with a smaller amplitude, and therefore with a smaller contribution. The expression for a second-order Stokes wave profile in deep water is given by:

$$\zeta(t) = \frac{H}{2}\cos(kx-\omega t) + \frac{\pi H}{8\lambda}\frac{\cosh kd}{\sinh^3 kd}[2+\cosh 2kd]\cos 2(kx-\omega t) \tag{3.9}$$

The profile is shown in Figure 3.9, together with a first order wave profile. It clearly shows a higher peak and more shallow trough, making it more recognizable with waves seen at sea. The wave particle kinematics of second-order Stokes also include a second, higher order component

H	wave height, crest to trough
λ	wave length
d	water depth

as does the wave profile. It can be shown however, that for deep water the contribution from this second component can be neglected.
Fifth-order Stokes waves are comprised of five components, with the frequencies of the higher order components multiples of the first frequency. As the higher order components decay more rapidly with depth then the first, their effects are only most notable near the surface. For many submerged offshore structures, linear theory is sufficiently accurate for design purposes. The wave profile of a fifth-order Stokes wave is shown in Figure 3.10 together with a linear wave profile.
Stream function theory is an additional non-linear theory in which the wave is described by its stream function rather with potential theory. There are two types, *regular* and *irregular*. The first is appropriate for describing waves that are symmetric front-to-back, but that are asymmetric trough-to-crest. The parameters are wave height, period and water depth as in potential theory. The irregular stream function theory is suitable in a situation in which the wave profile is known, such as for a design wave.
The regular stream function theory describes a wave by:

$$\psi(x,y) = (c-U)y + \sum_{n=1}^{N} X(n)\sinh nky\cos nkx \tag{3.10}$$

N	order of the theory used
U	current velocity
c, X_n	unknown quantities

The appropriate order to apply can by found by consulting Figure 3.6. Stream function theory has is this way a broad range of application, from small waves to large, steep waves, which can be seen in Figure 3.11 [3].

Figure 3.9: Second-order Stokes wave profile

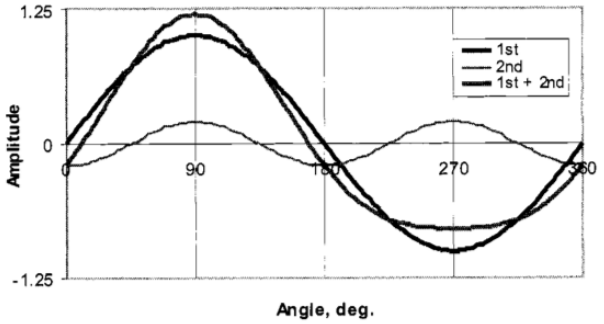

Figure 3.10: Fifth-order Stokes wave profile

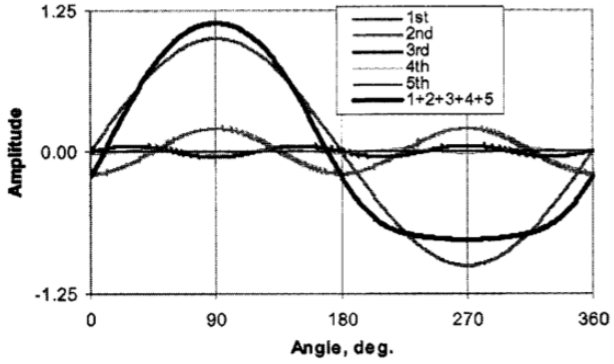

Figure 3.11: Seventh-order stream function theory wave

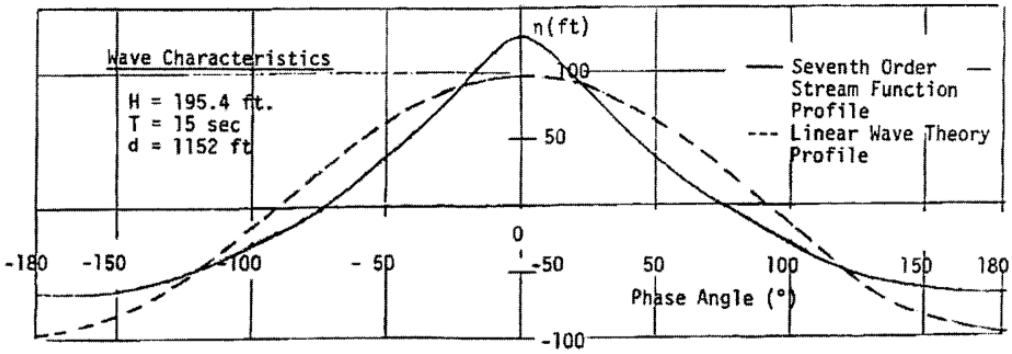

3.3 Theoretical background

3.3.1 Direct pressure integration

The main parameters of interest when describing a slamming load is the pressure on the wetted surface. In order to calculate the pressure it is necessary to also have an accurate description of the wetted surface as it enters the water surface. For simplicity, constant velocity is assumed during submergence, meaning that the added mass pressure resulting from rate of change of velocity $\frac{dV}{dt}$ is zero [15]. The problem is illustrated below, in Figure 3.12

Figure 3.12: Description of impact problem of a circular cylinder

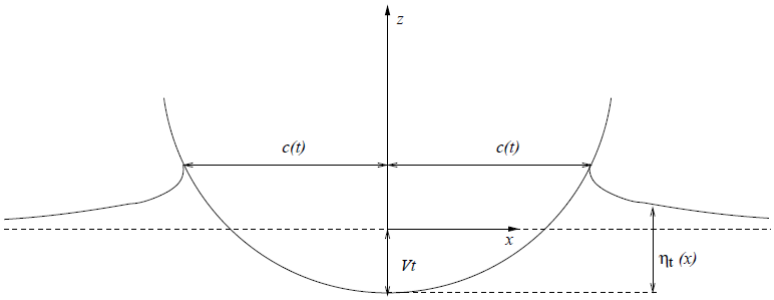

In order to solve the problem, the fluid is assumed to be irrotional, inviscid and incompressible, enabling potential flow theory. The boundary conditions of the problem are transferred to a flat plate, see Figure 3.13.

Figure 3.13: Boundary value problem

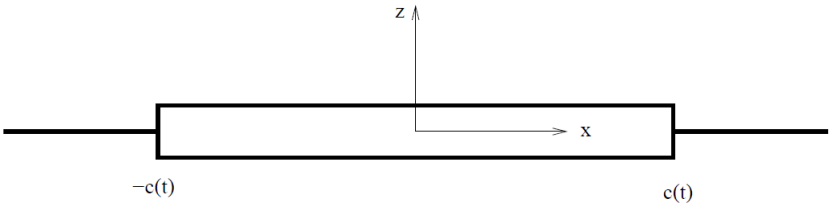

Along with potential flow theory, several other assumptions must be made [22]. The angle β between the body and the surface is required to be small. This means that the body boundary condition may be written:

$$\frac{\partial \phi}{\partial n} = n_1 \frac{\partial \phi}{\partial x} + n_3 \frac{\partial \phi}{\partial z} \tag{3.11}$$

Because of the small angle β, $n_1 << n_3$ and the body boundary condition becomes:

$$\frac{\partial \phi}{\partial n} = n_3 \frac{\partial \phi}{\partial z} \approx -V n_3 \tag{3.12}$$

so that

$$\frac{\partial \phi}{\partial z} = -V \text{ on } z = 0 \text{ for } -c(t) < x < c(t) \tag{3.13}$$

ϕ potential function
n_i normal vectors
V vertical velocity of body
$c(t)$ length of submerged section at time t

A second assumption is that the fluid accelerations are much smaller than g. The free surface condition:

$$\frac{\partial^2\phi}{\partial^2 t} + g\frac{\partial\phi}{\partial z} = 0 \tag{3.14}$$

is reduced to:

$$\frac{\partial^2\phi}{\partial^2 t} \Rightarrow \phi = 0 \text{ on } z = 0 \text{ for } |x| > c(t) \tag{3.15}$$

Assuming that spacial derivatives are small compared to the time derivatives, and that the submergence of the body is small, the pressure on the body can be found by the Bernoulli equation. With a constant downwards velocity, the expression for the pressure is now reduced to:

$$p = -\rho\frac{\partial\phi}{\partial t} = \rho V\frac{c}{\sqrt{c^2 - x^2}}\frac{dc}{dt} \tag{3.16}$$

Integrating the pressure over the wetted surface to find the vertical force on the body:

$$F_3 = \int_{-c}^{c} p\,dx = V\frac{d}{dt}\left(\rho\frac{\pi}{2}c^2\right) \tag{3.17}$$

F_3 vertical force on body
p pressure
ρ density of sea water

It remains to find an expression for the wetted surface on a cylinder body. There are two different methods for calculating the wetted surface, the *von Karman* method and the *Wagner* method.
Von Karman does not take the water rise-up during impact into consideration, so that the wetted surface may be taken as the distance to the vertical point on the structure that intersects the water surface at $z = 0$. Using this, $c(t)$ is by geometric considerations found to be [15]:

$$c(t) = \sqrt{2VtR - V^2t^2} \tag{3.18}$$

R radius of cylinder

The Wagner method takes consideration to the water-rise up. It can be shown how the expression for the wetted surface $c(t)$ is achieved by finding the distance to the vertical point of the cylinder which intersects with the free surface elevation [21]:

$$c(t) = 2\sqrt{VtR} \tag{3.19}$$

3.3.2 Conservation of fluid momentum

Water entry of a horizontal circular cylinder during the first time stages of impact is also possible to describe using conservation of mass momentum.

$$\frac{d\mathbf{M}}{dt} = -\rho \iint_s \left[\left(\frac{p}{\rho} + gz \right) \mathbf{n} + \mathbf{V}(V_n - U_n) \right] ds \tag{3.20}$$

$\mathbf{M}$	momentum of fluid inside body
g	gravity constant
s	surface
$\mathbf{V}$	velocity vector
V_n	vertical velocity
U_n	horizontal velocity

where $\mathbf{M}$ may be written as:

$$\mathbf{M}(t) = \iint_s \rho \phi \mathbf{n} ds \tag{3.21}$$

Requiring that the velocity potential satisfies the body boundary conditions:

$$\frac{\partial \phi}{\partial n} = -V n_3 \tag{3.22}$$

and free surface conditions:

$$\phi = 0 \text{ for } z = 0 \tag{3.23}$$

The vertical force on the body as it pierces the surface with velocity V becomes:

$$F_3 = \frac{d}{dt}(A_{33} V) \tag{3.24}$$

F_3	vertical force on body
A_{33}	added mass in heave
ρ	density of sea water

when neglecting buoyancy and with calm water with no incident waves. Von Karman simplified the problem of the circular cylinder by instead assuming a flat plate, with the added mass value as $\omega \to \infty$ being $A_{33} = \rho \frac{\pi}{2} c^2$. Inserting this into Equation 3.24, the same result as in Equation 3.17 is obtained in the case of constant velocity.
Introducing the slamming coefficient C_s for the circular cylinder:

$$C_s(t) = \frac{F_3(t)}{\frac{1}{2}\rho V^2 2R} \tag{3.25}$$

C_s slamming coefficient
D cylinder diameter

So that we can write the vertical slamming force on the body as a function of C_s:

$$F_3(t) = \frac{1}{2}\rho C_s D V^2 \tag{3.26}$$

Experiments conducted by Campbell & Weynberg for a smooth circular cylinder experiencing water entry at constant vertical velocity are discussed in more detail in [17]. The results are shown in Figure 3.14. The slamming coefficient is plotted as a function of submergence $\frac{h}{R}$, together with the analytic formula given by von Karman.

Figure 3.14: Water entry of circular cylinder

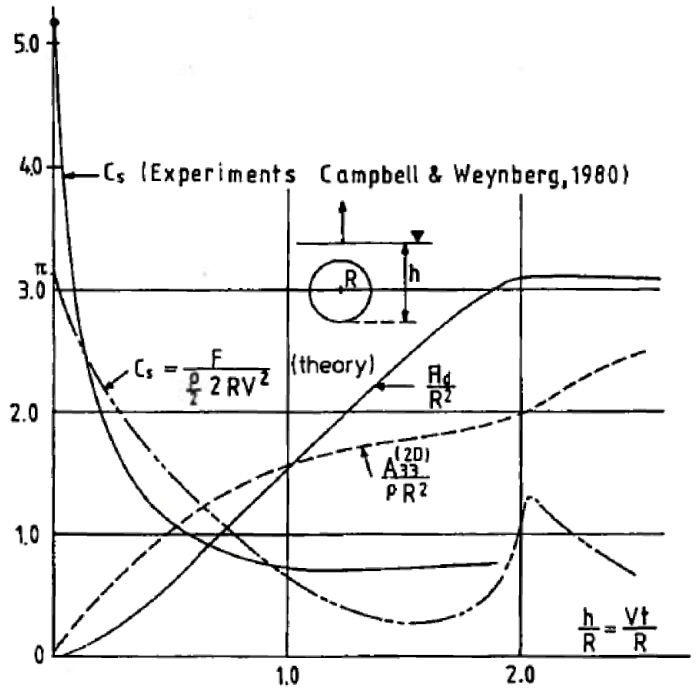

An analytic fit to the experimental data has been provided by Campbell & Weynberg [8], given by:

$$C_s = 5.15\left[\frac{D}{D+19h} + \frac{0.107h}{D}\right] \tag{3.27}$$

h submergence of cylinder

For the experimental results, the figure reports a significantly higher starting value for C_s than for von Karmans analytical result. Table 3.1 displays the initial slamming coefficients for the von Karman and Wagner methods and experimental results by Campbell & Weynberg.

Table 3.1: Initial slamming coefficients

	von Karman	Exp. Campbell & Weynberg	Wagner
C_s	π	5.15	2π

Wagner yields an initial value twice as large as that of von Karman. It is natural that von Karman under-predicts the coefficient, as he does not consider that water rise-up. Comparing with the experimental results, Wagner seems in turn to over-predict the initial value of the coefficient. It can be said that the two methods give lower and upper limits, respectively. It is apparent that the force seems to be highly dependent on the formulation of the wetted surface $c(t)$. Looking at the differences for the coefficient value displayed in Figure 3.14 for larger submergence, they can no longer be explained by the effect of water rise-up. The empirical formula 3.27 also considers buoyancy during submergence, while von Karman does not. It is clear that buoyancy will have an increasing importance with larger $\frac{h}{R}$.
The previously introduced methods are easily applicable in the estimation of slamming loads as a function of time as a horizontal cylinder pierces the water surface. As mentioned previously, fluid accelerations are much larger than g. This means that gravity does not enter into the problem, and thus it is also possible to apply the method for a breaking, near vertical wave impacting with a vertical circular cylinder, so that the situation can be modeled in a simple way as shown in Figure 3.15.

Figure 3.15: Wave slamming on vertical cylinder

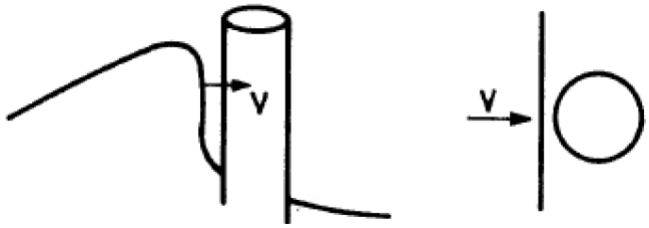

3.3.3 Slamming loads from steep incoming waves

The slamming model used in this thesis is based upon the model suggested by Nestegård in his paper on the topic of slamming loads on riser guide tubes [8]. In conversation [20] in the later stages of the thesis work, Nestegård stated that this model is not intended for waves applicable to linear theory. In this respect the thesis must be considered as an attempt to investigate the relevance of including slamming in a linear load model. Linear, irregular waves are hereby assumed to be able to induce slamming loads as they propagate past the riser. For a single strip with sufficiently small incremental length, the submergence may be considered in the same way as illustrated in Figure 3.15. The slam load occurs in the interval in between the strip impacts with the wave front and it is fully submerged [8], as shown in Figure 3.16.

Figure 3.16: Slam load zone

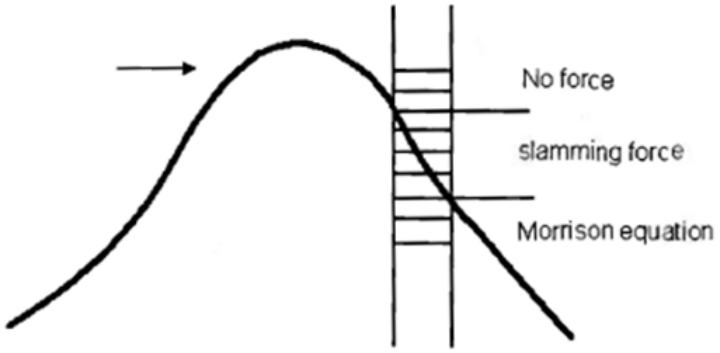

Slamming is in this case due to water entry of the circular strip or section of the cylinder, and is dependent on the relative motion between the structure and the fluid. The following expressions are based upon the vertical water entry of a circular cylinder, but are applicable for slamming due to incoming waves on a vertical riser, due to gravity not being a parameter.
The main differences in the problem of an incoming wave with a slope is that:

- The horizontal water particle velocity will vary along the height of the pile.
- The submergence of the pile will vary along the length, meaning that the slamming load will not occur instantaneously over the length, but rather be induced in a subsequent manner as each strip is submerged in turn.

Nestegård [8] proposes that this can be managed by representing the slamming loads by summing up the forces acting on strips on the slender drilling riser, in a similar fashion to strip theory. The load is governed by the change of added mass momentum, as covered in Section 3.3.2. The force on each strip is given by:

$$dF_x = \frac{d}{dt}[A^{2D}(t;z)u] = \frac{d}{ds}[A^{2D}(s;z)]u^2 = \frac{1}{2}\rho C_s D u^2 \tag{3.28}$$

dF_x	horizontal force on each strip
A^{2D}	strip high-frequency added mass
u	relative horizontal velocity

3.3.4 Morisons equation

Wave loads on cylindrical structures are usually calculated using Morison's Equation [21]. These loads will hereby be referred to as conventional wave loads. Slamming loads are in this thesis included in the load model on the basis that the waves are especially steep, and only

during submergence. The horizontal drag and mass forces on a strip of a moving cylinder due to waves are formulated by Morison's equation:

$$dF_x = \frac{1}{2}\rho C_D D dz(u - \dot{\eta}_1)|u - \dot{\eta}_1| \tag{3.29}$$

$$+ \rho CM \frac{\pi D^2}{4} dz a_1 - \rho(C_M - 1)\frac{\pi D^2}{4} dz \ddot{\eta}_1 \tag{3.30}$$

dF_x	horizontal force on each strip
a_1	horizontal water particle acceleration
u	horizontal water particle velocity
$\dot{\eta}_1$	surge velocity of cylinder
$\ddot{\eta}_1$	surge acceleration of cylinder
C_M	mass coefficient
C_D	drag coefficient

The mass and drag coefficients must be determined numerically or empirically. Potential flow theory gives a mass coefficient value of $C_M = 2.0$ for a circular cylinder, where the contributions are equally divided between Froude-Kriloff and diffraction forces. The drag coefficient depends on amongst several factors the smoothness of the cylinder. For a smooth cylinder it has been shown that $C_D = 0.7$ [21]. Assuming that the drilling riser is not entirely smooth, some modification should be done. DNV's recommended practice C205 [13] gives some approximate values for C_D, depending on the roughness ratio. Based on this estimate, the drag coefficient is set to $C_D = 1.0$.

The drag and mass forces have a phase difference of 90°. The drag force reaches its absolute maximum when there is a wave trough or crest at the cylinder axis. The mass force will have a maximum in absolute value when there is a wave node in the position of the cylinder axis.

Chapter 4

Pulse excitations

In the case of slamming loads, the load is of short duration, usually well below the natural period of the total riser system. Further, the load is neither periodic nor harmonic, and so it is of interest to investigate the dynamic response of the system due to such a load, or *pulse*.

4.1 Duhamel's integral

It is desirable to find a way to evaluate a load varying arbitrarily with time, such as pulse loads. The response of the system may be described by the equation of motion:

$$m\ddot{u} + c\dot{u} + ku = p(t) \tag{4.1}$$

with initial conditions:

$$u(0) = 0 \quad \dot{u}(0) = 0 \tag{4.2}$$

m	mass of the system
c	damping of the system
k	stiffness of the system
p(t)	arbitrary load
u	displacement
$\dot{u}$	velocity

Considering a unit impulse with duration ε, *p(t)*. As $\varepsilon \to 0$, *(p(t)* approaches infinite. The magnitude of the impulse, defined by the time integral of *p(t)*, will however remain equal to unity. Newton's second law gives:

$$p = m\ddot{u} \tag{4.3}$$

Integrating both sides with respect to time, t yields:

$$\int_{t_1}^{t_2} p\,dt = m(\dot{u}_2 - \dot{u}_1) \tag{4.4}$$

For a unit impulse with infinite short duration, it is possible to neglect the spring and damping of a system because they do not have time to respond. At the end of the impulse duration, τ, the velocity is:

$$\dot{u}(\tau) = \frac{1}{m} \tag{4.5}$$

However, as the time duration is considered small, the displacement may be taken as zero:

$$u(\tau) = 0 \tag{4.6}$$

Taking Equations 4.5 and 4.6 as initial conditions for an undamped system with free vibrations induced by the unit pulse, the solution may be written:

$$h(t-\tau) \equiv u(t) = \frac{1}{m\omega_n} \sin\left[\omega_n(t-\tau)\right] \quad t \geq \tau \tag{4.7}$$

ω_n natural frequency of system
τ time instant of pulse

A sequence of such infinitesimally pulses can represent an arbitrary load. The response to one such load may be expressed as:

$$du(t) = [p(\tau)d\tau]h(t-\tau) \quad t > \tau \tag{4.8}$$

The sum of the responses from each impulse up to time t is the total response of the system, known as the *convolution integral*:

$$u(t) = \int_0^t p(\tau)h(t-\tau)d\tau \tag{4.9}$$

Substituting for the unit response function gives [6]:

$$u(t) = \frac{1}{m\omega_n} \int_0^t p(\tau) \sin\left[\omega_n(t-\tau)\right] d\tau \tag{4.10}$$

4.2 Dynamic response to pulse excitations

Evaluating the response of a system to a pulse force is done by dividing the problem into two phases. The first phase being the time until the cease of the pulse load. The second phase is the subsequent period of time when the system is excited into free vibration. The displacement and velocity found for the first phase are used as initial conditions for the second phase.
The nature of the response is dependent of the duration and shape of the pulse load. Generally, it can be said that for durations t_d longer than $T_n/2$, the maximum displacement occurs during the pulse phase. The dynamic amplification factor (DAF) is effected by how rapidly the pulse reaches its maximum value, as illustrated in Figure 4.1. For a pulse with an instantaneous build-up, represented by a rectangular shaped load, the DAF approaches a value of 2. For pulses with

Figure 4.1: Pulse spectra for three force pulses with equal amplitude

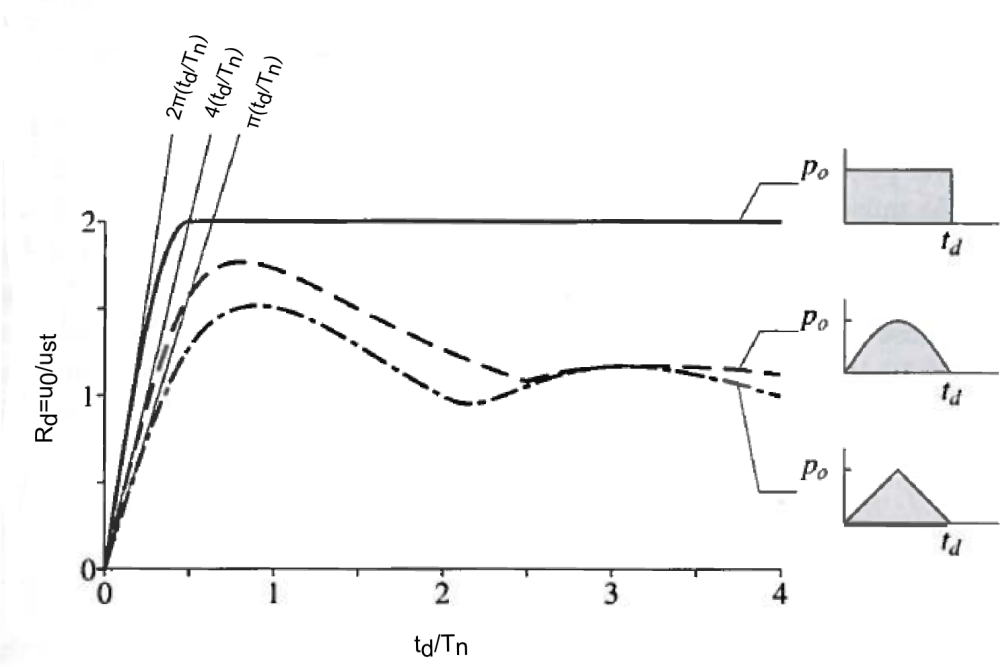

a finite rise time from 0, the DAF lies between 1 and 2.
For pulse durations $t_d < 0.2T_n$, figure 4.1 shows that there is a nearly linear relation between the DAF and duration t. Considering the limit case as t_d/T_n approaches zero. The response becomes the unit impulse response times the impuls magnitude

$$u(t) = I\left(\frac{1}{m\omega_n}\right)\sin\omega_n t \tag{4.11}$$

Where

$$I = \int_0^{t_d} p(t)dt \tag{4.12}$$

I magnitude of impulse

The maximum displacement is given by

$$u_0 = \frac{I}{m\omega_n} = \frac{I}{k}\frac{2\pi}{T_n} \tag{4.13}$$

and is proportional to the impulse magnitude. The maximum displacement values corresponding to the shape of the pulse are shown in figure 4.1. These values provide upper bounds for the true values, and are only excact at $t_d/T_n = 0$, but give good estimates for $t_d/T_n < \frac{1}{4}$. This means that for this time interval, the shape of the pulse becomes insignificant. Also, the maximum displacement occurs during the systems free vibration phase [6].

Chapter 5

Fatigue theory

5.1 S-N curve

Marine structures exposed to constant harmonic loading from the sea environment must take into account the effects of fatigue. Fatigue damage is due to cyclic loading, and is an accumalativ process. The load cycles are most often much smaller than the materials yield stress, but seeing as marine structures often have substantial life cycle durations, fatigue damage might often be an issue.
The relation between the stress range ΔS and the number of cycles N is given by a S-N diagram. The high cycle range of fatigue life exceeds 10^5 cycles and has mostly elastic deformation. Stress ranges that are so small that they do not effect the fatigue life of the structure in any reasonable life time fall below the *fatigue limit*. The relation between S and N is presented in a log-linear curve, or the S-N curve, expressed by:

$$\log N = \log \bar{a} - m \log \Delta\sigma \tag{5.1}$$

N	predicted number of cycles to failure at stress range $\Delta\sigma$
$\Delta\sigma$	stress range [MPa]
m	negative inverse slope of S-N curve
$\log \bar{a}$	intercept of log N-axis by S-N curve

The S-N curves are chosen on the basis of fatigue tests performed on the material in laboratories. Design S-N curves are readily available, in DNV's recommended practice for instance [12]. The curves themselves are shown in Figure 5.1. It is noted that the curves are bilinear, meaning that they have varying steepness depending on cycle range. In the case of the hydraulic cylinders, S-N curve B1 is chosen.

S-N curve	$N \leq 10^7$ *cycles*		$N > 10^7$ *cycles* $\log \bar{a}_1$ $m_2 = 5.0$	*Fatigue limit at* 10^7 *cycles*	*Thickness exponent k*	*Structural stress conc. embedded in the detail*
	m_1	$\log \bar{a}_1$				
B1	4.0	15.117	17.146	106.97	0.00	
B2	4.0	14.885	16.856	93.59	0.00	
C	3.0	12.592	16.320	73.10	0.15	
C1	3.0	12.449	16.081	65.50	0.15	
C2	3.0	12.301	15.835	58.48	0.15	
D	3.0	12.164	15.606	52.63	0.20	1.00
E	3.0	12.010	15.350	46.78	0.20	1.13
F	3.0	11.855	15.091	41.52	0.25	1.27
F1	3.0	11.699	14.832	36.84	0.25	1.43
F3	3.0	11.546	14.576	32.75	0.25	1.61
G	3.0	11.398	14.330	29.24	0.25	1.80
W1	3.0	11.261	14.101	26.32	0.25	2.00
W2	3.0	11.107	13.845	23.39	0.25	2.25
W3	3.0	10.970	13.617	21.05	0.25	1.00
T	3.0	12.164	15.606	52.63	0.25 for SCF$\leq$10.0 0.30 for SCF>10.0	1.00

5.2 Damage accumulation

The damage obtained over a certain period may be found through *Miner-Palmgren linear damage accumulation theory*:

$$D(t) = \sum \frac{n_i}{N_i} \tag{5.2}$$

- D total accumulated damage
- n_i number of cycles corresponding to stress range S_i
- N_i number of cycles to fracture, at stress range S_i

Fatigue damage is related to the stochastic response of the structure, and may also be calculated on the basis of the stochastic process. In the time domain, the number of cycles at certain stress cycles are simply counted and summarized.

5.3 Cycle counting

A commonly used counting method is *Rainflow counting*, suitable for broadband processes. The definition of a rainflow cycle is as follows: *From each local maximum M_k one shall try to*

Figure 5.1: S-N curve for air environment

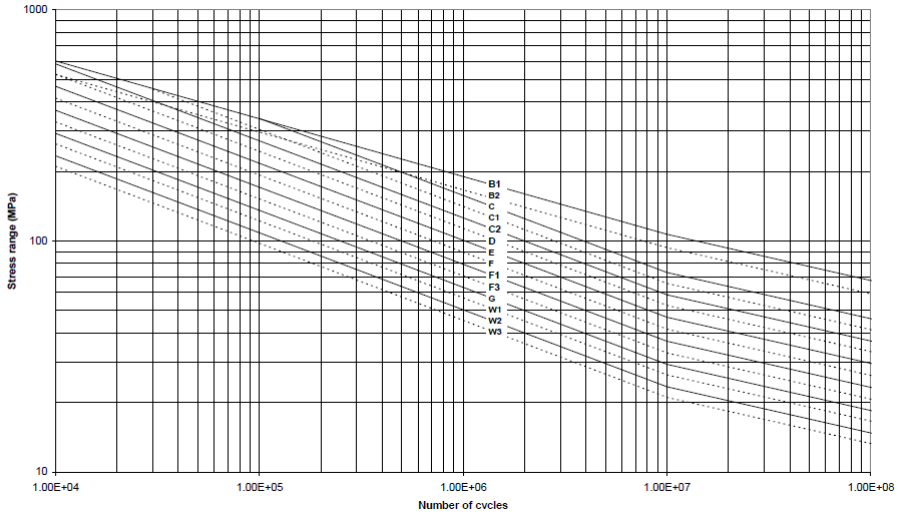

reach above the same level, in the backward (left) and forward (right) directions, with an as small downward excursion as possible. The minima, m_k^- and m_k^+, on each side are identified. The minimum that represents the smallest deviation from the maximum M_k is defined as the corresponding rainflow minimum m_k^{RFC}. The k'th rainflow cycle is defined as (m_k^{RFC},M_k). The principle is illustrated in Figure 5.2. Using rainflow cycles, the damage may be predicted

Figure 5.2: Definition of a rainflow cycle

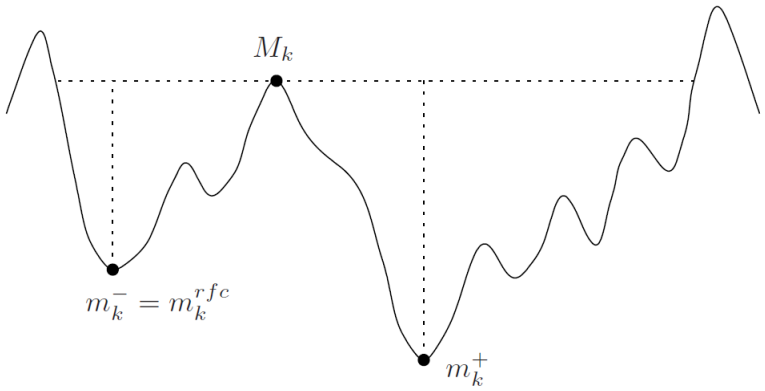

by [11]:

$$D(t) = \sum_{t_k \leq t} \frac{1}{N_{S_k}} = \sum_{t_k \leq t} K(S_k^{RFC})^{\beta} \tag{5.3}$$

Where

$$S_k^{RFC} = (M_k - m_k^{RFC})/2 \tag{5.4}$$

and

$$K = \frac{1}{\bar{a}} \tag{5.5}$$

The normal stresses must be calculated from the bending moments and axial forces obtained

β	slope of S-N curve according to WAFO terminology
S_k^{RFC}	stress range [MPa] according to WAFO terminology
K	material constant, intercept of y-axis according to WAFO terminology

from the simulation in Riflex. In the local axis system of the cross-section of the cylinder, the normal stresses may be found by:

$$\sigma = \frac{N}{A} + \frac{M_z}{I_z} y + \frac{M_y}{I_y} z \tag{5.6}$$

N	Axial force
A	Area of cross section
$M_{z,y}$	Moment about z- and y-axis
$I_{z,y}$	Area moment about z- and y-axis

5.4 WAFO

WAFO (Wave Analysis for Fatigue and Oceanography) is a freely available Matlab toolbox developed at the Faculty of Engineering at Lund University. The toolbox is intended for analysis and simulation of stochastic processes, especially sea waves and loads. Some of the features of the toolbox include wave/load data analysis, extreme value and other statistical analyses, spectral distributions and fatigue life calculations.
This thesis has utilized some of the possibilities that the toolbox offers with regard to data analysis, rainflow cycle analysis and fatigue calculation. The modules that have been used are:

data2tp	finds turning points from data set
tp2rfc	calculates rainflow cycles
cc2dam	calculates damage from information yielded from the rainflow cycles

Chapter 6

Implementation of slamming loads into Riflex

6.1 Approximations

For the implementation of slamming loads in the Riflex simulation the following assumptions and approximations are taken:

- Displacements induced by slamming loads are small compared to those induced by vessel motion and forces formulated in Morison's equation
- Wave kinematics are calculated at static positions
- The error committed due to the stretching of wave kinematics is neglected
- Negligible vertical motion of drilling riser

The slamming loads are expected to induce small displacements on the riser. It is therefore assumed in the calculation of the slamming loads that it is sufficient to use the displacements and velocities induced by conventional wave loads and vessel motion calculated by Riflex. The process will be further described in Section 6.2.
As the vessel motion will be the dominating motion of the system close to the surface, the wave kinematics are calculated at static position to insure consistency between terminal point motions and wave kinematics [1].
The slamming forces act on the riser from the mean water line up to the free-surface elevation, and a stretching method is used to describe the wave kinematics in this region. An error is thus introduced, because the kinematics used to calculate the forces given by Morison's equation in Riflex are limited to the mean water level. The kinematics are therefore duplicated to some extent. A correction for the forces calculated with duplicated kinematics should be made. It is however doubtful that the correction will be calculated accurately enough to have any meaning. On the assumption that the effect of the duplicated kinematics are small, this is

therefore neglected. The last item corresponds well with the assumption of near constant top tension of the riser, due to the heave compensation system.

6.2 Modeling procedure

The time domain simulation of the riser response including slamming loads is done iteratively as follows:

- **Step 1:** Time domain simulation in order to obtain riser displacements
- **Step 2:** Slamming load formulation
- **Step 3:** Time domain simulation with slamming loads

A time domain analysis is carried out with the FEM based program Riflex to provide a solution to the riser response, subjected to conventional wave loads. A self-developed Matlab program has been written to formulate the slamming loads on the riser. However, as the riser is under constant motion due to vessel motion and response to wave loads, it is necessary to implement the results obtained from step 1 to include the updated riser displacements. Derivation of the displacements yields the riser velocity so that the relative velocity between the riser and incoming water particles may be calculated, which is a key parameter when calculating the slamming forces. This is done in step 2. The slamming loads are then implemented into a second time domain analysis in Riflex in step 3. This is described schematically in Figure 6.1.
It is in this case deemed sufficient with just one iteration including slamming loads, in coherence with the approximations outlined in Section 6.1. The two time domain simulations performed also give the advantage of comparison of results - with and without slamming, which indeed is the main goal of this thesis.
The calculations for the slamming load formulation are done with a simple Matlab code. The time series of the riser nodal displacements and the Fourier wave components are input to the program. A load time series file is the output. The flowchart for obtaining the riser response with and without slamming forces is shown in Figure 6.2.

1. A simulation is run in Riflex in order to obtain the nodal displacements, given in binary format in *noddis.bin*.
2. Also, the dynmod.exe and outmod.exe functions of Riflex are run to obtain the Fourier wave components necessary to reproduce the wave elevation, given in *fouriercomponents.txt*.
3. The sea states are specified in *casespec.m*.
4. *noddis.bin* is read by *binread.m*.
5. *nodaldispvel.m* differentiates the nodal displacements in order to obtain the riser velocity.

Figure 6.1: schematic modeling procedure

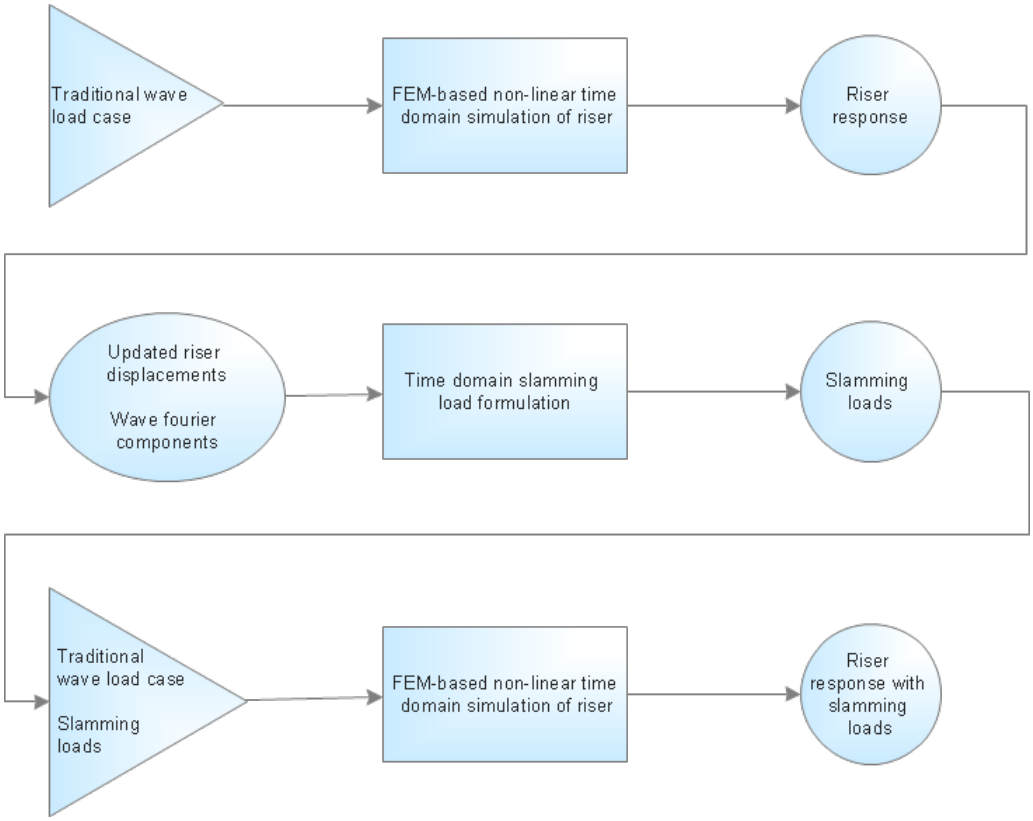

6. Wave kinematics and elevation are produced in *waveel.m*.

7. Relative riser velocity is calculated in *nodevelocities.m*.

8. *waveslam.m* calculates the slammings loads.

9. The load file is written in *writeslam* in ASCII format.

10. The second time domain simulation, including slamming loads, is run in Sima Riflex.

Figure 6.2: Flowchart riser response calculations

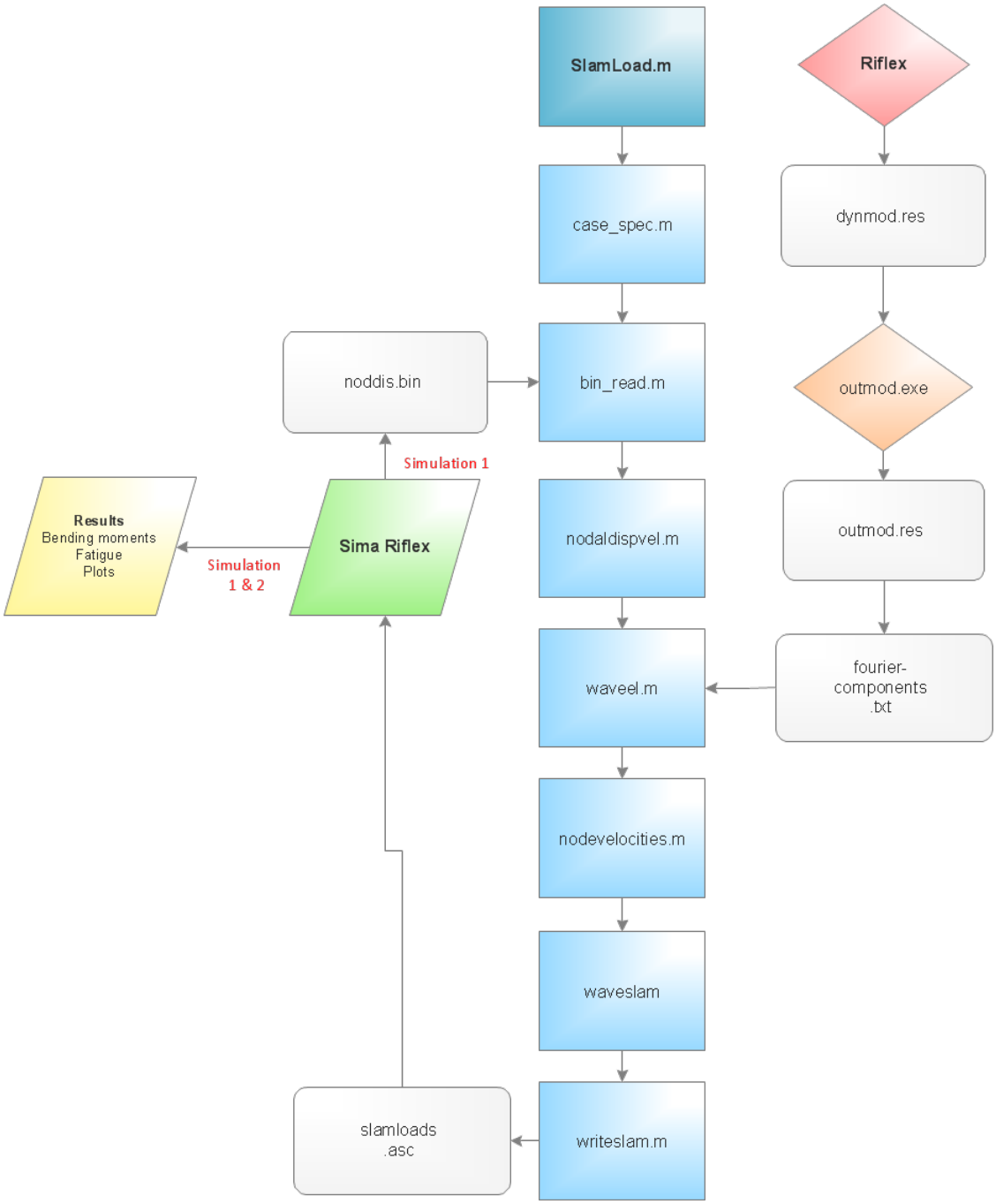

6.3 Sea state generation and kinematics

6.3.1 Irregular wave time series

Riflex is capable of modeling an irregular sea state using first-order theory, or *Airy waves*. The option for combining wind generated waves and swell exists, although the latter is altogether omitted with regards to this thesis. The sea state may be described by:

$$S_{\zeta,TOT}(\beta\omega) = S_{\zeta,1}\phi_1(\beta-\beta_1) + S_{\zeta,2}\phi_2(\beta-\beta_2) \tag{6.1}$$

Where $S_{\zeta,1}$ and $S_{\zeta,2}$ contain information about the frequency distribution of the wind sea and swell, and β is the wave propagation direction, as shown below in Figure 6.3 The realization

Figure 6.3: Definition of wave directions

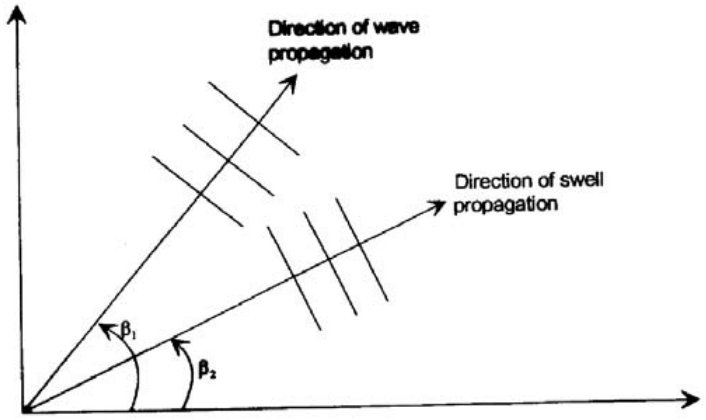

of the sea state is a set of discrete wave components generated from the appropriate wave spectrum, as discussed in Section 3.2.1. Riflex samples the random wave phase angle ϕ_{jk} from a uniform distribution over $-\pi$ and π. A position dependent phase angle is also included:

$$\phi^p_{jk} = -k_k x\cos\beta - k_k \sin\beta_j \tag{6.2}$$

So that the surface elevation may be found by:

$$\zeta(t) = \sum_{j=1}^{N_\beta}\sum_{k=1}^{N_{\inf}} \zeta_{a,jk}\sin(\omega_k t + \phi^p_{jk} + \phi_{jk}) \tag{6.3}$$

At a given position, with a zero angle wave propagation direction and wind generated waves, Equation 6.3 reduces to Equation 3.3 in Section 3.2.1. Riflex calculates the surface elevation with the use of a Fast Fourier transformation algorithm [1].

There are various parameters needed in order for Riflex to run an irregular wave time domain analysis. For the generation of the random phase angles, Riflex requires a seed, i.e. an input parameter which the random number generator algorithm uses to produce the phases. One

seed will always produce the same set of random phase angles, making it possible to reproduce the same irregular sea state provided the same seed is used. Further, the duration of the time series must be chosen, along with the time increment with which it is to be calculated. Riflex requires reasonably enough that the length of the time series exceeds that of the simulation time.
It is vital in the estimation of the slamming loads that the irregular waves, along with the water particle kinematics, are accurately reproduced in Matlab. To do this, the OUTMOD module allows the discrete wave components to be printed in the OUTMOD result file using the FOURIER COMPONENTS WAVES data group. The wave components are printed as in Figure 6.4. The superposition of these discrete wave components, according to Equation 6.3, will yield in

Figure 6.4: Print result of fourier wave components in OUTMOD

Freq no	Frequency (RAD/T)	Amplitude (L)	Phase angle (DEG)
1	0.261	0.000	-58.282
2	0.262	0.000	-88.939
3	0.264	0.000	-51.873
4	0.265	0.000	-2.266
5	0.267	0.000	-43.860
6	0.268	0.000	68.552
7	0.270	0.000	-134.114
8	0.272	0.000	112.852

a irregular sea state realization. Illustrated in Figure 6.5 is a comparison of the wave elevation print obtained from the OUTMOD function in Riflex and the wave elevation resulting from the summation of the Fourier components.

6.3.2 Nodal displacements and velocities

As the riser will move due to vessel motion and hydrodynamic forces, the impact velocity with which the slamming loads are to be calculated must be taken from the water particle velocity relative to the riser motion. In its current state, Riflex does not store the nodal velocities and accelerations [1], so that in order to obtain the velocities, a numerical differentiation of the displacements must be performed. A numerical differentiation method symmetric about the desired time value is used, called *central differentiation*. In other words, the approximation to the derivative at a is found by using the values on both sides of a, $f(a-h)$ and $f(a+h)$. A polynomial that interpolates the values at $(a-h)$ and $(a+h)$ is used to approximate the derivative at t, so that it may be expressed by:

$$f^{'}(a) \approx p_2^{'}(a) = \frac{f(a+h) - f(a-h)}{2h} \tag{6.4}$$

Figure 6.5: Irregular sea state

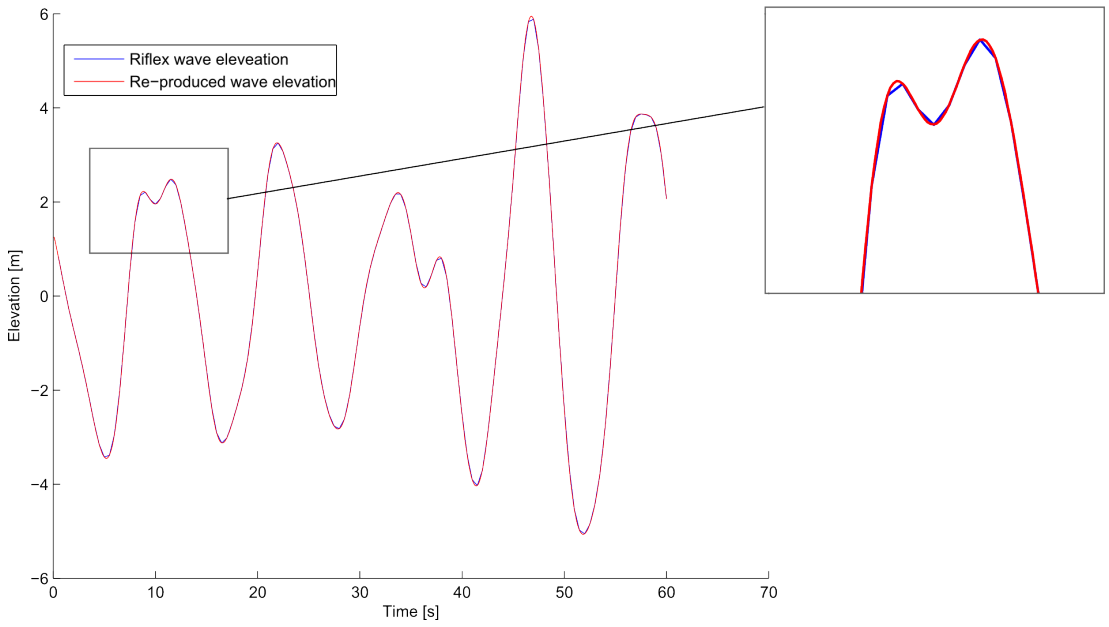

At either end of the time series, i.e. the first and the last time steps, the derivative is found by *forward* and *backward numerical differentiation*, respectively [5]:

$$f'(a) \approx \frac{f(a+h) - f(a)}{h} \tag{6.5}$$

and

$$f'(a) \approx \frac{f(a) - f(a-h)}{h} \tag{6.6}$$

The nodal displacements are stored during the dynmod-run using the DISPLACEMENT RESPONSE STORAGE data group. The desired line is specified (Line 8), along with the specific segment number and node numbers. The displacements are stored in a binary file format. The Matlab program is capable of reading the binary file and using the data for the calculations. The resulting derivative of the nodal displacement for a certain node is plotted in Figure 6.6.

6.3.3 Wheeler stretching

As mentioned in Section 3.2.2, it is desirable to make a modification to the linear wave theory to properly describe the kinematics in the wave profile. This can be done with the *Wheeler stretching method* by attaching the velocity to the free-surface elevation instead of the mean water line, as described by Wheeler [18]. The vertical coordinate is simply stretched, by:

$$z = \frac{z_s - \eta}{1 + \eta/d} \tag{6.7}$$

Where

$$-d < z < 0; \quad -d < z_s < \eta \tag{6.8}$$

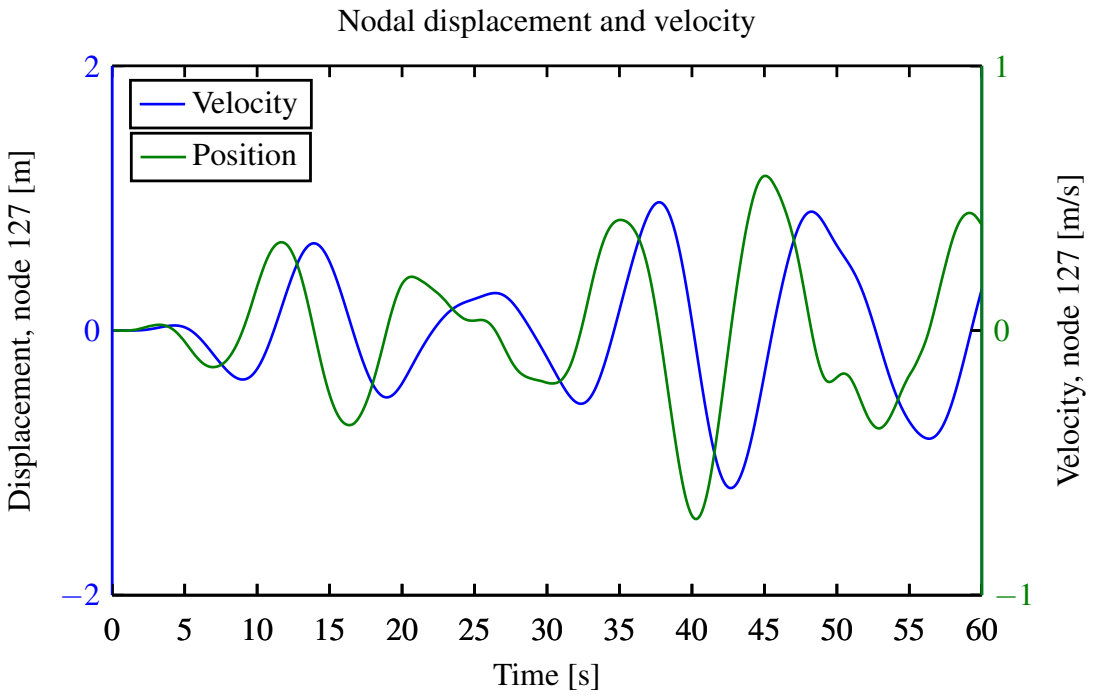

Figure 6.6: Nodal displacement and velocity

The principle is shown in Figure 6.7 For a regular wave, the calculation of the horizontal ve-

Figure 6.7: Stretched velocity profile

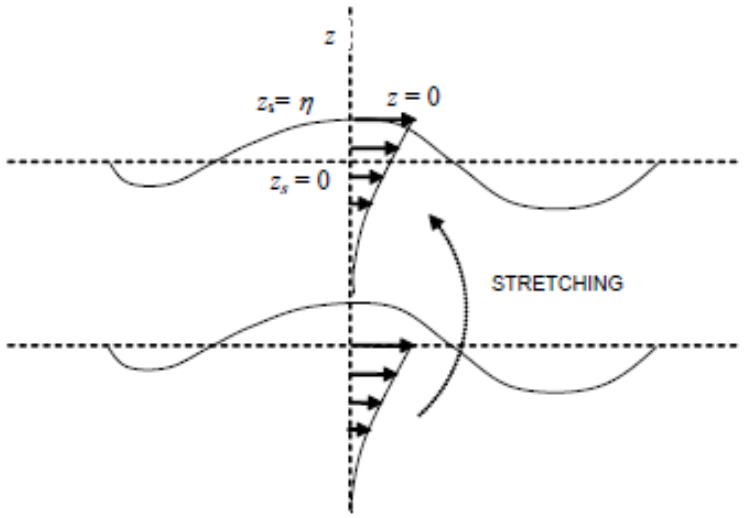

locity at a desired position at a given time becomes a fairly simple matter of stretching the z-coordinate and applying it to Equation 3.7. Figure 6.12 shows how the horizontal water particle velocity profile at the position of the riser varies in amplitude and vertical position, as the riser is submerged by the wave front.

The water particle velocity profile for an irregular wave is also connected to the free-surface elevation, using *Wheeler stretching*. The horizontal velocities of all the wave components are calculated at the static position of the riser, in compliance with the method used in Riflex. This

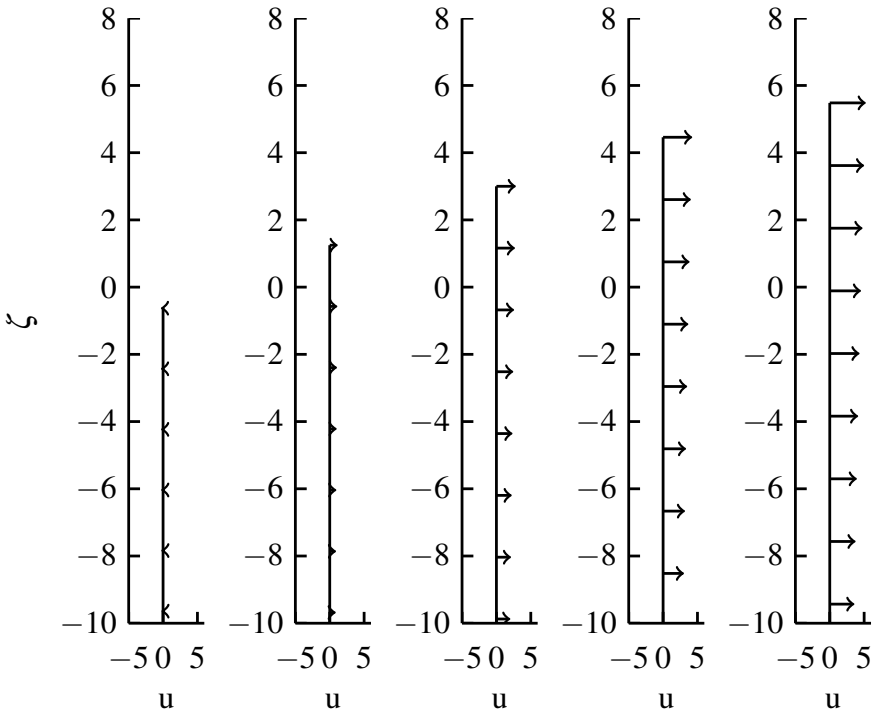

Figure 6.8: Horizontal water particle velocity profile for a regular wave at subsequent time instants during riser submersion

is an option chosen for simplicity and also recommended by [1]. The principle is shown in Figure 6.9 The velocities of all the wave components are superposed as by Equation 3.8, as shown in Figure 6.10. The relative velocity with which the wave impacts with the riser is the sum of riser velocity and water particle velocity:

$$u_{relativ} = u_{waterparticles} + u_{riser} \tag{6.9}$$

Figure 6.9: Wave kinematics calculated at static positions

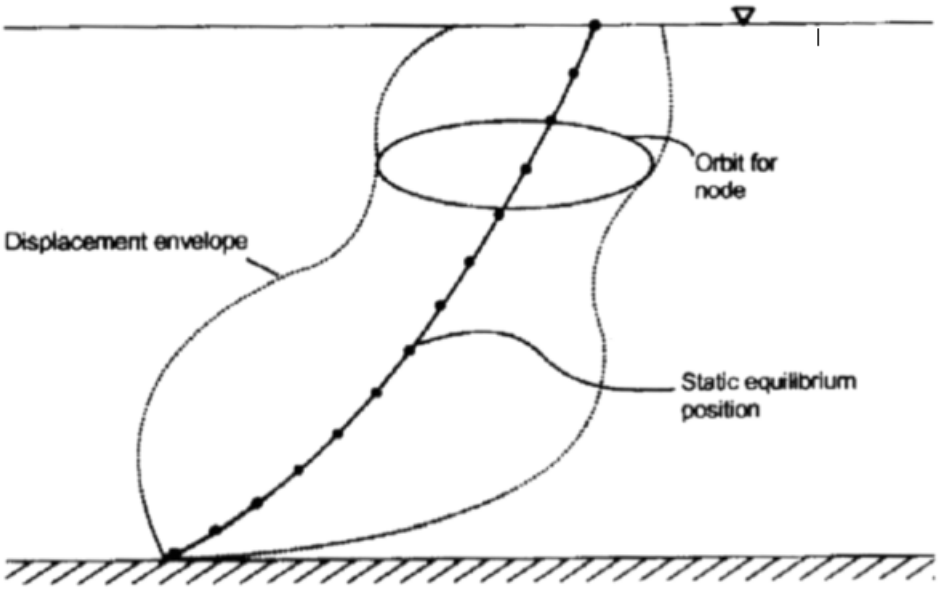

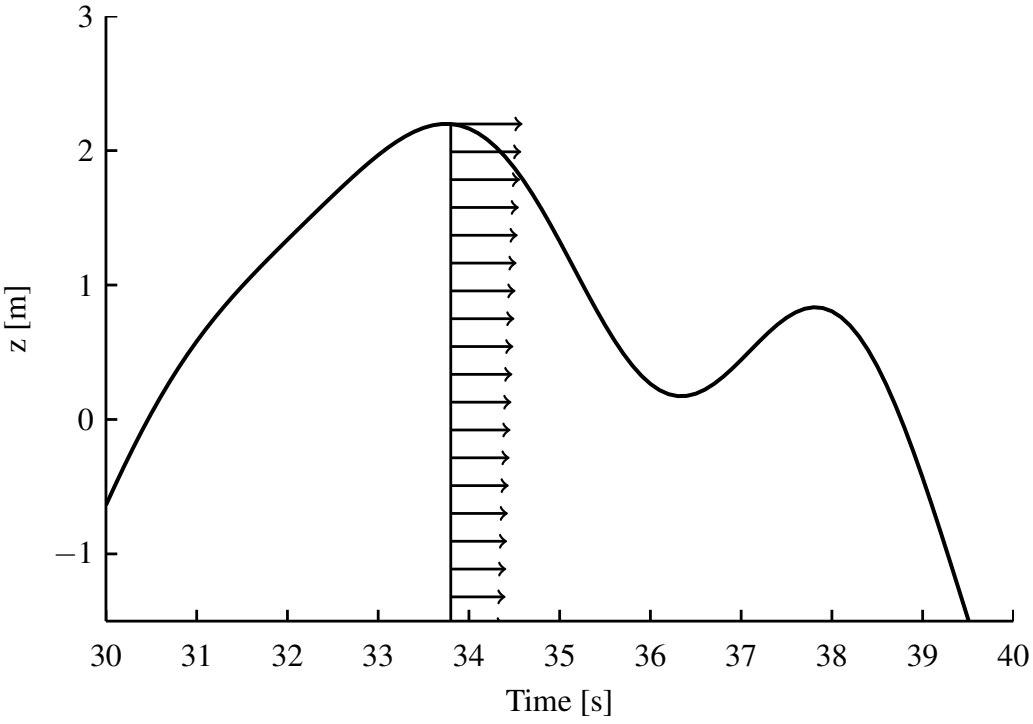

Figure 6.10: Wave velocity profile for an irregular wave

6.4 Estimation of slamming forces

6.4.1 Calculation method

The external forces on the drilling riser have two components, the higher order slamming load and the forces formulated by Morison's equation. The slamming load is only active during the submergence of the riser. In the calculations, this is handled by requiring two things, proposed by [8]:

- The incident wave elevation must be above mean water level for the slamming load to be activated.
- The submergence $s = s(t)$ to be less than the diameter D of the cylinder.

The submergence s is a function of velocity and time. In Sections 3.3.1 and 3.3.2 the expression found for the slamming force requires constant velocity during submergence, so that the submergence must be:

$$s(t) = Vt \tag{6.10}$$

And when utilizing the slamming coefficient given by Equation 3.27, the submergence for each time step is given by:

$$\Delta s = V\Delta t \tag{6.11}$$

When performing the numerical calculations it is therefore necessary to have both sufficiently small Δt and length between nodes, dL, to describe the load over time. The convergence of the result is discussed in Section 7.4.
The two load components act on separate regions of the riser and are divided in the following way:

- The slamming forces are calculated in Matlab and act from the mean water line up to the free surface elevation
- Morison's equation is used up to the mean water line and is calculated in Riflex

6.4.2 Integration of strips

The slamming forces are calculated in a strip-wise manner using Equation 3.28 earlier discussed. In order to obtain the total load on the riser, the forces on each strip must be integrated along the submerged part of the riser, i.e. from the free-surface elevation ζ_1 where $s = D$, and up to the free surface elevation ζ_2 where $s = 0$. The total force is found by:

$$F(t) = \int_{\zeta_1}^{\zeta_2} dF_x dz = \int_{\zeta_1}^{\zeta_2} \frac{1}{2}\rho C_s D u^2 dz \tag{6.12}$$

The areas over which the slamming forces and Morison forces are integrated are shown in Figure 6.11 The integration is performed numerically, and Matlab has several built-in numerical

Figure 6.11: Area over which the forces acting on riser are to be integrated

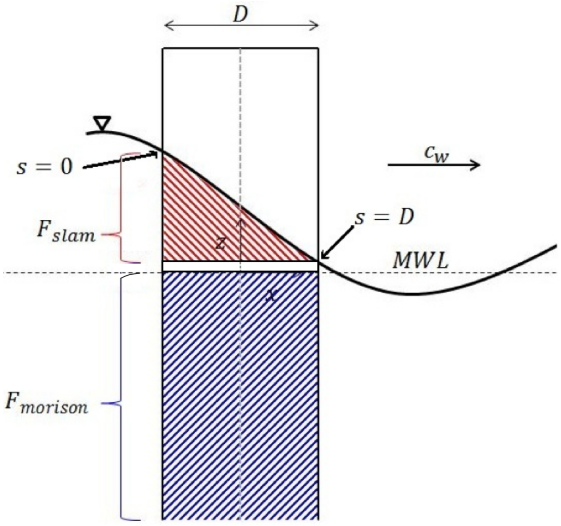

integration procedures, among them the trapezoidal method which is used in this case. The trapezoidal method approximates the integral by calculating the area of a trapezoid given by the function values at two points, a and b, and the distance between them, dL:

$$I = \int_a^b f(x)dx \approx (b-a)\frac{f(b)+f(a)}{2} \tag{6.13}$$

Dividing the integration length into n segments, the integral is approximated as [5]:

$$\int_a^b f(x)dx \approx \sum_{i=0}^{n-1} \frac{1}{2}(x_{i+1}-x_i)(f(x_{i+1}+f(x_i)) \tag{6.14}$$

6.4.3 Slamming loads from an incoming regular wave

A simulation of a steep regular wave impacting on a drilling riser resulting in a slamming load has been made. The chosen case has been to implement a regular incident wave with height $H = 12m$ and period $T = 12.39s$. The ratio between H and T is the maximal permissible by linear theory, as discussed in Section 3.2.1. The horizontal wave particle velocity is computed based on linear wave theory, and subsequently stretched to the wave surface using the *Wheeler method*. The slamming coefficient presented by Campbell & Weynberg is used. The diameter of the drilling riser is set to $D = 0.533m$. The riser is in this case assumed fixed, so that the velocity is only comprised of the water particle velocity of the incoming wave.
The load is induced as the incident wave impacts with the riser. The resulting slamming load is integrated along the riser length and plotted together with the incident wave in Figure 6.12, and shows how the total slamming load is distributed over time during impact.
The jagged curve of the slamming load in Figure 6.12 is due to the numerical issue of dividing the riser into strips. The total load has the appearance of an impulse load, with a magnitude of around 1000 N and duration of close to three seconds as the wave impacts with the riser and submerges an increasing amount of strips. The slamming forces acting on each strip is shown in

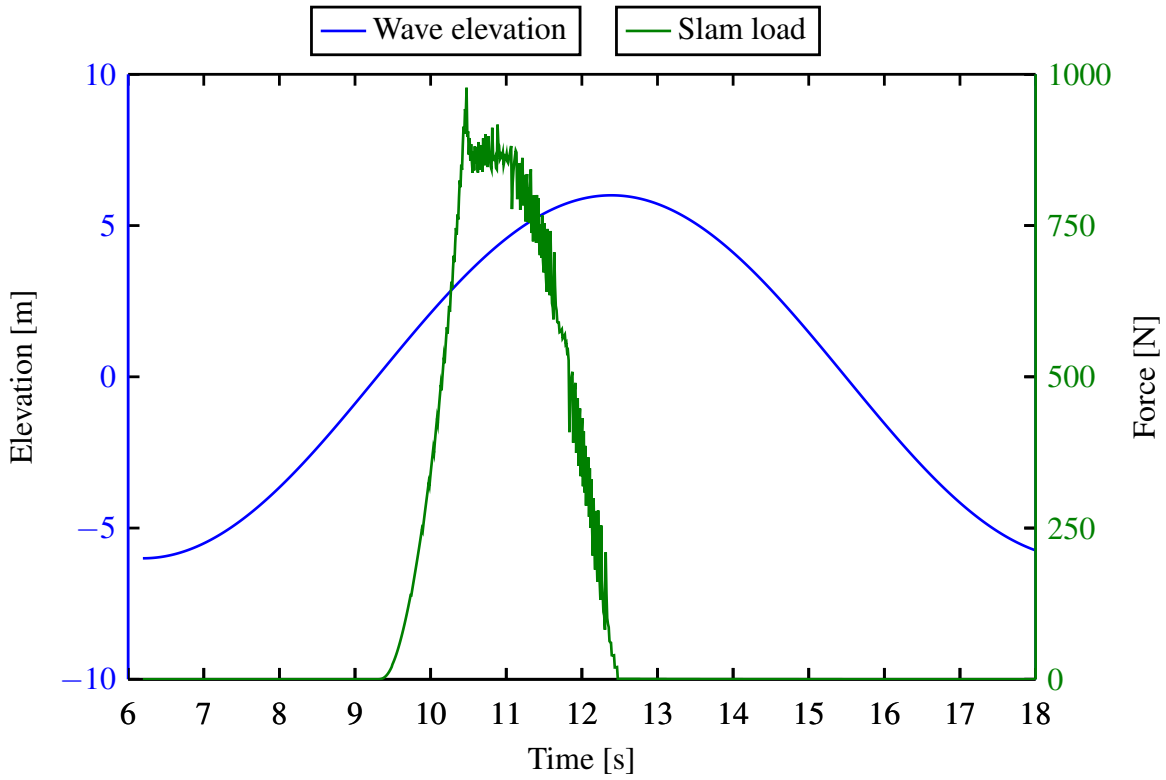

Figure 6.12: Wave elevation and slamming forces

Figure 6.13, illustrating how the wave impacts and induces loads on increasingly higher located strips. Also, the figure illustrates how the increasing wave particle velocity towards the wave crest induces a higher load, and also has a shorter duration due to a more rapid submergence of the riser.

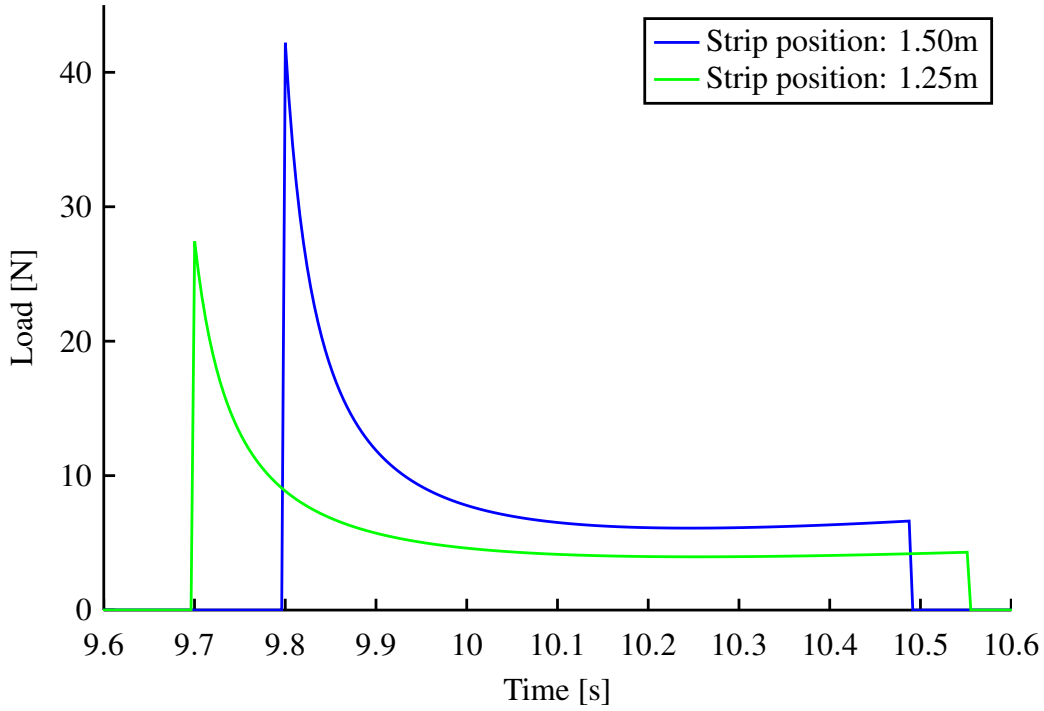

Figure 6.13: Slamming force on individual strips

6.4.4 Generation of load file

The slam loads are added in addition to the traditional wave loads incorporated in Riflex, and are implemented as an additional input load file to Riflex. Riflex includes the option of including dynamic current forces and dynamic nodal forces, defined either by a simple expression or as a separately defined load file. The option of including a separate load file is chosen. The file is of ASCII-format, and is described by assigning magnitude values to certain nodes at specified time instants. The loads are designated to the nodes simply by order of sequence from top to bottom on the line segment. The line segment and nodes are also specified in the input file.
The dynamic nodal force is applied at the specified node and segment number, together with the degree of freedom and coordinate system. The forces are given in kN, consistent with the unit used by Riflex.

Chapter 7

Simulation model

7.1 Selection of sea states

The purpose of the simulation is to investigate the importance of slamming loads on the marine drilling riser due to steep incoming waves. Slamming loads are most noticeable when the wave steepness is high, i.e. when ζk is high, because the wave kinematics reach high velocities and the wave front impacts with larger areas of the riser during a shorter period of time. To this end, it is helpful to consult a scatter diagram, in order to investigate the occurrence frequency of the various sea states. A scatter diagram is a account of the number of occurrences of different sea states, determined by the parameters H_s and T_p, during a certain amount of time. The diagram is often used for estimating the probability of occurrence of a given sea state. The Ekofisk-field scatter diagram is chosen in this case. The most severe and steep sea states are taken from the scatter diagram shown in Table 7.1.

Table 7.1: Selection of Ekofisk-field scatter diagram, 1980-1993

Hm0\Tp	**7-8**	**8-9**	**9-10**	**10-11**	**11-12**	**12-13**
4.5-5.0	2	113	271	190	40	19
5.0-5.5		23	154	136	49	23
5.5-6.0		4	61	109	52	26
6.0-6.5			20	58	35	14
6.5-7.0			6	23	35	14
7.0-7.5			2	21	16	13
7.5-8.0				4	8	9
8.0-8.5				2	8	3
8.5-9.0					2	5

The highlighted cells indicate the steepest combinations of H_s and T_p observed at this site, and thus give the sea states in which slamming loads will be most important. The combinations are listed in Table 7.2.

The appropriate wave spectrum is chosen with basis in the chosen combination of H_s and T_p.

Table 7.2: Selected combinations of H_s and T_p

H_s [m]	T_p [s]
6	8
7	9
8	10
8	11
8	12

The Pierson-Moskowitz (PM) spectrum is based on data from the North Atlantic Ocean for fully developed sea states, given on the form:

$$S_{PM}(\omega) = \frac{5}{16} H_s^2 \omega_p^4 \omega^{-5} exp\left(-\frac{5}{4}\left(\frac{\omega}{\omega_p}\right)^{-4}\right) \tag{7.1}$$

Data measured in the south-east parts of the North Sea resulted in the JONSWAP spectrum, a modification to the PM spectrum, yielding a sharper peak:

$$S_J(\omega) = \frac{\alpha g^2}{\omega^5} exp\left(-\beta\left(\frac{\omega_p}{\omega}\right)^4\right) \gamma^{exp\left(-\frac{(\omega/\omega_p-1)^2}{2\sigma^2}\right)} \tag{7.2}$$

The spectrum consists of five parameters [2]

- α spectral parameter
- ω_p peak frequency, $\omega_p = 2\pi/T_p$
- γ peakedness parameter
- β form parameter, usually taken as $\beta = 1.25$
- σ spectral parameter, taken as
  $\sigma_a = 0.07$ for $\omega < \omega_p$
  $\sigma_b = 0.09$ for $\omega > \omega_p$

The effects of the peakedness parameter γ are shown in Figure 7.1.
[13] states that the JONSWAP spectrum is appropriate to use in the range:

$$3.6 \leq T_p/\sqrt{H_s} \leq 5.0 \tag{7.3}$$

based on a parametrization of the JONSWAP spectrum, see Figure 7.2.

Figure 7.1: JONSWAP spectrum under various γ values

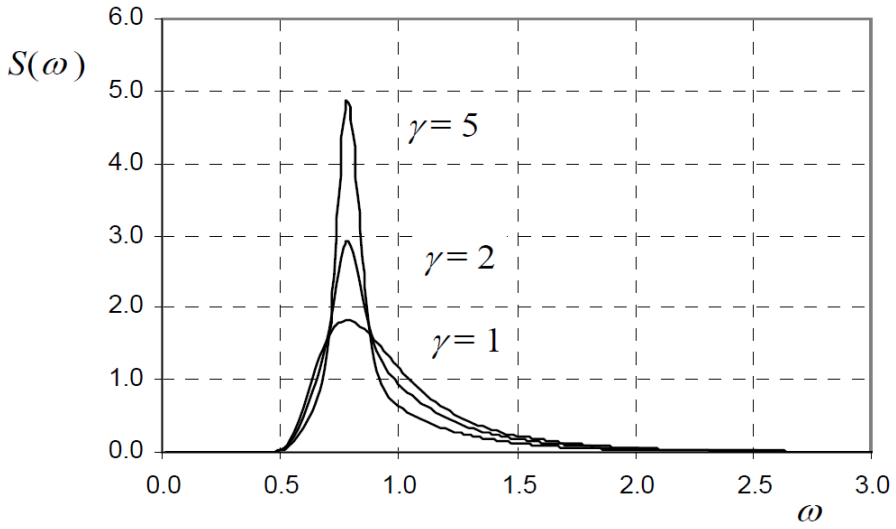

Figure 7.2: JONSWAP area of application

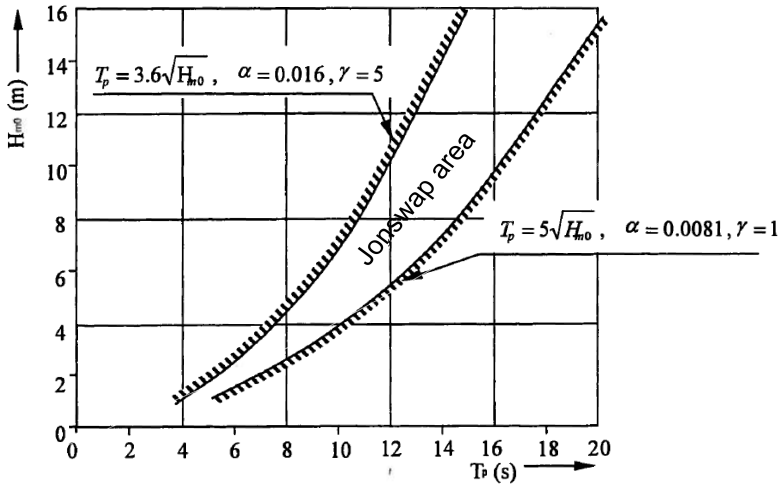

For the selected values of H_s and T_p, this corresponds to the values found in Table 7.3.
It is noted that the three first values do not fit into the stated interval. However, [13] states that γ may be taken on the basis of H_s and T_p:

$$\gamma = 5 \text{ for } T_p/\sqrt{H_s} \leq 3.6 \tag{7.4}$$

$$\gamma = exp\left(5.75 - 1.15\frac{T_p}{\sqrt{H_s}}\right) \text{ for } 3.6 < T_p/\sqrt{H_s} < 5.0 \tag{7.5}$$

$$\gamma = 1 \text{ for } 5 \leq T_p/\sqrt{H_s} \tag{7.6}$$

Subsequently, the parameter γ is chosen as 5 for all cases, accepting that the application of the JONSWAP spectrum might not be accurate for all combinations of H_s and T_p.

Table 7.3: Values of H_s and T_p in the JONSWAP area

H_s [m]	T_p [s]	$T_p/\sqrt{H_s}$
6	8	3.266
7	9	3.402
8	10	3.536
8	11	3.889
8	12	4.243

7.2 Tensioner layout

The heave compensation system comprises of six cylinders, arranged in a circular fashion around the riser. One end of the cylinder is attached to the tension ring fastened to the circumference of the riser joint, the other to a square frame following the motions of the vessel. This thesis will only concern itself with long-crested sea states with unidirectional incident waves propagating along the x-axis. The layout and numbering of the cylinders and the lines used in the Riflex model is illustrated in Figure 7.3.

Figure 7.3: Cylinder layout

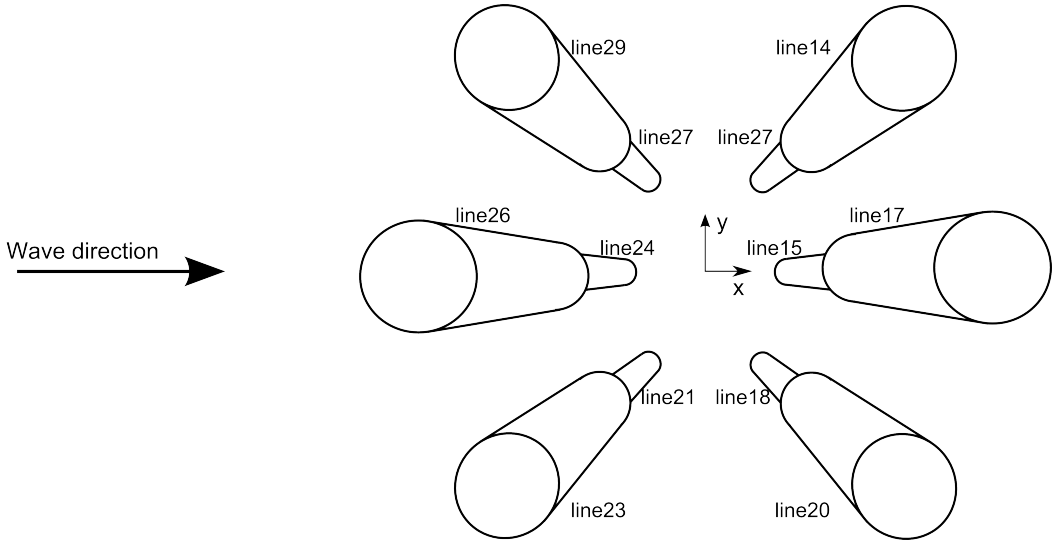

The illustration shows that two cylinders symmetric about the y-axis will only have in-line forces, while the four remaining cylinders will have both in-line and transverse force components. The cylinder itself is comprised of a piston rod and piston housing, each represented by a line in the Riflex model. The dimensions are found in Table 7.4.

Table 7.4: Cylinder layout

Component	Dimension [mm]
Cylinder chamber diameter	560
Rod diameter	230
Piston thickness	365
Packbox	678
Rod length	17429
Cylinder chamber length	16665

The contact points are at the head of the rod and the bottom of the cylinder housing, as shown in Figure 7.4.

Figure 7.4: Cylinder contact points

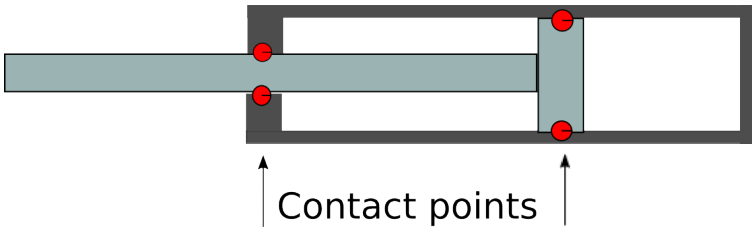

7.3 Eigenmodes

A simplified FEM model is made in order to calculate the most important eigenmodes of the tensioner cylinder. The eigenmodes are useful in several ways. First, they may be used in order to identify any secondary peaks in the response spectrum of the cylinder. Further, the ratio between the eigenperiod and the pulse duration is of interest with regards to dynamic effects. The tensioner cylinder is in reality a fairly complex object due to it being a pipe-in-pipe model. The length will constantly vary and the mass and stiffness are unevenly distributed. Also, a tension is applied which will contribute to its bending stiffness. For this case, it is appropriate to establish only a simple model. By dividing the tensioner cylinder into three parts with different mass, cross-section area and stiffness, it is a fairly simple task to make an estimate of the eigenfrequencies. The middle section of the model represents the overlapping rod and cylinder chamber. The simplified model is illustrated in Figure 7.5.

Figure 7.5: FEM model of tensioner cylinder

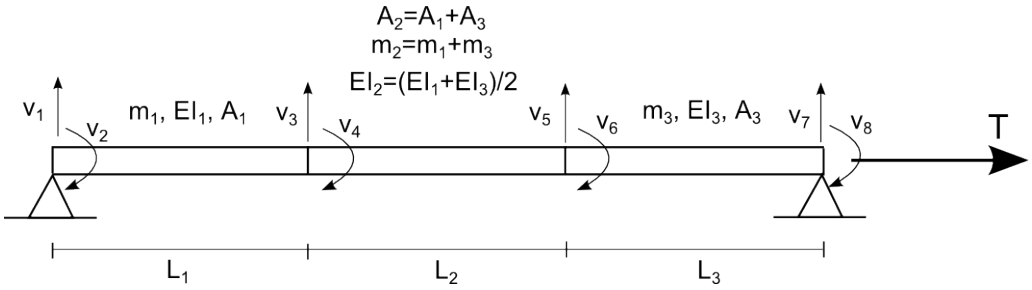

The applied tension will give a contribution to the total stiffness in the form of a geometric stiffness. The elastic and geometric stiffness matrices are:

$$k_{elast.} = \frac{2EI}{L^3}\begin{bmatrix} 6 & & symm. & \\ -3L & 2L^2 & & \\ -6 & 3L & 6 & \\ -3 & L^2 & 3L & 2L^2 \end{bmatrix} \tag{7.7}$$

$$k_{geom.} = \frac{P}{30L}\begin{bmatrix} 36 & & symm. & \\ -3L & 4L^2 & & \\ -36 & 3L & 36 & \\ -3L & -L^2 & 3L & 4L^2 \end{bmatrix} \tag{7.8}$$

Along with the mass matrix:

$$m = \frac{\rho AL}{420}\begin{bmatrix} 156 & & symm. & \\ -22L & 4L^2 & & \\ 54 & -13L & 156 & \\ 13L & -3L^2 & 22L & 4L^2 \end{bmatrix} \tag{7.9}$$

Dynamic equilibrium for a system without damping may be written as:

$$\mathbf{M}\ddot{\mathbf{r}} + \mathbf{K}\mathbf{r} = 0 \tag{7.10}$$

where

$$\mathbf{r} = \Phi \sin \omega t \tag{7.11}$$

- $\mathbf{M}$ system mass matrix
- $\mathbf{K}$ system stiffness matrix
- $\mathbf{r}$ response
- Φ eigenmode

The solution to Equation 7.10 is given by the eigenvalue problem, on general form:

$$(\mathbf{K} - \omega^2\mathbf{M})\Phi = 0 \tag{7.12}$$

Equation 7.12 may also be expressed by the special eigenvalue problem:

$$(\mathbf{A} - \lambda \mathbf{I})\mathbf{x} = 0 \tag{7.13}$$

Where

$$\mathbf{A} = \mathbf{L}^{-1}\mathbf{K}(\mathbf{L}^{T})^{-1} \tag{7.14}$$

and

$$\mathbf{M} = \mathbf{L}\mathbf{L}^{T} \tag{7.15}$$

L lower triangular matrix by Cholesky decomposition

Calculating the eigenvalues of **A** with a Matlab function yields the values found in Table 7.5.

Table 7.5: Standard deviation of bending moment

Eigenvalue nr.	Eigenfrequency [rad/s]	Eigenperiod [s]
1	27.4388	0.2290
2	53.2803	0.1179
3	73.6332	0.0853
4	120.0164	0.0524
5	216.8150	0.0290
6	395.9481	0.0159

7.4 Convergence

Slamming loads are of very short duration, as seen in Figure 6.13. For a cylinder section entering the water surface, the time it takes it to be fully submerged is in our case only a fraction of a second for the sections at the location of the maximum velocity. For this reason it is necessary to have a very small time increment to describe the development of the load in time. In a likewise manner, the length of the riser must have a small length increment to avoid a jagged curve. The load case in Section 6.4.3 is examined. Figure 7.6 shows the slamming load on an individual strip integrated over time using Matlab's built in trapezoidal integration function, using *dt* as the incremental length. The total force integrated over time is plotted as a function of the number of time increments.

Without a sufficiently small time increment, the force is not correctly described over time, and the Matlab code seems to over-predict the total load. The matter is naturally a balance between obtaining sufficiently accurate results and computational time. The situation would be simple if only one slamming load would to be calculated, but this thesis aims to calculate slamming forces on a riser in an irregular sea state. It is not only the slamming force, but riser dynamics

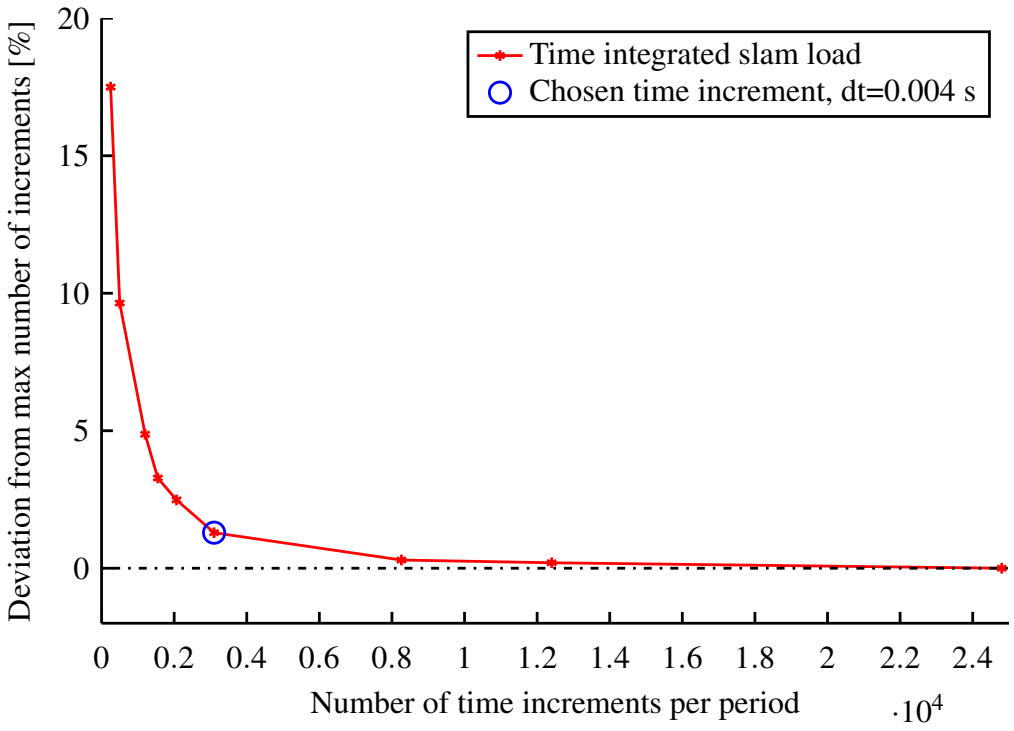

Figure 7.6: Convergence of slam load

and wave kinematics that must be calculated at the same time instant. Therefore, there is a limit to reasonable computational time. With reference to Figure 7.6, the time increment of $dt = 0.004s$ is chosen as sufficient, with less than 2% deviation from the result obtained by even smaller increment.

Chapter 8

Simulation results and discussion

The results from the analyses performed in Riflex and Matlab are presented in this chapter. There are two simulation models undergoing 5 different sea states with a duration of 1 hour. The first model will only include conventional wave loads. The second will take into account slamming loads on the riser in the splash zone in addition to the conventional wave loads. Neither of the models include current forces as the intention of the simulations are to highlight the differences between the load models with and without slamming. The results presented here will focus on:

- Load and response time series
- Bending moments, maximum values and time series
- Effect on fatigue

Dynamic effects related to the load duration and eigenperiods of the hydraulic cylinder will also be examined in order to further determine whether slamming loads represent a significant factor in the load formulation.

8.1 Time series

8.1.1 Load time series

The occurrence of slamming loads is dependent on the incoming wave. The load is induced during submergence of the riser from the mean water line up to the wave crest. The magnitude of the load is dependent on the kinematic properties of the incoming wave as well as the steepness and height. The height determines how many of the strips that are effected, while the steepness of the wave determines how many of the strips are submerged simultaneously. It is suitable to present a time series illustrating the relation between the wave elevation and occurrence and magnitude of slamming loads. Figure 8.1 shows a time series for a short duration. The relation between wave height and steepness and the load amplitude is clearly visible. The wave appearing after 45 s with an amplitude of around 6 m and short period produces the

largest force in the depicted time series, while the waves in the interval between 80 and 110 s hardly produce any force at all.

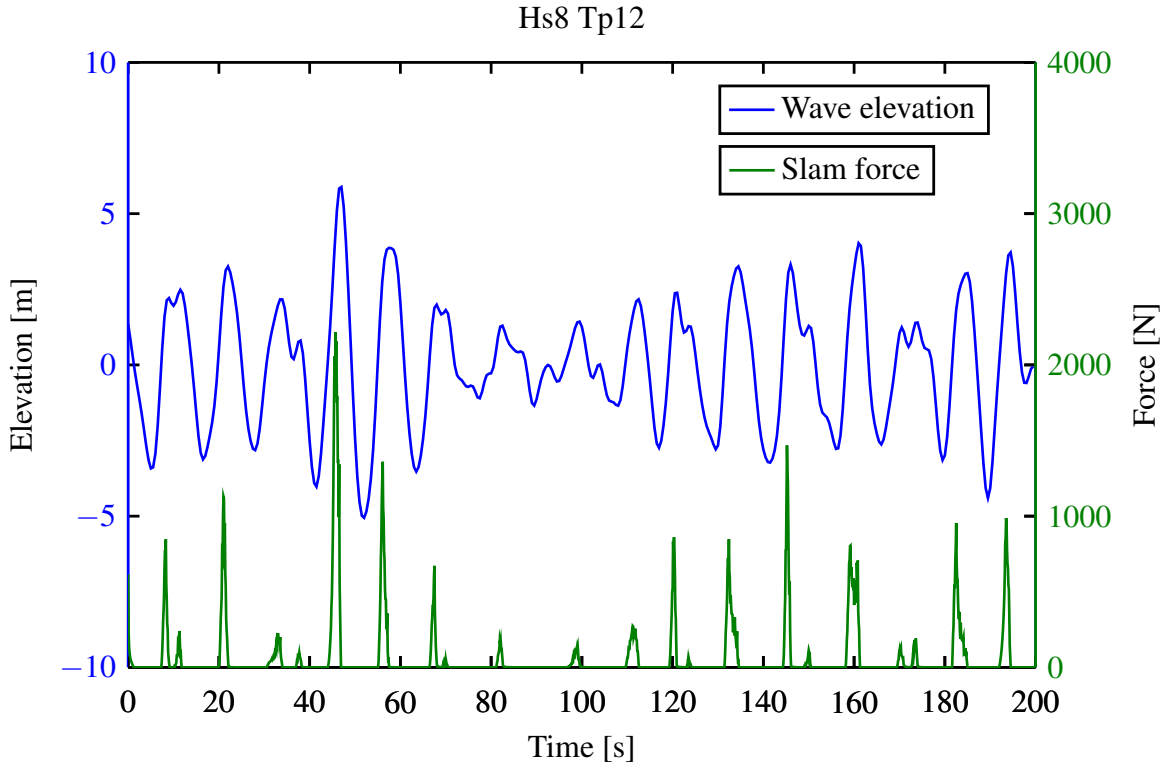

Figure 8.1: Wave elevation and slamming forces

The forces depicted in Figure 8.1 reach values up to 2500 N, most of them around 1000 N. A result file with the forces calculated by Riflex is not available, so a direct comparison with the Morison forces as calculated by Riflex is unfortunately not possible. In comparison with the results achieved in previous work by Nestegård [8] and Sten [29], both utilizing the same purpose made slamming program WAVESLAM developed at DNV, the forces are small. Referring to Figures 3.2 and 3.3, the forces calculated in this thesis are of the order of magnitude 1:10. Compared with the results obtained by Sten, the order of magnitude is 1:100. The most probable reason is the difference in the utilized relative velocities. Nestegård and Sten approximate the water particle velocities by multiplying a factor of 0.3 with the phase velocity of the incoming wave, giving much higher velocities than the water particle velocities used in this thesis. As the slamming force is a function of the square of the velocity, this will have a decisive influence.

8.1.2 Cylinder response time series

The response was found to be largest on the cylinders located on the right hand side of the tensioner ring and riser (positive x-axis), relative to the incoming wave direction. Further, the cylinders with an angle to the x-axis, i.e. those of line 12 and 14 and those of line 18 and 20, see Figure 7.3, were found to have the largest responses. The slamming loads act upon the riser

joint located in the splash zone, to which the tensioner ring is fastened, to which the hydraulic cylinders, in turn, are attached. The displacements are largest at the point on the cylinder rod where it meets the tensioner ring, following the motion of the riser. In order to check for any structural vibrations of the hydraulic cylinder, the point of the largest displacements was located and a time series of the responses, with and without slamming, plotted in Figure 8.2. The wave elevation is included in the plot to illustrate any coherence between the elevation and the response. The figure reveals very small differences in the response with and without slamming, the two time series are almost identical. It is mostly in the case of when the largest slamming loads occur, near to the wave elevation peaks, that a slightly higher amplitude of the response with slamming is observed. An enlarged illustration of the cylinder response for $H_s = 6$ m and $T_p = 8$ s is found in Figure 8.3. Here, it is possible to see that there are occasionally higher peaks added to the response, due to slamming. None of the time series seem to reveal any sign of structural vibrations.

Key results from the response time series are found in Table 8.1. Naturally, the responses are highest for the most severe sea states in terms of significant wave height. The standard deviation of the response is slightly higher with slamming for all cases. It is also noted that the largest difference is for the $H_s = 6$ m and $T_p = 8$ s, which is also the sea state containing the most steep waves. The last sea state, $H_s = 8$ m and $T_p = 12$ s, has the smallest differences in standard deviation, and is also the sea state with the least steep waves.

Table 8.1: Standard deviation of cylinder response

	No slamming	With slamming
Hs6 Tp8	0.23831	0.25228
Hs7 Tp9	0.24111	0.25441
Hs8 Tp10	0.2572	0.26744
Hs8 Tp11	0.34667	0.35205
Hs8 Tp12	0.47834	0.48185

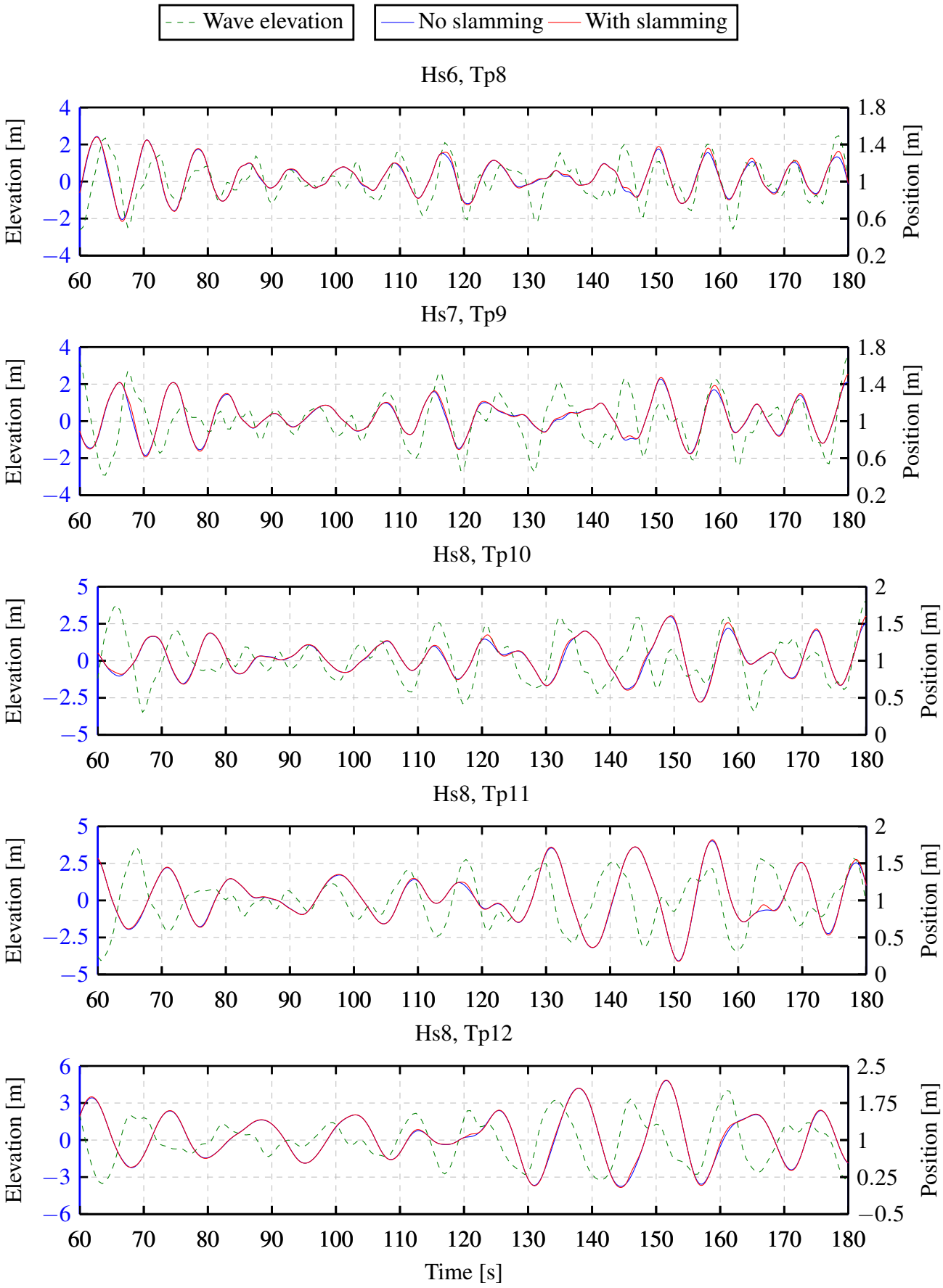

Figure 8.2: Cylinder response time series

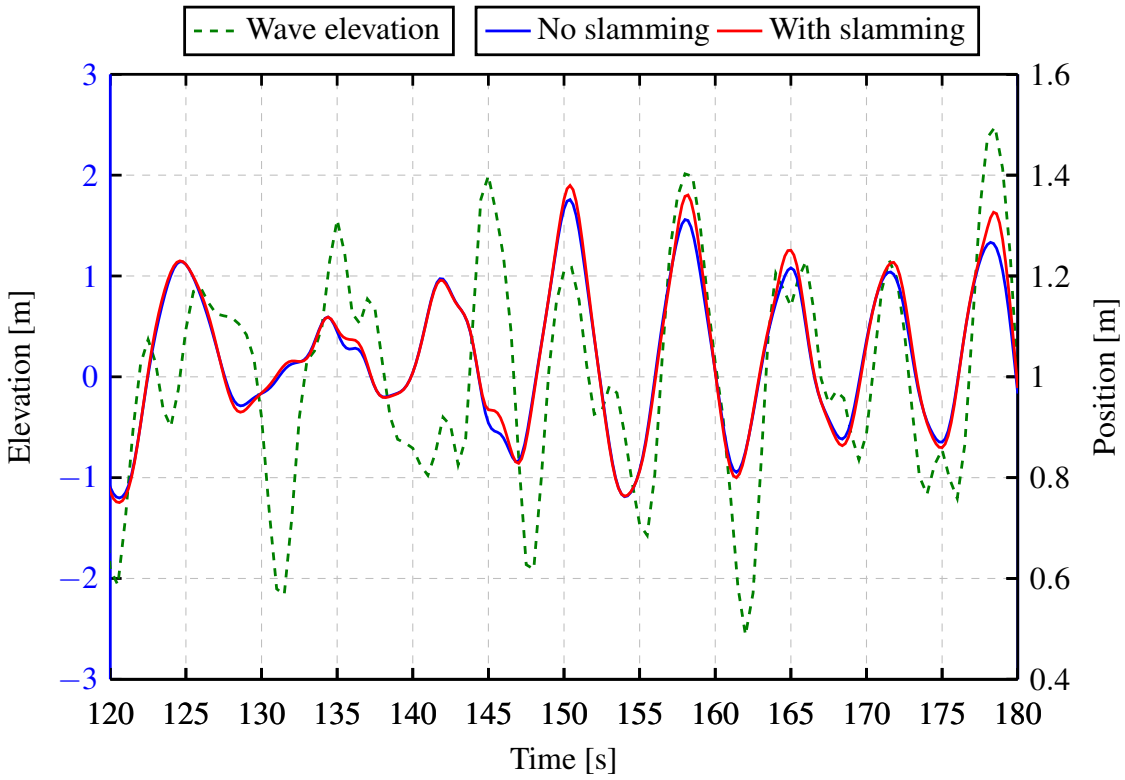

Figure 8.3: Close-up of cylinder response time series, Hs6 Tp8

8.2 Dynamic effects

8.2.1 Effects of pulse duration

From the appearance of Figures 6.12 and 8.1 it can be assumed that a slam load has a duration, t_d, between 1 and 2 seconds. The eigenperiods of the tensioner cylinder are found in Table 7.5, estimated by using the simplified FE model discussed in Section 7.3. The natural period is found to be 0.23 seconds. The short natural period is mostly due to the large tension the cylinder is subjected to. With regards to this natural period, the load duration may be considered much longer. On the basis of this, two observations can be made. The maximum response to such a load will occur during the first phase, i.e. the pulse duration. Further, the shape of the pulse will influence the DAF. The shape of the slam load is relatively irregular, as Figure 6.13 shows, though it seems appropriate to approximate its shape as a rectangle because it acts suddenly. As the ratio t_d/T_n is large, the DAF will most likely convergence towards 2, referring to Figure 4.1. This means that the dynamic displacement due to slamming will be twice that of the static.

8.2.2 Response spectrum

The motion of the hydraulic cylinder is due to vessel motion and waves loads. By finding the response spectrum of the cylinder, it is possible to identify the various load components by their frequencies. It is most interesting to identify any trace of excitation from higher order slam-

ming loads. The displacements are so dominated by the vessel motion that it is more practical to use the curvature or bending moment for this purpose. The spectra for the bending moments in Element 6 of Line 14 for the various sea states are found in Figure 8.6, plotted both with and without slamming.

The spectra are clearly dominated by linear response. On the basis of the transfer function of the vessel displayed in Figure 2.7, the same cancellation effects are observed around the frequencies 0.7 and 1 [rad/s]. There is also a response due to higher-order drag force components, most prominent for $H_s = 6$ m and $T_p = 8$ s, $H_s = 7$ m and $T_p = 9$ s and $H_s = 8$ m and $T_p = 10$ s. The intention of plotting the spectra with and without slamming is to make visible any frequency components that might occur in one load case, but not the other. For $H_s = 8$ m and $T_p = 10$ s there appears to be a small amount of energy in the frequencies between 2.8 and 4 [rad/s] when slamming is included, suggesting vibrations that are not present for any of the other sea states. They are, however, notably small. Altogether, the spectra show no evidence of significant response due to slamming.

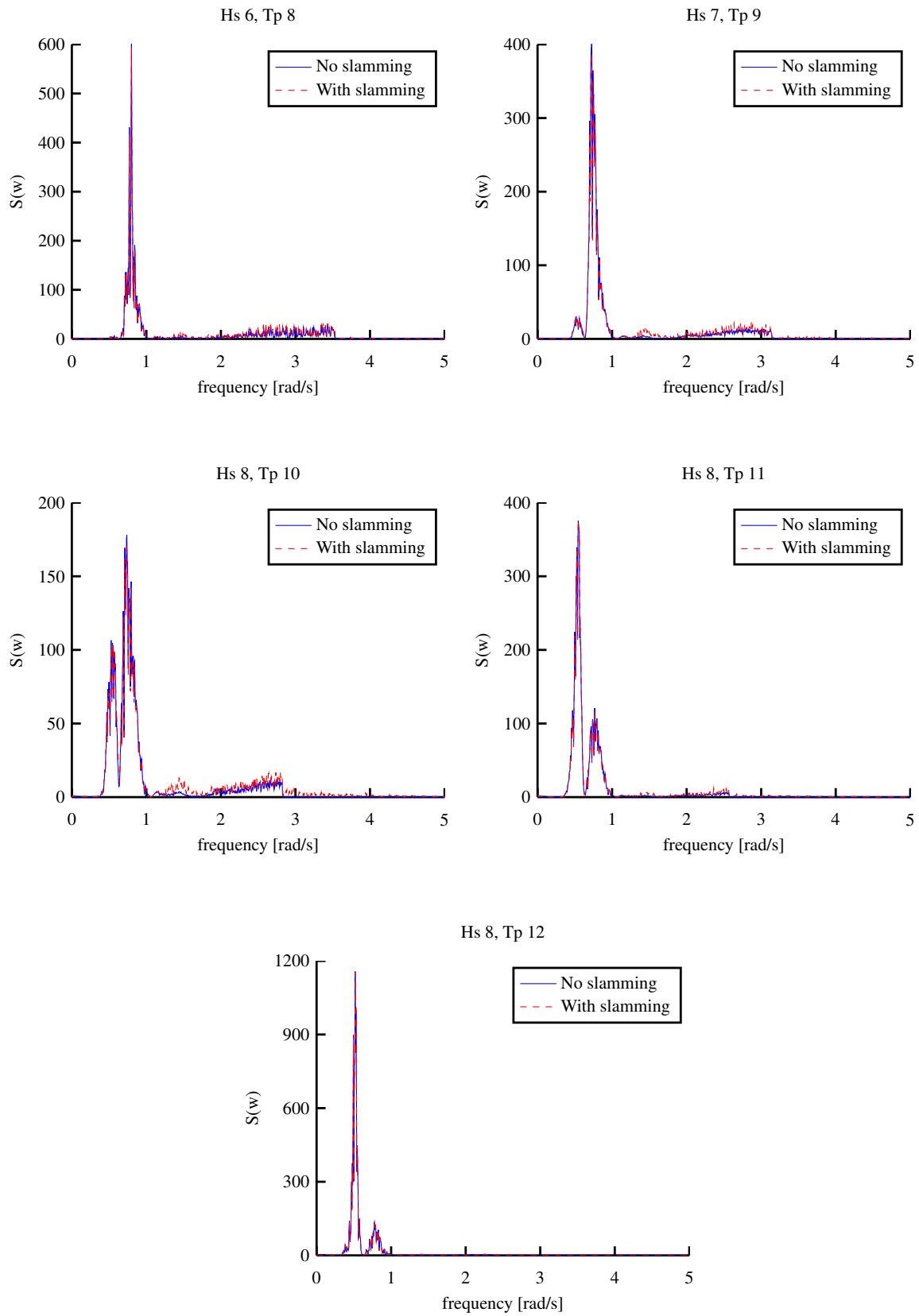

Figure 8.6: Response spectra

8.3 Bending moments

There is a constant motion of the vessel and therefore a continuous extension and retraction of the cylinders. The contact points between the head of the cylinder rod and the cylinder housing, and of the bottom of the cylinder housing and the rod, will also vary continuously. This means that the node or point in which the largest forces occur will vary with time. The bending moments have been examined in two ways. The maximum bending moment occurring on the riser at every time increment is traced and plotted as a time series. The largest maximum bending moment of the simulation is also found. The bending moment along the length of the hydraulic cylinder is plotted at the corresponding time instant.

8.3.1 Bending moment time series

Figure 8.7 shows the time series of the maximum bending moments on the hydraulic cylinder composed of line 12 and 14. In other words, the maximum bending moment has been traced throughout the cylinder length at every time step, meaning that it is the largest values that are at all times plotted. In Figure 8.7, the largest bending moments on the cylinder in the model including slamming are found, and subsequently the bending moments at the same points on the cylinder in the model without slamming.

Occasional large amplitude peaks are observed, compared to the bending moments without slamming. Mostly, this is in the case of the largest oscillations. For smaller amplitude oscillations, the bending moments with and without slamming are found to be almost equal.

It is observed that in most cases, the additional peaks provided by the slamming forces oscillate with the same frequency as the bending moments without slamming. However, there are some seldom cases in which there is an additional oscillation due to slamming. This will be further discussed in Section 8.4.

The standard deviation of the bending moments with and without slamming are provided in Table 8.2. The standard deviation is in all cases slightly higher for slamming than without. The first and last sea states, $H_s = 6$ m and $T_p = 8$ s and $H_s = 8$ m and $T_p = 12$ s, respectively have the largest values, presumably due to steepness and wave height respectively. The largest difference is found for $H_s = 8$ m $T_p = 10$ s.

Table 8.2: Standard deviation of bending moment

	Std, Bending moment	
	No slamming	With slamming
Hs6 Tp8	7.8956	8.291
Hs7 Tp9	7.4426	7.8233
Hs8 Tp10	6.6794	7.107
Hs8 Tp11	7.2454	7.5074
Hs8 Tp12	8.6355	8.7423

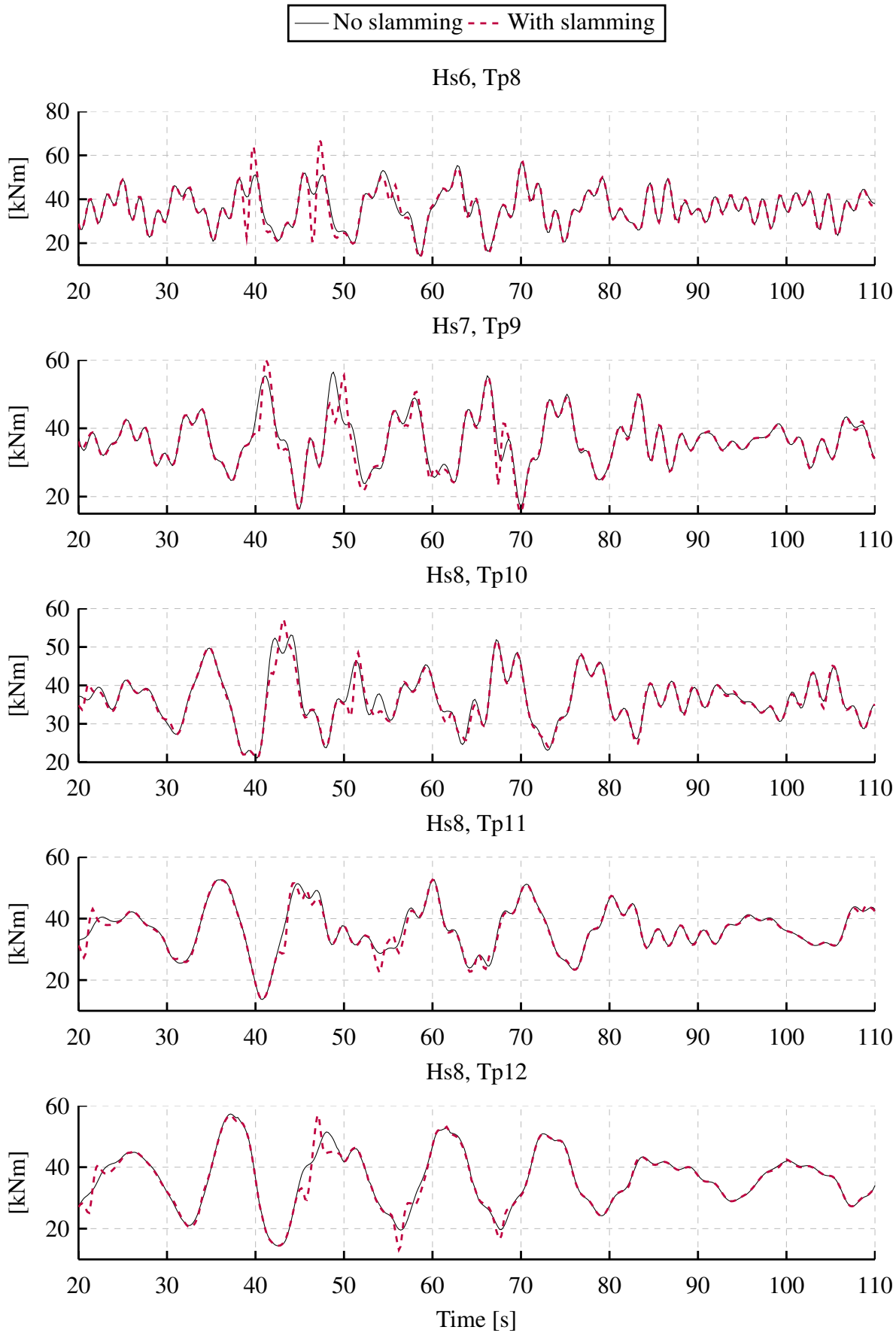

Figure 8.7: Maximum bending moment time series

8.3.2 Maximum bending moment

The time instant in which the maximum bending moment occurs on the tensioner cylinder is found, and the corresponding bending moments along the entire length plotted. The plot is an envelope plot, but a snapshot of the time instant in which the largest value occurs. The tensioner cylinder is a pipe-in-pipe body, composed of two lines. At static positions there is an overlap between the two lines of 8.7 m. The total length is 27.3 m. The tension ring is located at x=0 m. The tensioner cylinder will in reality extend and retract according to the vessel heave motion. For simplicity however, the bending moments are plotted at the static positions of the master and slave pipes. This might lead to some displacement of the bending moment values in comparison to their true positions. The maximum bending moments are plotted for the all sea states, with and without slamming, see Figures 8.8 and 8.9. Figure 8.8 show that

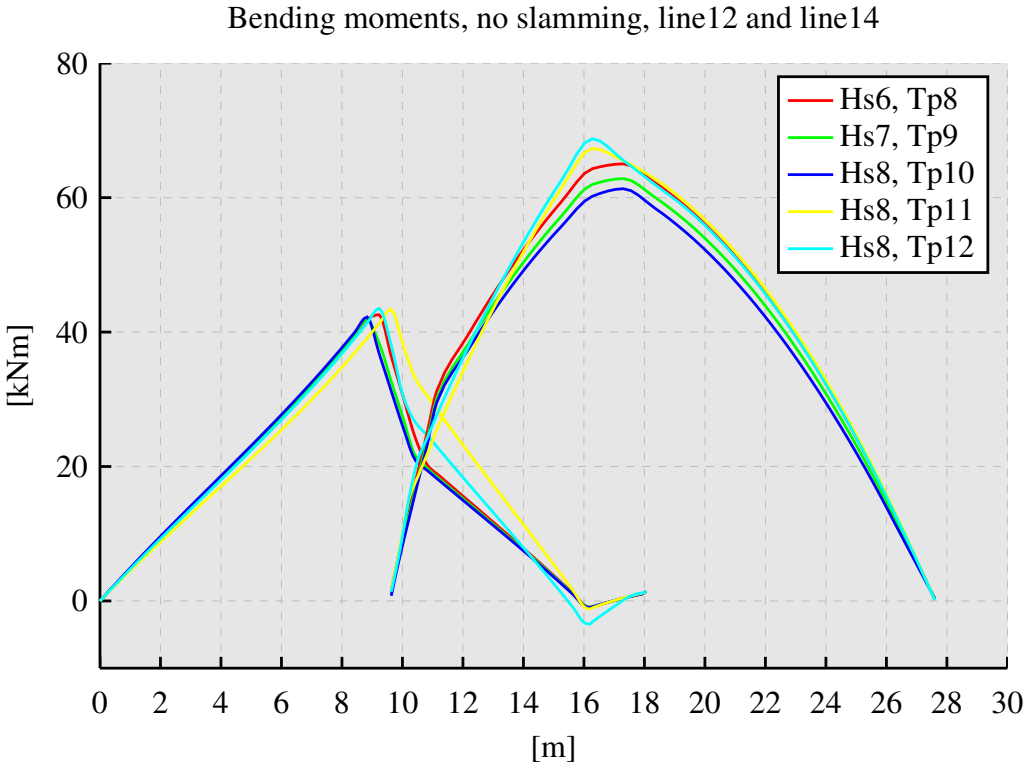

Figure 8.8: Maximum bending moment, without slamming, line12 and line14

the maximum bending moments occur on the cylinder chamber, between 16 and 18 m from the tension ring. This is the location of the contact point between the head of the rod and the cylinder. Correspondingly, the largest bending moments for the rod are at the contact points between the rod and the pack box, between 8 and 10 m from the tension ring. The maximum bending moments are fairly joined between 60 and 70 kNm for the cylinder, and somewhat above 40 kNm for the rod. The two most severe sea states have the largest maximum bending moments.

For the slamming load case there is an increase in maximum bending moments for all sea states, as displayed in Figure 8.9. For $H_s = 8$ m and $T_p = 12$ s and for $H_s = 8$ m and $T_p = 11$

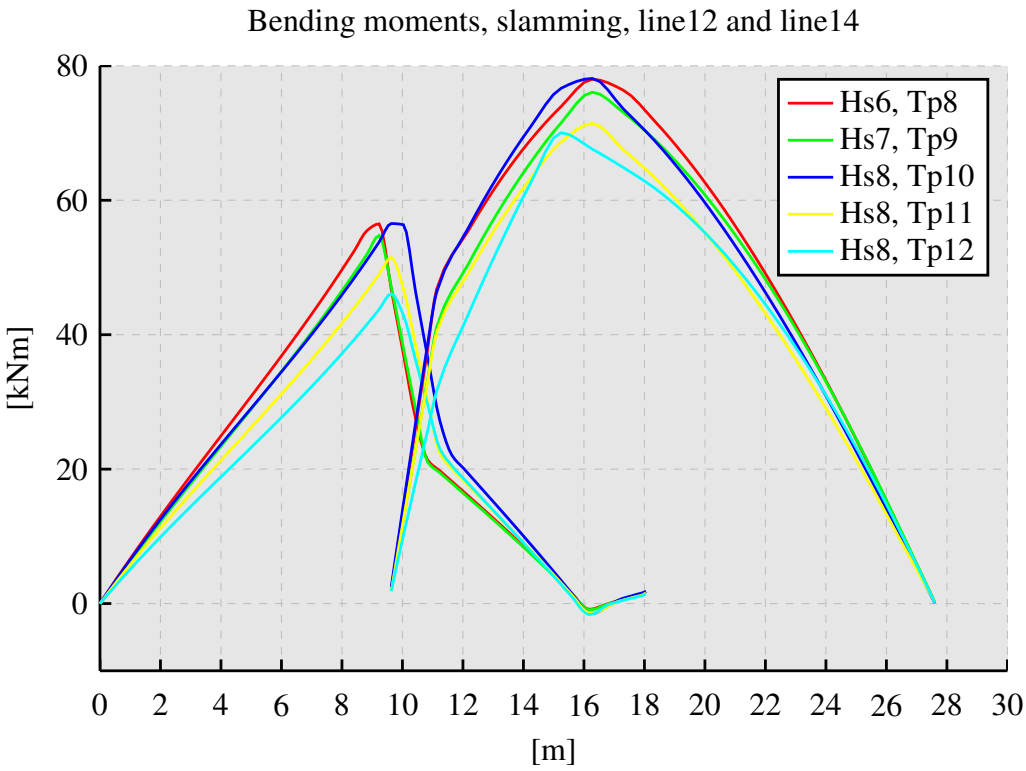

Figure 8.9: Maximum bending moment, with slamming, line12 and line14

s there is only a slight increase in the maximum values, while sea states $H_s = 6$ m and $T_p = 8$ s and $H_s = 8$ m and $T_p = 10$ s have the largest maximum bending moments when slamming is included. The maximum bending moments both with and without slamming for all sea states are found in Table 8.3.

Table 8.3: Maximum bending moments, line 14

	No slamming, [kNm]	With slamming [kNm]	Increase [%]
Hs6 Tp8	65.02	78.01	19.97
Hs7 Tp9	62.83	76.08	21.08
Hs8 Tp10	61.32	78.12	27.39
Hs8 Tp11	67.32	71.43	6.11
Hs8 Tp12	68.77	70.04	1.85

8.4 Fatigue

The significance of slamming loads may be studied through the effects it has on the fatigue life of the tensioner cylinders. The axial stress does not vary significantly along the length of the tensioner, and the bending moments about the local y-axis of the element is found to be the dominating varying force. The location of the maximum bending moment was investigated

with regards to fatigue and damage accumulation.

8.4.1 Rainflow cycles

The time series of the normal stresses in the cross section are calculated from the axial tension and bending moments. WAFO was used for analysis of this data. First the peaks and troughs, or the turning points, of the time series were found. This is shown for a short time duration in Figure 8.10. For some sea states especially, some amount of white noise was observed. An amplitude filter was applied to reduce the noise, filtering out the smallest oscillations, that might have been caused due to some numerical reasons. It is noted that this noise was later found to have close to no effect on damage anyway, as the stress range they represent is of such small order that they fall beneath the fatigue limit of the chosen S-N curve.

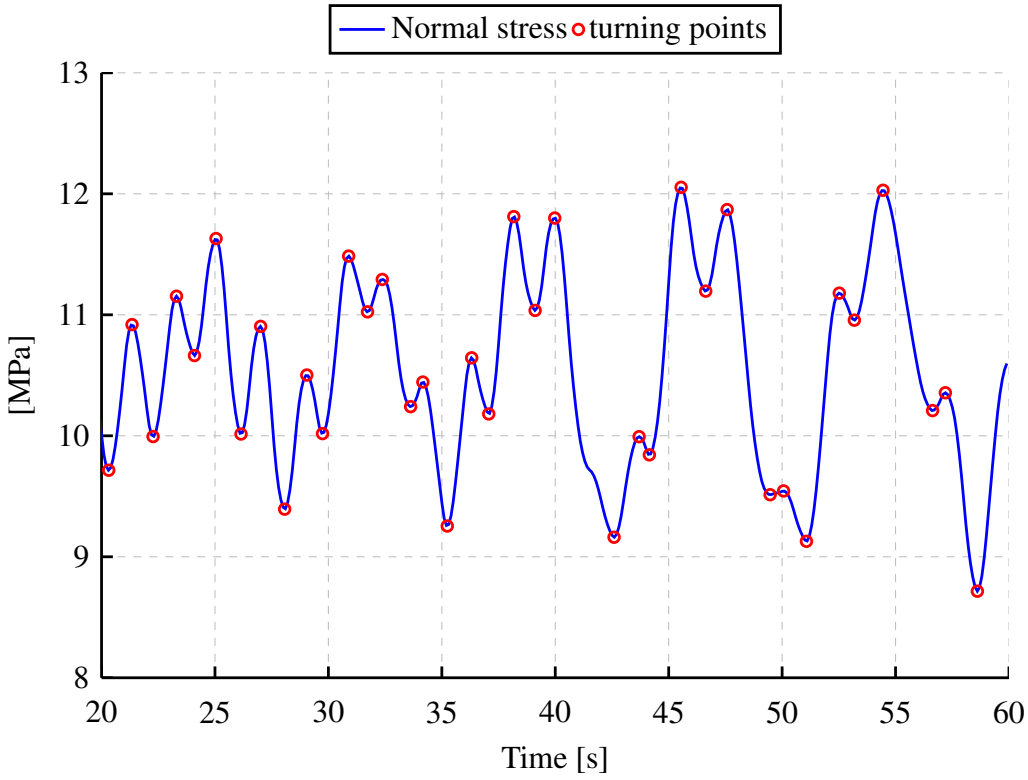

Figure 8.10: Normal stress time series with turning points, Hs6 Tp8

The rainflow cycles were counted, according to their definition found in Section 5.3. The results of the cycle count are shown in Figure 8.11. Each cycle has a maximum and minimum value, a dot is plotted corresponding to these two values. For the smallest amplitude rainflow cycles there is a linear relation between the maximum and minimum values. The larger amplitude cycles move away from the linear line towards larger maximum values. In the case of the second load model including slamming, there is an increase of high-amplitude cycles, as well as increased scattering.

The cycles are counted and arranged by amplitude into a histogram chart, shown in Fig-

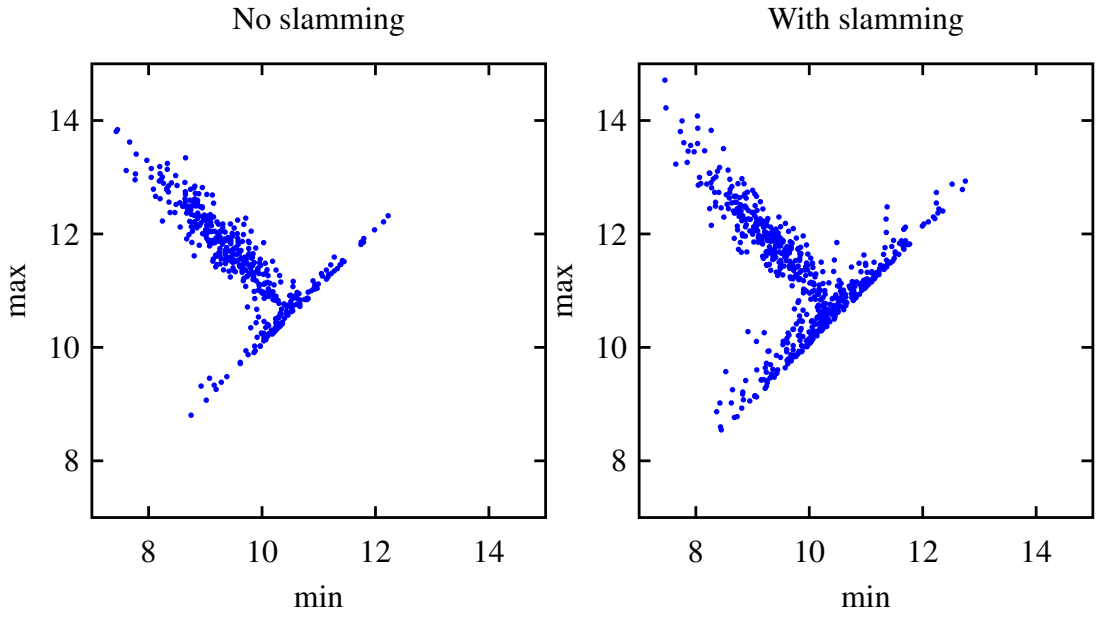

Figure 8.11: Rainflow cycle count, Hs8 Tp12

ure 8.12. As the histogram shows, there is a large increase of low-amplitude cycles. In some instances, the largest amplitudes have increased.

The intention of these figures are to illustrate that slamming effects the rainflow cycles by

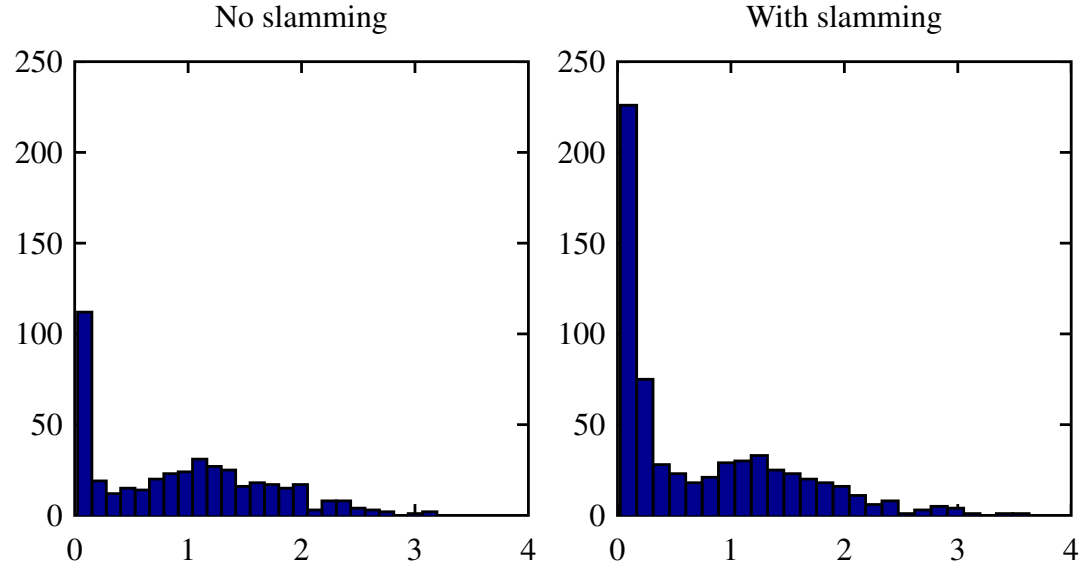

Figure 8.12: Rainflow amplitude distribution, Hs8 Tp12

slightly increasing the amount of energy in the response of the tensioner cylinder, especially of the smallest oscillations. The amount of total cycles are found in Table 8.4. There is an increase of total cycles for all sea states, mostly so for the two most severe sea states.

Table 8.4: Number of rainflow cycles after 1 hour simulation

	Rainflow cycles, 1 hour	
	No slamming	With slamming
Hs6 Tp8	1653	1741
Hs7 Tp9	1821	1860
Hs8 Tp10	1018	1160
Hs8 Tp11	652	854
Hs8 Tp12	436	626

8.4.2 Fatigue damage

Usually, it is the smallest amplitude cycles that are of concern with regards to fatigue life and damage accumulation, because they are the most numerous. The accumulated damage is found in Table 8.5.

Table 8.5: Accumulated damage after 1 hour simulation

	Accumulated damage, 1 hour	
	No slamming	With slamming
Hs6 Tp8	$1.0448 \cdot 10^{-14}$	$1.8281 \cdot 10^{-14}$
Hs7 Tp9	$7.337 \cdot 10^{-15}$	$1.4248 \cdot 10^{-14}$
Hs8 Tp10	$5.4019 \cdot 10^{-15}$	$1.2623 \cdot 10^{-14}$
Hs8 Tp11	$8.5531 \cdot 10^{-15}$	$1.4678 \cdot 10^{-14}$
Hs8 Tp12	$1.619 \cdot 10^{-14}$	$2.0307 \cdot 10^{-14}$

It is clear that the large increase of low-amplitude oscillations have a large effect on the fatigue life of the tensioner cylinder. The increase varies between 25.43 and 133.67 % for the different sea states, the largest being for $H_s = 8$ m and $T_p = 10$ m.

Chapter 9

Concluding remarks

9.1 Conclusion

The intention of the work during this thesis has been to investigate the significance of including slamming loads into the load model in a time domain simulation of the response of a marine drilling riser with a complete pipe-in-pipe heave compensation system. The slender marine structure simulation program Riflex was used. Simulations for 5 severe sea states were run in Riflex, both with and without slamming forces. The comparison has been on the basis of load formulation and magnitude on one hand, and effects on the time domain simulation on the other. Conclusions from the thesis include:

- The time increment used during time domain analysis is crucial for the result. Too large increments tend to over-estimate the slam force and do not adequately describe the force over time. This leads to long analysis time and large amounts of data.

- The results obtained regarding the force magnitudes were substantially smaller than those achieved in previous works on the subject, most likely due to differences in choice of wave kinematics. Linear wave theory is limited in its capacity for calculating slamming loads because linear waves are not steep enough to impact with a large enough front on the riser, and has relatively small wave particle velocities. This indicates that the slamming model used is unsuited for linear waves. Indeed, it seems questionable that slamming loads occur in waves applicable for linear theory at all.

- A time series of the response of the hydraulic cylinder show that there are very small variations between the two load models. The standard deviations show small increases for all sea states. It seems that the steepness of the sea state is influential to the significance of slamming loads

- The response spectra show no indication of any structural vibrations in the frequency range of slamming loads. The spectra including slamming loads are observed to contain somewhat more energy, but have close to identical shapes.

- There are observed occasional higher amplitude oscillations of the maximum bending moment on the hydraulic cylinder when slamming is included. This is also reflected in the slightly larger standard deviations for all sea states. The largest maximum bending moment during the one hour simulation is found to have increased for all sea states, at the most 27.39 %.
- The fatigue life of the hydraulic cylinder is found to be influenced by including slamming. The total amount of rainflow cycles is increased, especially on the number of low stress range cycles, but also somewhat to the amount of high stress range cycles. The accumulated damage has at most a growth of 133.67 %, which is considerable

Slamming loads in conditions which are applicable for linear theory are small compared to Morison forces. In addition, the duration of a slamming load using linear theory is far to long to cause structural vibrations on the hydraulic cylinders, which have very short natural periods. On the other hand, a significant effect of the fatigue life of the tensioner cylinders can be attributed to slamming loads. The increase of maximum bending moment occurring during the one hour simulation is also significant for some sea states, and might be of interest with regards to maximum permissible values for design purposes. Altogether it is doubtful whether slamming should be included in the general load model for marine riser analyses. It can appear more relevant to investigate slamming loads in individual cases with the application of sufficiently steep or even breaking waves. In time domain simulations using linear wave theory, slamming loads do not represent a significant factor.

9.2 Further work

Due to lack of time, a statistical consideration of the slamming loads has been omitted. Such a consideration could have included establishing a probability distribution and even Monte Carlo simulations. The parameter variation used in the simulations in this thesis are few and simple. For further work it would be natural to take use of the load possibilities already offered by Riflex. Current forces have been omitted in this thesis, but it might be interesting to investigate the effects of current have on slamming forces. There are some challenges in this regard because little is known about the physics of the combination of wave crests and current.
Riflex provides the possibility of regular wave simulations using second-order Stokes waves, which are more suitable for modeling of slamming forces. On this note, investigating even higher-order wave theories, such as fifth-order Stokes waves and Stream Function Theory could provide an even better basis to simulate slamming forces on cylinder structures.

Bibliography

[1] *RIFLEX Theory Manual*.

[2] *SIMO Theory Manual*.

[3] *Handbook of Offshore Engineering*. Elsevier Ltd., 2005.

[4] *Subsea Pipelines and Risers*. Elsevier Ltd., 2005.

[5] *Advanced Engineering Mathematics*. John Wiley and Sons, inc, 2006.

[6] *Dynamics of Structures, Theory and Applications to Earthquake Engineering*. Pearson, 2007.

[7] *Marin Dynamikk, Uregelmessig sjø*. Institute for marine technology, 2007.

[8] S.Haver A.J.Kalleklev Y.L.Wu E.Lehn A. Nestegård, K.Hagatun. Resonant vibrations of riser guide tubes due to wave impact. Proceedings of OMAE2004, OMAE04-51545 2004.

[9] Maritimt magasin, September 2009.

[10] B.Pettersen. *Kompendium for TMR 4247 Marin Teknikk 3, Hydrodynamikk*. Institutt for Marin Teknikk 2007.

[11] P.A. Brodtkorb, P. Johannesson, G. Lindgren, I. Rychlik, J. Rydén, and E. Sjö. WAFO - a Matlab toolbox for the analysis of random waves and loads. In *Proc. 10'th Int. Offshore and Polar Eng. Conf., ISOPE, Seattle, USA*, volume 3, pages 343–350, 2000.

[12] DNV RP C203. Fatigue design of offshore steel structures.

[13] DNV RP C205. Environmental conditions and environmental loads 2007.

[14] C.T.Stansberg C.Pakozdi, T.E.Kendon. Breaking wave impact on a platform column: an introductory cfd study. Proceedings of OMAE2011, OMAE2011-49976 2011.

[15] Marilena Greco. Tmr 4215:sea loads lecture notes 2012.

[16] N.G.Jacobsen H.Bredmose. Vertical wave impacts on offshore wind turbine inspection platforms. Proceedings of OMAE2011, OMAE2011-49785 2011.

[17] P.A.Weynberg I.M.C.Campbell. Measurement of parameters affecting slamming. Technical report, Wolfson unit for Marine Technology Report 1980.

[18] J.D.Wheeler. Method for calculating forces produced by irregular waves. Offshore Technology Conference 1969.

[19] T.Rung N.A.Lange. Impact tests in pure and aerated water. Proceedings of OMAE2011, OMAE2011-49725 2011.

[20] A. Nestegård. Personal conversation.

[21] O.M.Faltinsen. *Sea loads on ships and offshore structures*. Cambridge University Press 1990.

[22] O.M.Faltinsen. Slamming in marine applications. *Theoretical Easter Physics*, 2004.

[23] Csaba Pakozdi. Marintek review. Technical report, Marintek 2012.

[24] Samuel Ransau. Lecture notes for course: Numerical methods in marine hydrodynamics 2012.

[25] R.A.Dalrymple R.G.Dean. *Water wave mechanics for engineers and scientists*. World Scientific 1984.

[26] S.Sævik C.M.Larsen R.Sten, M.R.Hansen. Force variations of heave compensating system for ultra-deepwater drilling risers. Proceedings of OMAE2010, OMAE2010-20011.

[27] C.P. Sparks. *Fundamentals of Marine Riser Mechanics*. PennWell 2007.

[28] S.Sævik. Lecture notes in offshore pipeline technology.

[29] Ronny Sten. *Dynamic Simulation of Deep Water Drilling Risers with Heave Compensating System*. PhD thesis, NTNU 2012.

Appendix A

Matlab code

A.1 Slamming load calculations

```
%%%%%%%%%%%%%%%%%%%%%%%%--Parent function of SlamLoad--%%%%%%%%%%%%%%%%%%%%%%%%

tic
clear all
clc

g=9.81;                             %Gravitational constant
d=204.5;                            %Model water depth
rho=1025;
D=0.660;                             %Riser diameter

%%%%%%%%%%%%%%%%%%%%%%%%%%%%%%%%%%%%%%%%%%%%%%%%%%%%%%%%%%%%%%%%%%%%%%%%%%%%%%%
Hs=8;
Tp=12;

%%%%%%%%%%%%%%%%%%%%%%%%%%%%%%%%%%%%%%%%%%%%%%%%%%%%%%%%%%%%%%%%%%%%%%%%%%%%%%%
simtime=120;                         %Length of simulation time [s]
dt=0.004;                             %Time increment used in Riflex
incnum=simtime/dt;                   %Number of time steps in simulation
nn=250;                              %Number of nodes in line 8:

%%%%%%%%%%%%%%%%%%%%%%%%%%%%%%%%%%%%%%%%%%%%%%%%%%%%%%%%%%%%%%%%%%%%%%%%%%%%%%%
R_wavedt=0.5;                           %Riflex wave simulation time
    increment
R_wavesimtime=3800;                     %Riflex wave simulation time
R_waveincnum=R_wavesimtime/R_wavedt;    %Number of wave simulation time
    increments

%%%%%%%%%%%%%%%%%%%%%%%%%%%%%%%%%%%%%%%%%%%%%%%%%%%%%%%%%%%%%%%%%%%%%%%%%%%%%%%
```

```
wavedt=0.004;                          %Matlab-generated wave simulation time
    increment
wavesimtime=simtime;                 %Matlab-generated wave simulation time
waveincnum=wavesimtime/wavedt;       %Number of wave simulation time
   increments

%%%%%%%%%%%%%%%%%%%%%%%%%%%%%-Specifying seastate-%%%%%%%%%%%%%%%%%%%%%%%%%%%%%

[folder,lowfreq,highfreq]=casespec(Hs,Tp);

%%%%%%%%%%%%%%%%%%%%%%%-Reading nodal displacement file-%%%%%%%%%%%%%%%%%%%%%%%

[timesteps,noddisp_x,noddisp_y,noddisp_z,A]=bin_read(fullfile(folder,'
   sima_noddis.bin'),nn,incnum);

%%%%%%%%%%%%%%%%%-Numerical differentiation of nodal displacements-%%%%%%%%%

[nodvel_x]=nodaldispvel(incnum,dt,nn,timesteps,noddisp_x,noddisp_y,
   noddisp_z);

%%%%%%%%%-Calculation of irregular wave elevation and kinematics-%%%%%%%%%%

[compn,freq,amp,phase,time,timeriflex,zs,u,ncpup,zeta_tot]=waveel(g,nn,
   R_wavesimtime,R_wavedt,R_waveincnum,wavesimtime,wavedt,dt,waveincnum,
   timesteps,d,incnum,lowfreq,highfreq,folder);

%%%%%%%%%%%%%-Calculation of relative velocities at riser nodes-%%%%%%%%%%%%%

[vertpos,velint,dL,nvertpos,rel_vel]=nodevelocities(timesteps,d,incnum,nn,
   noddisp_z,nodvel_x,zs,u,ncpup);

%%%%%%%%%%%%%%%%%-Calculating wave slam forces on nodes-%%%%%%%%%%%%%%%%%%%

[sumSlam,dFslam,s]=waveslam(timesteps,incnum,vertpos,velint,zeta_tot,D,time
   ,rho,dt,dL,nvertpos,rel_vel,simtime,Hs,Tp);

%%%%%%%%%%%%%%%%%-Writing forces to file for use in Sima-%%%%%%%%%%%%%%%%%%%

writeslam(incnum,timesteps,nvertpos,sumSlam,dFslam,folder);
toc
```

```
function [folder,lowfreq,highfreq]=casespec(Hs,Tp)

if Hs==6 && Tp==8
    folder=('C:\Users\Balder\Documents\Masteroppgave\Matlab\Hs6Tp8');
    lowfreq=0.3927;
    highfreq=3.5328;
elseif Hs==7 && Tp==9
    folder=('C:\Users\Balder\Documents\Masteroppgave\Matlab\Hs7Tp9');
    lowfreq=0.3482;
    highfreq=3.1401;
elseif Hs==8 && Tp==10
    folder=('C:\Users\Balder\Documents\Masteroppgave\Matlab\Hs8Tp10');
    lowfreq=0.3129;
    highfreq=2.8256;
elseif Hs==8 && Tp==11
    folder=('C:\Users\Balder\Documents\Masteroppgave\Matlab\Hs8Tp11');
    lowfreq=0.2853;
    highfreq=2.5679;
elseif Hs==8 && Tp==12
    folder=('W:\Matlab\Hs8Tp12');
    lowfreq=0.2608;
    highfreq=2.3547;
end

end
```

```
function [timesteps,noddisp_x,noddisp_y,noddisp_z,A] = bin_read(name,nn,
    incnum)%'206m_PIP_utenslam_noddis.bin')
id = fopen(name);
%number of columns in .bin file, 3 dofs per node
ncolumns=nn*3+3;
A = fread(id,[ncolumns incnum],'float32');
A = A';
%removing unuseful FORTRAN code in first and last column
A(:,1) = [];
A(:,end) = [];

%%%%%%%%%%%%%%%%%%%%%%%%%%%%%-Timestep vector-%%%%%%%%%%%%%%%%%%%%%%%%%%%%
timesteps=zeros(incnum,1);
for i=1:incnum
    timesteps(i,1)=A(i,1);
end
%%%%%%%%%%%%%%%%%%-nodal x-displacements for all timesteps-%%%%%%%%%%%%%%%
noddisp_x=zeros(incnum,nn);
tellerx=0;
for i=2:3:ncolumns-2
    tellerx=tellerx+1;
    for j=1:incnum
        noddisp_x(j,tellerx)=A(j,i);
    end
end
%%%%%%%%%%%%%%%%%%-nodal y-displacements for all timesteps-%%%%%%%%%%%%%%%
noddisp_y=zeros(incnum,nn);
tellery=0;
for i=3:3:ncolumns-1
    tellery=tellery+1;
    for j=1:incnum
        noddisp_y(j,tellery)=A(j,i);
    end
end
%%%%%%%%%%%%%%%%%%-nodal z-displacements for all timesteps-%%%%%%%%%%%%%%%
noddisp_z=zeros(incnum,nn);
tellerz=0;
for i=4:3:ncolumns
    tellerz=tellerz+1;
    for j=1:incnum
        noddisp_z(j,tellerz)=A(j,i);
    end
end
disp('bin_read done')
end
```

```
function [nodvel_x] = nodaldispvel(incnum,dt,nn,timesteps,noddisp_x,
    noddisp_y,noddisp_z)

%%%%%-numerically differentiating displacements to obtian velocities-%%%%%
nodvel_x=zeros(incnum,nn);
for i=1:incnum
    for j=1:nn
        if i==1
            nodvel_x(i,j)=(noddisp_x(i+1,j)-noddisp_x(i,j))/dt;
        elseif i==incnum
            nodvel_x(i,j)=(noddisp_x(i,j)-noddisp_x(i-1,j))/dt;
        else
            nodvel_x(i,j)=(noddisp_x(i+1,j)-noddisp_x(i-1,j))/(2*dt);
        end
    end
end

%%%%%%-plotting displacement of riser node around MWL to illustrate-%%%%%%%

node located around MWL:
nodemwl=nn/2+2;

displvel=figure;
[AX,H1,H2] = plotyy(timesteps(1:600,1),noddisp_x(1:600,nodemwl),timesteps
    (1:600,1),nodvel_x(1:600,nodemwl),'plot');
set(get(AX(1),'Ylabel'),'String',['Displacement, node ',num2str(nodemwl) '
    [m]'])
set(get(AX(2),'Ylabel'),'String',['Velocity, node ',num2str(nodemwl) ' [m/s
    ]'])
xlabel('Time [s]')
set(H1,'LineWidth',1)
set(H2,'LineWidth',1.2)
title('Nodal displacement and velocity')
matlab2tikz(strcat('displvel.tikz'), 'height', '\figureheight', 'width', '\
    figurewidth','showInfo', false,'checkForUpdates',false);
fclose('all');
fpath=('C:\Users\Balder\Documents\Masteroppgave\Latex\tikz');
movefile(strcat('displvel.tikz'),fpath)
fpath=('C:\Users\Balder\Documents\Masteroppgave\Latex\pics');
saveas(displvel,fullfile(fpath,'displvel.png'))
disp('nodaldispvel done')
end
```

```
function [compn,freq,amp,phase,time,timeriflex,zs,u,ncpup,zeta_tot] =
    waveel(g,nn,R_wavesimtime,R_wavedt,R_waveincnum,wavesimtime,wavedt,dt,
    waveincnum,timesteps,d,incnum,lowfreq,highfreq,folder)

%%%%%%%%%%%%%%%%%%%%-reads wave elevation time series-%%%%%%%%%%%%%%%%%%%%%%%%
waveelevation=fopen(fullfile(folder,'waveel.txt'),'r');

zeta_riflex=fscanf(waveelevation,'%f',[inf]);

%%%%%%%%%%%%%%%%%-Reads fourier wave components input file-%%%%%%%%%%%%%%%%%

fourwavecomp=fopen(fullfile(folder,'fourwavecomp.txt'),'r');

components=fscanf(fourwavecomp,'%f',[4,inf])';

%Building array structure
wavecomp.n=components(:,1);
wavecomp.freq=components(:,2);
wavecomp.amp=components(:,3);
wavecomp.phas=components(:,4);

compn=wavecomp.n;
% freq=wavecomp.freq;
amp=wavecomp.amp;
phase=wavecomp.phas*(pi/180);          %converting to radians

%number of frequency components
nfreq=length(phase');

%%%%%%%%%%%%%%%%%%%%%%%%%%%%%%%%%%%%%%%%%%%%%%%%%%%%%%%%%%%%%%%%%%%%%%%%%%%%%%
%%%%%%%%%%%-Generating irregular wave time series surface profile-%%%%%%%%%%
%%%%%%%%%%%%%%%%%%%%%%%%%%%%%%%%%%%%%%%%%%%%%%%%%%%%%%%%%%%%%%%%%%%%%%%%%%%%%%

time=(0:wavedt:wavesimtime)';       %Generating wave timestep vector

timeriflex=(R_wavedt:R_wavedt:wavesimtime);
length(timeriflex);

%%%%%%%%%%%%%%Calculating frequencies with correct number of digits%%%%%%%%%%
domega=(highfreq-lowfreq)/(nfreq-1);
for i=1:nfreq
    if i==1
        freq(i,1)=lowfreq;
    else
        freq(i,1)=freq(i-1,1)+domega;
    end
end
```

```
tic
for i=1:waveincnum
    for j=1:nfreq
        zeta_j(j,i)=wavecomp.amp(j,1)*cos(freq(j,1)*timesteps(i,1)+(
            wavecomp.phas(j,1)*pi/180));
    end
    zeta_tot(1,i)=sum(zeta_j(:,i));
end
toc

irregwave=figure;
hold on
plot(timeriflex,zeta_riflex(1:wavesimtime*2))      %Plotting wave elevation
    by Riflex
plot(timesteps,zeta_tot,'r')  %Plotting wave elevation by Fourier
   components
xlabel('Time [s]')
ylabel('Elevation [m]')
legend('Riflex wave eleveation','Re-produced wave elevation','Location','
   Best')
fpath=('C:\Users\Balder\Documents\Masteroppgave\Latex\pics');
saveas(irregwave,fullfile(fpath,'irregwave.pdf'))

%%%%%%%%%%%%%%%%%%%%%%%%%%%%%%%%%%%%%%%%%%%%%%%%%%%%%%%%%%%%%%%%%%%%%%%%%%%%
%%%%%%%%%%%%%%%%%%-Generating irregular wave velocities-%%%%%%%%%%%%%%%%%%
%%%%%%%%%%%%%%%%%%%%%%%%%%%%%%%%%%%%%%%%%%%%%%%%%%%%%%%%%%%%%%%%%%%%%%%%%%%%

%%%%%%%%%%%%%%-Wheeler stretching to the velocity profile-%%%%%%%%%%%%%%%%%
%%%%%%%-Relating zs coordinate to wave height for each time step-%%%%%%%%%

ncp=1000;                                  %Number of calculation points from
   free surface to bottom
ncpup=200;                                 %Number of calculation points from
   top to a distance down the riser
zs=zeros(ncp,incnum,'single');            %Defining zs coordinate matrix

for i=1:incnum
    dwh=(zeta_tot(1,i)+d)/(ncp-1);         %Increment length for each time
       step
    for j=1:ncp
        if j==1
            zs(j,i)=zeta_tot(1,i);    %Top coordinate is equal to wave
               elevation
        else
            zs(j,i)=zs(j-1,i)-dwh;    %coordinates are distributed downwards
        end
    end
end
```

```
%%%%%%%%%%%%%%%—Calculating velocities for each timestep,—%%%%%%%%%%%%%%%%%%
%%%%%%%%%%%%%%%%%%%—at each node, for every freq—%%%%%%%%%%%%%%%%%%%%%%%%%%


z=zeros(ncp,incnum,'single');
u=zeros(ncpup,incnum,'single');

wavenumber=freq.^2./g;       %calculating wavenumber

progress=(0:incnum/40:incnum);

freqamp=freq.*amp;
tic
for i=1:incnum
    if zeta_tot(1,i)>=0
         for j=1:ncpup
             z(j,i)=(zs(j,i)-zs(1,i))/(1+(zs(1,i)/d));
             for k=1:nfreq
                 u(j,i)=u(j,i)+freqamp(k,1)*exp(wavenumber(k,1)*z(j,i))*cos
                     (freq(k,1)*timesteps(i,1)+phase(k,1));
             end
         end
    end
    for l=1:40
        if i==progress(l)
            fprintf('status: %d percent\n',(progress(l)*(100/incnum)));
        end
    end
end
toc
clear u_j
clear z
%%%%%%%%%%%%%%%—Plotting irregular velocity profile—%%%%%%%%%%%%%%%%%%%%%%%

irregwavevel=figure;
hold on
narrowpoints=20;
velocitypos=338;
v=0;
x=0;
v(1:narrowpoints,1)=0;
x(1:narrowpoints)=velocitypos*dt;
quiver(x',zs(1:narrowpoints,velocitypos),u(1:narrowpoints,velocitypos),v,'
    Color','k');
line([velocitypos*dt velocitypos*dt],[zs(narrowpoints,velocitypos) zs(1,
    velocitypos)],'Color','k')
plot(timesteps(300:400),zeta_tot(300:400),'k','LineWidth',1.5)
```

```
xlabel('u')
ylabel('z','rot',0)
axis([7 20 -12 5])
matlab2tikz(strcat('irregwavevel.tikz'), 'height', '\figureheight', 'width'
    , '\figurewidth','showInfo', false,'checkForUpdates',false);
fclose('all');
fpath=('C:\Users\Balder\Documents\Masteroppgave\Latex\tikz');
movefile(strcat('irregwavevel.tikz'),fpath)
fpath=('C:\Users\Balder\Documents\Masteroppgave\Latex\pics');
saveas(irregwavevel,fullfile(fpath,'irregwavevel.png'))
disp('waveeel done')
end
```

```
function [vertpos,velint,dL,nvertpos,rel_vel]=nodevelocities(timesteps,d,
    incnum,nn,noddisp_z,nodvel_x,zs,u,ncpup)

%%%%%%%%%%%%%%%%%%-Assigning nodes above MWL to vector-%%%%%%%%%%%%%%%%%%%%%
for i=1:nn
    vertpos(i,1)=noddisp_z(1,nn+1-i);
end

nvertpos=length(vertpos');              %Number of vertical positions above
    MWL
dL=vertpos(1,1)-vertpos(2,1);           %Distance between nodes

%%%%%%%%%%%%%%%-Allocating wave particle velocities to nodes-%%%%%%%%%%%%%%%

for i=1:incnum
    velint(:,i)=interp1(zs(1:ncpup,i),u(1:ncpup,i),vertpos,'linear',0);  %
        velocity interpolated at the riser coord.
end

%%%%%%%%%%%%%%%%%%-Allocating relativ velocity to nodes-%%%%%%%%%%%%%%%%%%%%%

nodvel_x=flipud(nodvel_x');

for i=1:incnum

    for j=1:nvertpos
        if velint(j,i)~=0
        rel_vel(j,i)=velint(j,i)+nodvel_x(j,i);
        end
    end
end
disp('nodevelocities done')
end
```

```
function [sumSlam,dFslam,s]=waveslam(timesteps,incnum,vertpos,velint,
    zeta_tot,D,time,rho,dt,dL,nvertpos,rel_vel,simtime,Hs,Tp)

U=zeros(nvertpos,1);                          %Velocity during submergence
s=zeros(nvertpos,incnum);                  %Submergence
dFslam=zeros(nvertpos,incnum,'single');          %Slamming forces on each
    node
sumSlam=zeros(incnum,1);
%%%%%%%%%%%%%%%%%-Calculating slamming forces on each node-%%%%%%%%%%%%%%%%%

for i=1:incnum
    if zeta_tot(1,i) >= 0                %Slamming force above MWL
        for j=1:nvertpos
                if s(j,i)<=D && vertpos(j,1)<=zeta_tot(1,i) && vertpos(j,1)
                    >=0
                    if s(j,i)==0 && rel_vel(j,i)>0
                        U(j,1)=rel_vel(j,i);  %Constant velocity during
                            submergence
                    end
                    Cs=5.15*((D/(D+19*s(j,i)))+(0.107*s(j,i)/D));
                    dFslam(j,i)=0.5*rho*Cs*D*U(j,1)^2;
                    if i==incnum;
                        %no further submergence, last time step
                    else
                        s(j,i+1)=U(j,1)*dt+s(j,i);
                    end

                elseif s(j,i)>D && vertpos(j,1)<=zeta_tot(1,i) && vertpos(j
                    ,1)>=0
                    s(j,i+1)=s(j,i);
                    U(j,1)=0;
                else
                    s(j,i+1)=0;
                end
        end
    end
    sumSlam(i,1)=dL*trapz(dFslam(:,i));     %Sum of nodal slamming forces
        on riser

end

%figure with time series of slam load and wave profile
waveelslamtimeseries=figure;
dur=incnum;                        %duration of plot length
[AX,H1,H2] = plotyy(time(1:dur,1),zeta_tot(1,1:dur),timesteps(1:dur,1),
    sumSlam(1:dur,1),'plot');
set(get(AX(1),'Ylabel'),'String','Elevation [m]')
set(get(AX(2),'Ylabel'),'String','Force [N]')
```

```
xlabel('Time [s]')
set(H1,'LineWidth',1)
set(H2,'LineWidth',1)
title(['Wave elevation and slamming forces, Hs',num2str(Hs),'Tp',num2str(Tp
    )])
legend('Wave elevation','Slam force')
fpath=(['W:\Matlab\Hs',num2str(Hs),'TP',num2str(Tp)]);
saveas(waveelslamtimeseries,fullfile(fpath,['waveelslamtimeseriestestHs',
    num2str(Hs),'Tp',num2str(Tp),'.png']))
disp('waveslam done')
end
```

```
function [] = writeslam(incnum,timesteps,nvertpos,sumSlam,dFslam,folder)
disp('writing load file')
fp=fopen(fullfile(folder,'slamloads.asc'),'w');      %Opening textfile,
    ascii format:asc

fprintf(fp,'%s\n','''NTDFO');
fprintf(fp,'%d\n',incnum);

for i=1:incnum

    fprintf(fp,'%s\t%s\n','''MDCOMP','TIMEDFO');
    fprintf(fp,'%d %f\n',nvertpos,timesteps(i,1));
    fprintf(fp,'%s\n','''RLMAG');
    for j=1:nvertpos
        fprintf(fp,'%f\n',dFslam(j,i)/1000);
    end

end
fclose(fp);

end
```

A.2 Selection of post-process

```
%%%%%%%%%%%%%%%%%%%%%%%%--Parent function of PostProcess
    --%%%%%%%%%%%%%%%%%%%%%%%%

%%%%%%%%%%%%%%%%%%%%%%%%%%%%%%%%-Seastate parameters-%%%%%%%%%%%%%%%%%%%%%%%%%%%%%%%%
tic
clear all
clc
n_seastates=5;
for s=5:n_seastates
    if s==1
        Hs=6;
        Tp=8;
    elseif s==2
        Hs=7;
        Tp=9;
    elseif s==3
        Hs=8;
        Tp=10;
    elseif s==4
        Hs=8;
        Tp=11;
```

```
    else
        Hs=8;
        Tp=12;
    end
%%%%%%%%%%%%%%%%%%%%%%%%%%-output file parameters-%%%%%%%%%%%%%%%%%%%%%%%%%%%%
nsegments=25;                    %number of segments in forces file
    6*2*2+1=25
masterel_seg1=40;                 %number of elements in master pipe,
    segment 1
masterel_seg2=15;                 %number of elements in master pipe,
    segment 2
slaveel_seg1=5;                  %number of elements in slave pipe, segment
    1
slaveel_seg2=16;                  %number of elements in slave pipe, segment
     2
masternode_seg1=masterel_seg1+1;   %number of nodes in master pipe, segment
     1
masternode_seg2=masterel_seg2;   %number of nodes in master pipe, segment 2
slavenode_seg1=slaveel_seg1+1;     %number of nodes in slave pipe, segment
    1
slavenode_seg2=slaveel_seg2;     %number of nodes in slave pipe, segment 2
ncylinders=1;                    %number of cylinders
masterlength_seg1=16.049;        %length of master line, segment 1
masterlength_seg2=2;             %length of master line, segment 2
slavelength_seg1=1.5;            %length of slave line, segment 1
slavelength_seg2=16.47;          %length of slave line, segment 2
%%%%%%%%%%%%%%%%%%%%%-Dynamic simulation parameters-%%%%%%%%%%%%%%%%%%%%%%%%%%
simtime=3600;                      %Length of simulation time [s]
dt=0.004;                          %Time increment used in Riflex
incnum=simtime/dt;                %Number of time steps in simulation
nn=250;                           %Number of nodes in line 8:
%%%%%%%%%-Matlab-generated irregular wave time series parameters-%%%%%%%%%%
wavedt=0.1;                        %Matlab-generated wave simulation time
    increment
wavesimtime=simtime;               %Matlab-generated wave simulation time
waveincnum=wavesimtime/wavedt;     %Number of wave simulation time
    increments
%%%%%%%%%%%%%%%%%%%%%%%%%%%%%-Specifying seastate-%%%%%%%%%%%%%%%%%%%%%%%%%%%%%

[folder1,folder2]=casespecpost(Hs,Tp);

%%%%%%%%%%%%%%%%%%%-Reading element forces file-%%%%%%%%%%%%%%%%%%%%%%%%%%

[Bendingmoments_withoutslam,Bendingmoments_slam,A,B,cylinder_elemnum,
    timesteps]=postbin_read(forces1,forces2,nsegments,masterel_seg1,
    masterel_seg2,slaveel_seg1,slaveel_seg2,ncylinders,incnum,s);

%%%%%%%%%%%%%%%%%%%%%%-Reading nodal displacement file-%%%%%%%%%%%%%%%%%%%%%%
```

```
[Displacements_withoutslam,Displacements_slam,zeta,A]=
    postbin_displacementread(disp1,disp2,waveelevation,masternode_seg1,
    masternode_seg2,slavenode_seg1,slavenode_seg2,incnum,s);

%%%%%%%%%%%%%%%%%%-Plotting maximum bending moment on cylinder-%%%%%%%%%%%%%%
if s==1
plotlinebendmom12_ws=zeros(221,n_seastates);
plotlinebendmom14_ws=zeros(221,n_seastates);
plotlinebendmom12_s=zeros(221,n_seastates);
plotlinebendmom14_s=zeros(221,n_seastates);
end
displacement_timeseries(Displacements_withoutslam,Displacements_slam,
    timesteps,Hs,Tp,s,zeta,incnum,simtime)

[masterelem_coord,slaveelem_coord,m_e_n,s_e_n]=maxbendingmoment(
    masterel_seg1,masterel_seg2,slaveel_seg1,slaveel_seg2,ncylinders,
    slavelength_seg1,slavelength_seg2,masterlength_seg1,masterlength_seg2,
    n_seastates,s,folder1,folder2);

%%%%%-Plotting max bending moment time series, independent max points-%%%%%

[maxbendmom_ws,maxbendmom_s]=bendmom_timeseries_indep(
    Bendingmoments_withoutslam,Bendingmoments_slam,s_e_n,slaveel_seg1,
    slaveel_seg2,dt,timesteps,Hs,Tp,s);

%%%%%%-Plotting max bending moment time series, dependent on slam max
    points-%%%%%

[timeseries_max_s]=bendmom_timeseries_dep(Bendingmoments_withoutslam,
    Bendingmoments_slam,s_e_n,slaveel_seg1,slaveel_seg2,timesteps);

%%%%%%%%%%%%%%%%%%%%%%%%%%%%-Fatigue analysis-%%%%%%%%%%%%%%%%%%%%%%%%%%%%%%

[tp_normstress_ws,tp_normstress_s,rfc_normstress_ws,rfc_normstress_s,
    damage_normstress_ws,damage_normstress_s]=fatigue(
    Bendingmoments_withoutslam,Bendingmoments_slam,incnum,timesteps,simtime,
    s);

[S_ws,S_s,xx_ws]=spectrum(Displacements_withoutslam,Displacements_slam,
    timesteps,s);

end
toc
```

```
function [tp_normstress_ws,tp_normstress_s,rfc_normstress_ws,
    rfc_normstress_s,damage_normstress_ws,damage_normstress_s] = fatigue(
    Bendingmoments_withoutslam,Bendingmoments_slam,incnum,timesteps,simtime,
    s)

%%%%%%%%%%%%%%%%%-Calculating normal stresses on cylinder-%%%%%%%%%%%%%%%%%

%%%%%%%%-Calculating geometric properties of cylinder cross-section-%%%%%%%

b=(0.632/2);       %outer radius (from Riflex model)
a=(0.560/2);       %inner radius
A=pi*(b^2-a^2);
I_z=pi*(b^4-a^4)/4;            %second moment of area about local z-axis
I_y=I_z;             %second moment of area about local y-axis


normstress_ws=zeros(incnum,2);
for i=1:incnum
    normstress_ws(i,2)=10^(-3)*(
        Bendingmoments_withoutslam.line14.seg2.element6.axial_force(i)/A+
        Bendingmoments_withoutslam.line14.seg2.element6.mom_y_axis_end1(i)*(
        a/I_z)+
        Bendingmoments_withoutslam.line14.seg2.element6.mom_z_axis_end1(i)*(
        a/I_y));
end
normstress_ws(:,1)=timesteps(:);

normstress_s=zeros(incnum,2);
for i=1:incnum
    normstress_s(i,2)=10^(-3)*(
        Bendingmoments_slam.line14.seg2.element6.axial_force(i)/A+
        Bendingmoments_slam.line14.seg2.element6.mom_y_axis_end1(i)*(a/I_z)+
        Bendingmoments_slam.line14.seg2.element6.mom_z_axis_end1(i)*(a/I_y))
        ;
end
normstress_s(:,1)=timesteps(:);

%%%%%%%%%%%%%%%%%%-Finding turning points with WAFO-%%%%%%%%%%%%%%%%%%%%%%%

addpath 'W:\Matlab\WAFO\wafo25'   %path to wafo package
initwafo('full',1,1)                                                    %
   Opening wafo package
tp_normstress_ws=dat2tp(normstress_ws,0.05);
                                  %finding turning points
tp_normstress_s=dat2tp(normstress_s,0.05);

rfc_normstress_ws=tp2rfc(tp_normstress_ws);                              %
   rainflow counting
```

```
rfc_normstress_s=tp2rfc(tp_normstress_s);
amp_normstress_ws=cc2amp(rfc_normstress_ws);
                                    %RFC amplitudes
amp_normstress_s=cc2amp(rfc_normstress_s);
%%%%%%%%%%%%%%%%%%%%-Calculating damage from S-N curve-%%%%%%%%%%%%%%%%%%%%%%
beta=4.0;                                           %S-N curve parameter
K=1/(10^17.146);                                    %S-N curve parameter
gam=5.5*10^-10;
damage_normstress_ws=cc2dam(rfc_normstress_ws,beta,K);%/simtime  %
    calculating damage
damage_normstress_s=cc2dam(rfc_normstress_s,beta,K);%/simtime
time_fail_ws=1/gam/damage_normstress_ws/3600;
time_fail_s=1/gam/damage_normstress_s/3600;

disp(strcat('damage, no slam, for s=',num2str(s),' is:',num2str(
    damage_normstress_ws)))
disp(strcat('damage, with slam, for s=',num2str(s),' is:',num2str(
    damage_normstress_s)))
disp(strcat('number of rfc, no slam, for s=',num2str(s),' is:',num2str(
    length(rfc_normstress_ws))))
disp(strcat('number of rfc, with slam, for s=',num2str(s),' is:',num2str(
    length(rfc_normstress_s))))

%%%%%%%%%%%%%%%%%%%%%%-Plotting fatigue plots-%%%%%%%%%%%%%%%%%%%%%%%%%%%%%%
if s==1
figure
grid on
hold on
plot(normstress_ws(1:60/0.004,1),normstress_ws(1:60/0.004,2),'b')
scatter(tp_normstress_ws(:,1),tp_normstress_ws(:,2),'r')
xlabel('Time [s]')
ylabel('[MPa]')
legend('Normal stress','turning points','Location','NorthOutside','
    Orientation','Horizontal')
axis([20 60 0.8*10^1 1.3*10^1])
title('No slamming')
figure
grid on
hold on
plot(normstress_s(1:60/0.004,1),normstress_s(1:60/0.004,2),'b')
scatter(tp_normstress_s(:,1),tp_normstress_s(:,2),'r')
xlabel('Time [s]')
ylabel('[MPa]')
legend('Normal stress','turning points','Location','NorthOutside','
    Orientation','Horizontal')
axis([20 60 0.8*10^1 1.3*10^1])
title('No slamming')
```

```
matlab2tikz(strcat('stressturningpoints.tikz'), 'height', '\figureheight',
    'width', '\figurewidth','showInfo', false,'checkForUpdates',false);
fclose('all');
fpath=('M:\Masteroppgave\Matlab\Tikz');
movefile(strcat('stressturningpoints.tikz'),fpath)
end
figure
subplot(1,2,1)
ccplot(rfc_normstress_ws)
title('No slamming')
subplot(1,2,2)
ccplot(rfc_normstress_s)
title('With slamming')
matlab2tikz(strcat('cyclecount',num2str(s),'.tikz'), 'height', '\
    figureheight', 'width', '\figurewidth','showInfo', false,'
    checkForUpdates',false);
fclose('all');
fpath=('M:\Masteroppgave\Matlab\Tikz');
movefile(strcat('cyclecount',num2str(s),'.tikz'),fpath)

figure
subplot(1,2,1)
hist(amp_normstress_ws,25);
title('No slamming')
subplot(1,2,2)
hist(amp_normstress_s,25);
title('With slamming')
matlab2tikz(strcat('histogram',num2str(s),'.tikz'), 'height', '\
    figureheight', 'width', '\figurewidth','showInfo', false,'
    checkForUpdates',false);
fclose('all');
fpath=('M:\Masteroppgave\Matlab\Tikz');
movefile(strcat('histogram',num2str(s),'.tikz'),fpath)


end
```

```
function [S_ws,S_s,xx_ws]=spectrum(Displacements_withoutslam,
    Displacements_slam,timesteps,s)

addpath 'W:\Matlab\WAFO\wafo25'    %path to wafo package
initwafo('full',1,1)

L0=6000;                %Smoothing parameter
xx_ws(:,1)=timesteps(1:50:end);
xx_ws(:,2)=Displacements_withoutslam(1:50:end,1);
xx_s(:,1)=timesteps(1:50:end);
xx_s(:,2)=Displacements_slam(1:50:end,1);
S_ws=dat2spec(xx_ws,L0);
S_s=dat2spec(xx_s,L0);
figure
hold on
plot(S_ws.w(1:5:end),S_ws.S(1:5:end))
plot(S_s.w(1:5:end),S_s.S(1:5:end),'LineStyle','--')
axis([0 1.5 0 2.0])
xlabel('frequency [rad/s]')
ylabel('S(w)[m^2 s/rad]')
legend('No slamming','With slamming')
matlab2tikz(strcat('spectrum',num2str(s),'.tikz'), 'height', '\figureheight
    ', 'width', '\figurewidth','showInfo', false,'checkForUpdates',false);
fclose('all');
fpath=('M:\Masteroppgave\Matlab\Tikz');
movefile(strcat('spectrum',num2str(s),'.tikz'),fpath)
end
```